ELECTROLYTE-BASED SIMULATIONS OF A LABORATORY SCALE CARBON DIOXIDE CAPTURE PROCESS

A Thesis Submitted to the
Graduate School of Engineering and Science of
İzmir Institute of Technology
in Partial Fulfillment of the Requirements for the Degree of

MASTER OF SCIENCE

in Chemical Engineering

by
Ateş Batıkan ÖZDAMAR

June 2020
İZMİR

ACKNOWLEDGEMENT

I would like to express my sincere gratitude to my thesis advisor, Co-Head of IZTECH Chemical Engineering Department Assist. Prof. Dr. Erdal UZUNLAR for his guidance, thoughtful advice, and continuous encouragement during the course of this work. I would also like to thank to committee members Assoc. Prof. Dr. Özgenç EBİL of IZTECH Chemical Engineering and Prof. Dr. Can ERKEY of Koç University Chemical and Biological engineering for their valuable discussions and contributions. I am also grateful to Prof. Dr. Erol ŞEKER for his precious advices and for introducing me to my thesis advisor Assist. Prof. Dr. Erdal UZUNLAR.

I am also grateful to our department secretary Fatma Aydoğan for her help and motivation.

I would like to thank to the professors of METU Chemical Engineering who made valuable contributions to my undergraduate education. Also, I wish to express my gratitude to Prof. Dr. Nevin Selçuk and Associate Dean Prof. Dr. Görkem Külah for their valuable suggestions, support and contributions in the first two years of graduate education in Middle East Technical University (METU).

I would like to thank my dearest members of “Rooftop”, Azime ARIKAYA, Günsev DİZOĞLU, Burcu SIRMA and my dear brother Yaşar Kemal RECEPOĞLU for their endless supports, encouragement and contributions. Their precious friendship brought me where I am.

Finally, I would like to express my heartfelt gratitude to my mother Gülay ÖZDAMAR and my father İsmail ÖZDAMAR for their unconditional love, encouragement, sacrifices and unshakable faith in me and endless support over my whole life. They are my luck. Their love enabled me to overcome difficulties. Without them, I cannot be the person I am right now.

ABSTRACT

ELECTROLYTE-BASED SIMULATIONS OF A LABORATORY SCALE CARBON DIOXIDE CAPTURE PROCESS

The aim of this thesis is to design and simulate a laboratory-scale CO_2 capture system on Aspen Plus. The studied CO_2 capture process is a post-combustion CO_2 capture process. The commonly employed monoethanolamine (MEA) sorbent is compared with the piperazine (PZ) sorbent in terms of reaction kinetics and energy consumption throughout the study.

Three main simulation studies were performed in order to compare MEA and PZ sorbents. First, an absorption column, then an open loop (single pass) process and finally a closed loop (recycle) process were designed and simulated on Aspen Plus. The simulations were carried out at various inlet gas pressures. After designing an absorber column, CO_2 loading, temperature, pressure, mole flow, packing details, column height and diameter constraints were determined. As a result of open loop and closed loop processes, the column operations in absorber and stripper columns regarding CO_2 reactions and energy consumption were investigated. The results showed that PZ absorbs and releases more CO_2, has a faster kinetics, and is more energy efficient compared to MEA in CO_2 capture processes.

ÖZET

LABORATUVAR ÖLÇEKLİ KARBONDİOKSİT TUTMA SÜRECİNİN ELEKTROLİT-TABANLI SİMÜLASYONLARI

Bu tezin amacı Aspen Plus üzerinde laboratuvar ölçekli bir CO_2 yakalama sistemi tasarlamak ve simüle etmektir. Çalışılan CO_2 yakalama süreci, bir yanma sonrası CO_2 yakalama işlemidir. Yaygın olarak kullanılan monoetanolamin (MEA) sorbenti, çalışma boyunca reaksiyon kinetiği ve enerji tüketimi açısından piperazin (PZ) sorbenti ile karşılaştırılmaktadır.

MEA ve PZ sorbentlerini karşılaştırmak için üç ana simülasyon çalışması yapılmıştır. İlk olarak, bir absorpsiyon kolonu, daha sonra bir açık döngü (tek geçiş) süreci ve son olarak bir kapalı döngü (geri dönüşüm) süreci Aspen Plus üzerinde tasarlanmıştır ve simüle edilmiştir. Simülasyonlar çeşitli giriş gazı basınçlarında gerçekleştirilmiştir. Bir absorplayıcı kolon tasarlandıktan sonra, CO_2 yükleme, sıcaklık, basınç, mol akışı, dolgu detayları, kolon yüksekliği ve çap kısıtlamaları belirlenmiştir. Açık döngü ve kapalı döngü süreçleri sonucunda, absorplayıcı ve sıyırıcı kolonlardaki CO_2 reaksiyonları ve enerji tüketimi ile ilgili kolon işlemleri incelenmiştir. Sonuçlar, PZ'nin daha fazla CO_2 absorpladığını ve serbest bıraktığını, daha hızlı kinetiğe sahip olduğunu ve CO_2 yakalama işlemlerinde MEA'ya göre enerji verimliliğinin daha fazla olduğunu göstermiştir.

TABLE OF CONTENTS

LIST OF TABLES

Table **Page**

LIST OF FIGURES

Figure **Page**

CHAPTER 1

INTRODUCTION

1.1. Environmental Effects of CO_2

Awareness on climate change, often called global warming, has been raising worldwide for the last few years. Even though global warming is a more stunning name, “climate change” is a more comprehensive and accurate phrase for the environmental changes observed [1].

Emissions of greenhouse gases contribute to global warming. Especially, carbon dioxide has received widespread attention. The concentration level of CO_2 in the atmosphere reaches over 410 ppm as it is mentioned later in this chapter and 410 ppm is considerably a high value for emission regulations. Effective CO_2 mitigation techniques will become increasingly demanding because of environmental problems. There are several sources that release CO_2 and combustion of fossil fuels plays the major role in it. Coal-fired power plants are one of the most prominent CO_2 emitting sources today. There are still challenges which remain unsolved despite various carbon reduction technologies available. Post-combustion based chemical absorption process is one of the most promising technologies for carbon mitigation. The operation of the chemical absorption process is deeply examined in the CO_2 capture systems [2].

In this chapter, background of global temperatures, the greenhouse effect, atmospheric CO_2 levels, general sources of CO_2 emissions, current status of CO_2 capture technologies, aqueous amine absorption/stripping including basics of mass transfer, general amine chemistry and Aspen Plus as a simulation tool are briefly explained.

1.1.1. Global Temperatures

Importance of greenhouse gas mitigation technology regarding CO_2 has been growing in the light of global climate change fears. Over the last 40 years, there has been

a raising concern because of increasing global temperatures [3]. The world-wide mean surface temperature and the average temperature from 1880 to 2020 increases which is illustrated in Figure 1.1 [4].

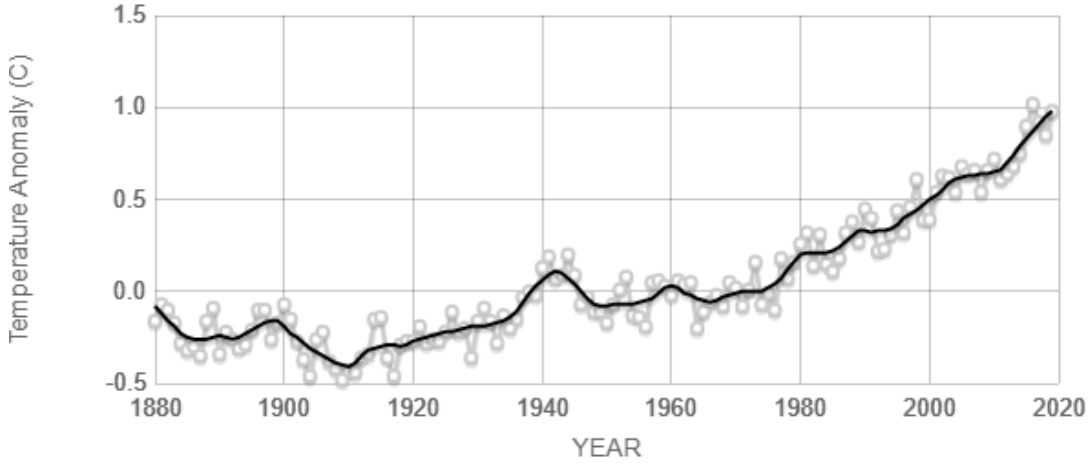

Figure 1.1 Change in global temperature from 1880 to 2020 [4]

Much of the temperature rise globally has been attributed to the enhanced CO_2 level in the atmosphere because of human activities [3]. This temperature data is consistent with the Climatic Research Unit and the National Oceanic and Atmospheric Administration. All the data coming from thousands of worldwide observation spots on land and sea was processed [1]. Grey marked dots linked to black line show annual mean temperature data. Since 2001, almost all the warmest years have occurred in the modern history. In 2016, temperature anomaly passed 1˚C for the first time in history [4].

1.1.2. The Greenhouse Effect

The greenhouse effect is one of the eminent planetary mechanisms that determines the temperature of planet "Earth" and is originally a natural phenomenon, i.e. not man-made. It has a partial benefit for making the climate on Earth livable for humans. However, humans have been changing the intensity of the greenhouse effect by increasing the proportion of the greenhouse gases in the air. Without an essential warming provided by greenhouse gases, the average global temperatures would be around –19˚C rather than 14˚C [5].

Increasing global temperatures have been frequently attributed to increasing atmospheric CO_2 levels. CO_2 is a known greenhouse gas which traps heat. When solar

radiation emitting from the sun strikes the Earth, it is converted to infrared radiation. Greenhouse gases absorb some of the infrared radiation reflected from Earth and emit that radiation them again to the Earth. This phenomenon is called heat trapping. Ozone, nitrous oxide, water vapor and methane are other major greenhouse gases. The report written by the National Center for Atmospheric Research (NCAR) mentions that water vapor is the major heat trapping gas. On a clear day, almost 60% of the greenhouse effect results from water vapor. CO_2, O_3, and the combination of CH_4 and N_2O make up 26, 8, and 6% of the greenhouse effect, respectively. The level of water vapor (H_2O) in the atmosphere cannot be controlled effectively [1]. The proportion of second important greenhouse gas, CO_2, has been increasing in the atmosphere due to the burning of fossil fuels since industrial revolution. To mitigate or reduce the heat trapping ability of the atmosphere, CO_2 should be the target between the greenhouse gases.

1.1.3. Atmospheric CO_2 Levels

The trend in monthly mean atmospheric CO_2 concentration globally averaged over marine surface sites is illustrated in Figure 1.2 [6].

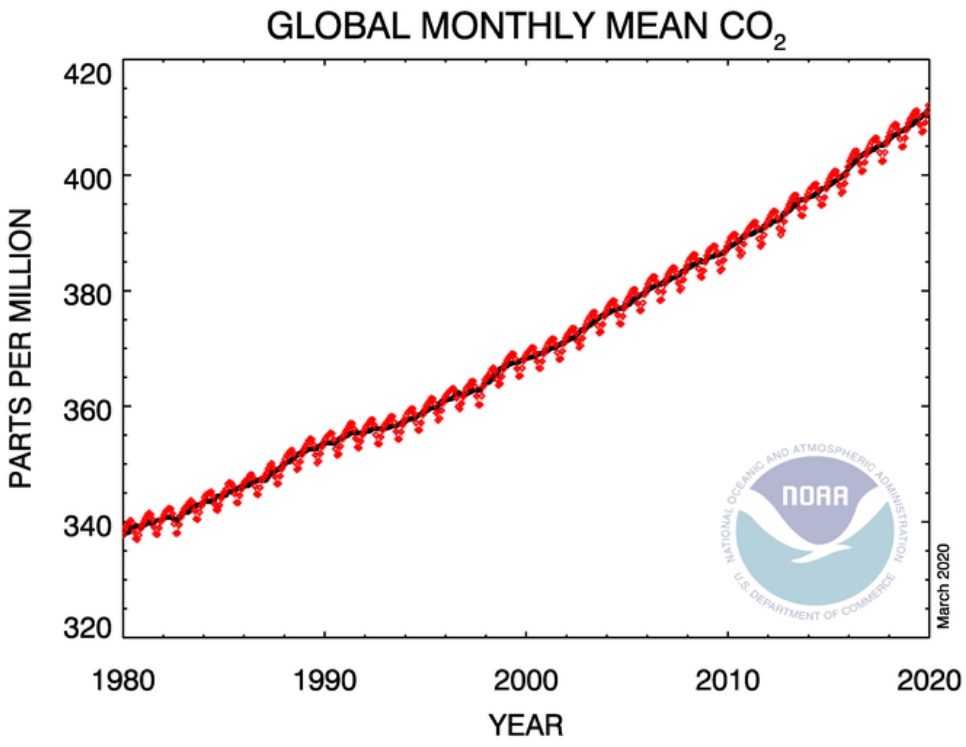

Figure 1.2 Global monthly mean CO_2 concentrations measured from marine surface sites from 1980 to 2020 [6]

The data for all years since 1980 are illustrated on this very graph. The CO_2 concentration data is given with respect to mole fraction of dry air. Parts per million (ppm) is used to express the mole fraction. The dashed red line, centered on the middle of each month, represents the monthly mean values. The black line represents the moving average of 7 adjacent seasonal cycles after correction for the average seasonal cycles. The black data are centered on the month that will be corrected, aside from the 1st and last 3.5 years of this record. It is because the seasonal cycle is averaged over the 1st and last 7 years. All measurements are done by the Global Monitoring Division of National Oceanic and Atmospheric Administration Earth System Research Laboratory [6]. From 1980 to 2020, CO_2 concentration increased from 340 ppm to almost 411 ppm as can be seen from Figure 1.2.

1.1.4. General Sources of CO_2 Emissions

In the most basic sense, carbon is extracted from deep underground and then emitted into the natural environment. This leads to atmospheric CO_2 concentrations to increase. The global carbon cycle is shown in Figure 1.3 [7].

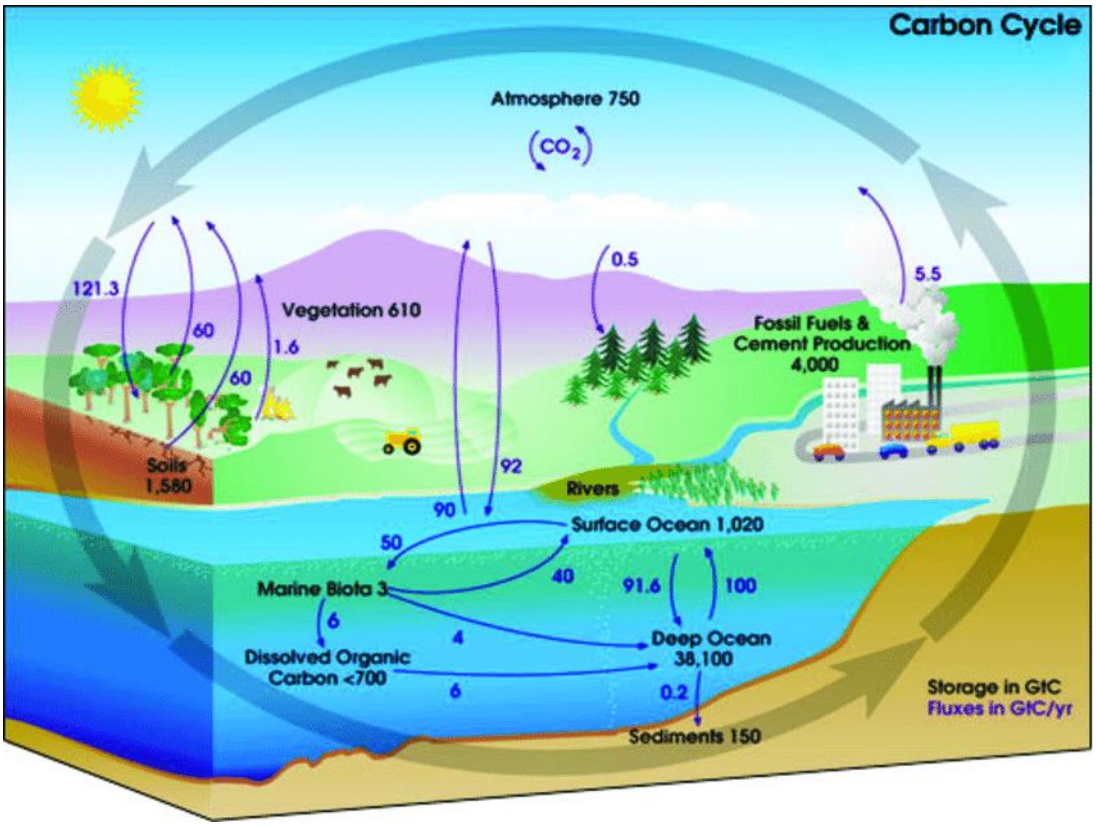

Figure 1.3 The global carbon cycle [7]

This diagram illustrates the storage and annual exchange of carbon between the atmosphere, geosphere and hydrosphere in gigatons of carbon (GtC). Most of the carbon transfer arises from natural environmental processes. Carbon dioxide dissolved in the ocean will move to the atmosphere and carbon dioxide in the atmosphere will finally shift to the ocean. It is a continuous cycle.

Man-made or anthropogenic CO_2 emissions cause atmospheric CO_2 concentration to enhance. This in turn represents a rise of the overall carbon in a closed system. Even though the ocean is by far the largest sink for carbon, with a sink capacity much larger than industrial emissions, the ocean cannot possibly absorb all the man-made CO_2 itself since there is a natural balance between the carbon in vegetation, the atmosphere, and the ocean.

It is significant to understand where the anthropogenic CO_2 emissions originate, so as to target a specific source before addressing the limitation measures that can be taken for those emissions [1]. Figure 1.4 shows yearly global CO_2 emissions from various fossil fuels, such as petroleum, coal and natural gas between the years 1990 and 2020 [8].

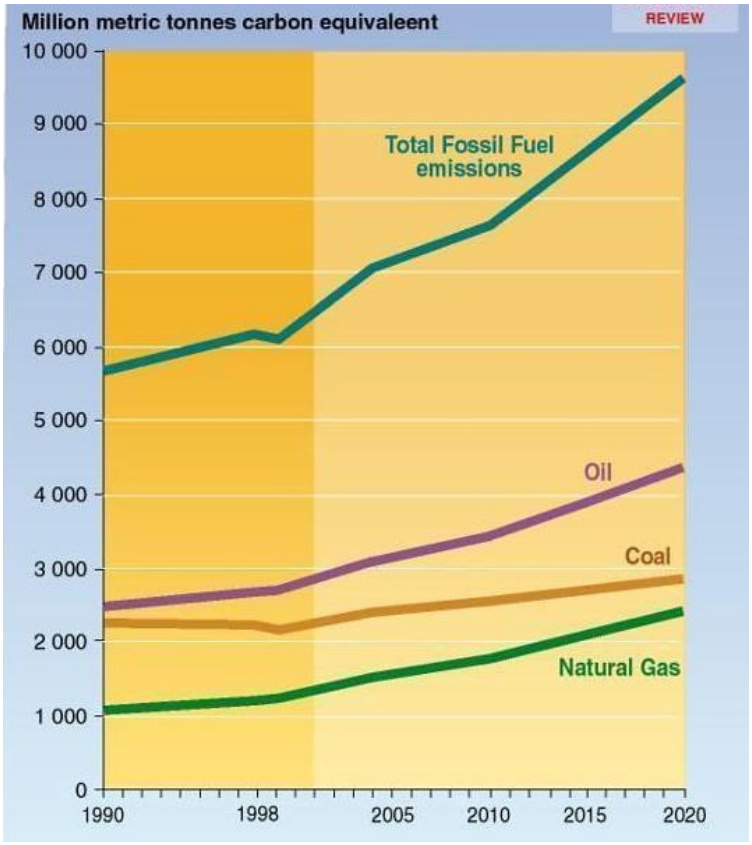

Figure 1.4 Change in fossil fuels-based CO_2 emissions between the years 1990 and 2020 [8]

The emissions are expressed as million metric tons carbon equivalent. As seen in Figure 1.4, oil, coal, and natural gas account for most of the CO_2 emissions. Oil (petroleum) is generally used as a fuel for transportation vehicles. Transportation vehicles which use oil as fuel result in a very large number of small emission sources [1]. Petroleum's contribution to total emission is higher than coal and natural gases. Also, another significant portion of CO_2 is emitted to the atmosphere by the large number of coal-fired power plants.

In short, all these CO_2 emissions contribute to global warming. In terms of the emission mitigation, it is relatively easier and more logical to target the sources in smaller numbers with large individual contributions, such as coal-fired plants, compared to the sources in larger numbers with smaller individual contributions, such as transportation vehicles. For that reason, we will study post-combustion CO_2 capture in coal-fired power plants in a laboratory-scale CO_2 capture system in this study.

1.2. Brief Overview of CO_2 Capture Systems

CO_2 capture has been applied in the industry for a long time. The basic reasons for capturing CO_2 can be listed as follows [9]:

- CO_2 is a greenhouse gas.
- The heating value of CO_2 is zero. So, removing CO_2 from a combustible mixture will increase the heating value of the mixture.
- If natural gas is intended to be transported using pipelines, CO_2 puts an extra load on compressors.
- The crystallization temperature of CO_2 is low. Because of that, CO_2 amount in natural gas should be kept below a certain limit while liquefying natural gas to LNG in order to prevent CO_2 crystallization inside the heat exchanger tubes.
- CO_2 creates an acidic environment in humid environment and that leads to corrosion of metals.
- CO_2 is marketable, that is, CO_2 can be used as a feedstock for chemical conversion to some valuable products, such as methanol.

Current global energy supply highly depends on coal. The future will bring rising demand on electricity. Therefore, new ways are needed to handle the CO_2 emissions from

the fossil fuel fired power plants. Basically, CO_2 can be captured by three different ways based on the order in process at which the capture happens [10–12]:

1. Oxy-fuel Combustion Capture
2. Pre-Combustion CO_2 Capture
3. Post-Combustion CO_2 Capture

A representative flow diagram of CO_2 capture and sequestration is shown in Figure 1.5.

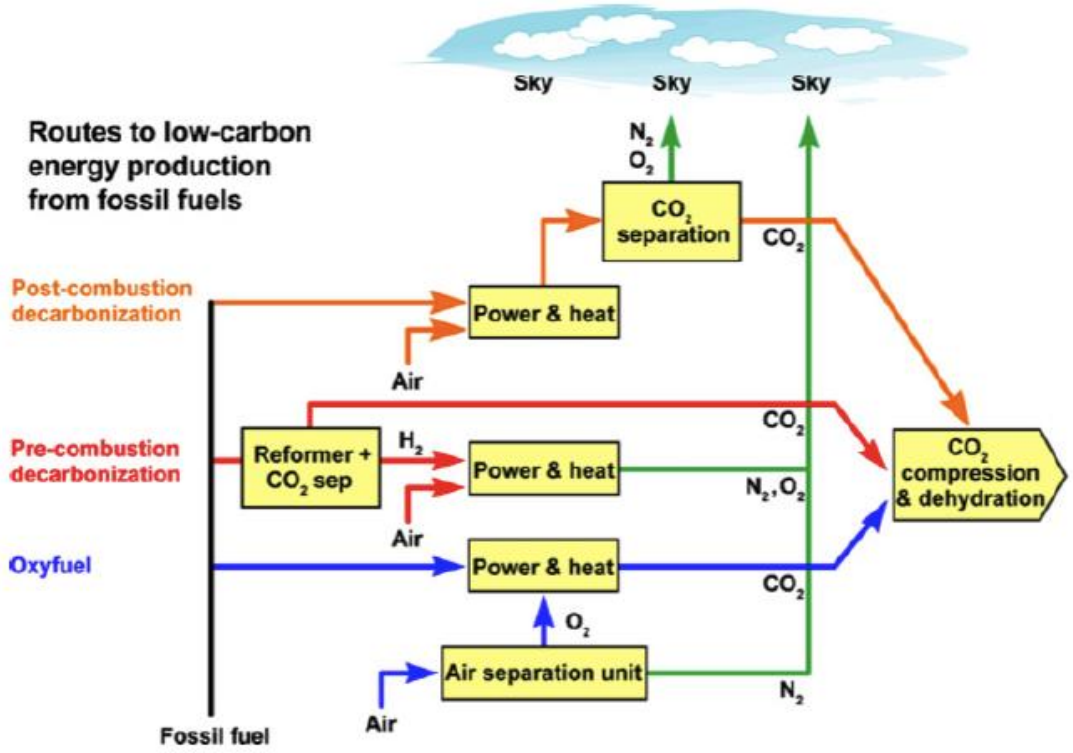

Figure 1.5 CO_2 Capture and Sequestration Flow Diagram [13]

1.2.1. Oxy-Fuel Combustion Capture

In oxy-fuel combustion, pure oxygen is used to obtain fuel gas rich in CO_2 and H_2O instead of air. A representative flowsheet of oxy-fuel combustion process is shown in Figure 1.6. By cryogenic separation of air components, the oxygen is obtained. Air Separation Unit, which is abbreviated as ASU, is utilized for separating O_2 from air. For the separation, a high amount of energy is required. Air separation unit consumes nearly 15% of the electrical energy produced by the power plant [10]. Flame temperature is extremely high in the oxy-fuel capture method since fuel is directly burnt in pure O_2. Control of flame temperature is provided by recycling the fuel gas, which is rich in CO_2

and H_2O, back to the combustion zone. In oxy-fuel combustion, CO_2 is captured after the combustion of fuel by pure O_2.

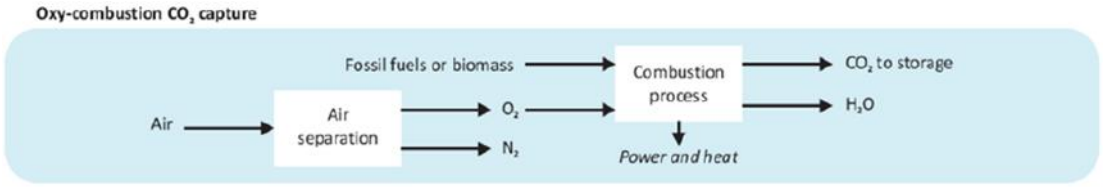

Figure 1.6 Oxy-combustion process flowsheet [14]

1.2.2. Pre-combustion Capture

In pre-combustion method, CO_2 is captured before the combustion of the fuel. A representative flowsheet of pre-combustion process is shown in Figure 1.7. Syngas is a mixture containing hydrogen and carbon monoxide. Syngas is produced by fuel reacting with air or oxygen. Then, carbon monoxide (CO) in syngas undergoes the water gas shift reaction to produce CO_2 and H_2. Then, CO_2 is separated from H_2 in a separation unit. Finally, CO_2-free H_2 is combusted with air to generate energy [10].

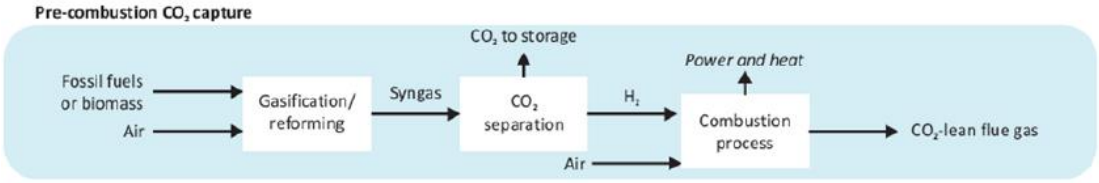

Figure 1.7 Pre-combustion process flowsheet [14]

1.2.3. Post-combustion Capture

As its name suggests, post combustion capture method separates CO_2 from the flue gas after the fuels are combusted. Figure 1.8 shows a typical post-combustion process flowsheet.

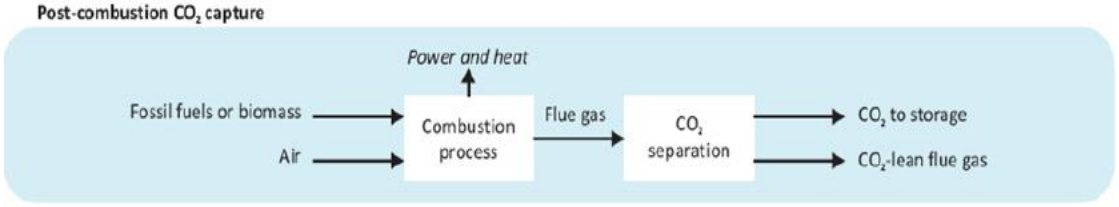

Figure 1.8 Post-combustion process flowsheet [14]

The flue gas is not released to the atmosphere, instead it is passed through the separation unit that separates the CO_2. This does not bother the design of the functioning power plant and therefore it is the most preferred capture method [10].

In order to remove or capture CO_2, several separation technologies are available which are shown in Figure 1.9. These technologies are membrane separation, adsorption, cryogenic separation, microbial separation, chemical absorption, and physical absorption. Each of these technologies has its own field of use in industry [9,10].

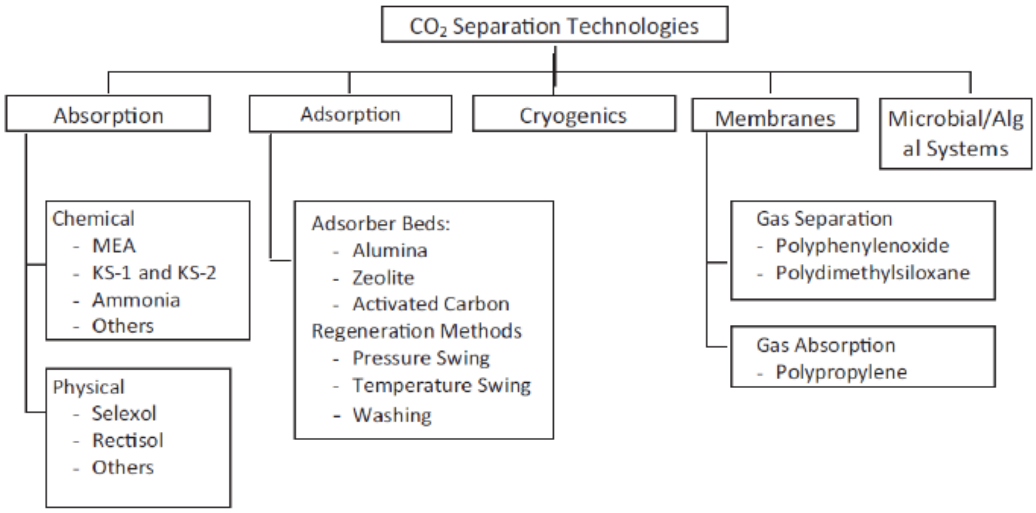

Figure 1.9 Gas separation technologies for CO_2 capture [15]

1.2.3.1. Membrane Separation

Membrane separation method is divided into two main topics which are gas separation with polyphenylene oxide and polydimethylsiloxane, and gas absorption with polypropylene as shown in Figure 1.9 [15]. In this separation method, a membrane is used that only allows CO_2 while blocking the other components to pass through it [16].

The membrane is composed of composite polymeric materials. One thin selective layer of rubber is bonded to a non-selective glassy, hard, and thick layer of polymer that supplies the mechanical support required by the membrane. Rubbery segment is soft and makes a thin film on hard support [17]. Besides polymeric ones, there are inorganic membranes, matrix membranes, carbon membranes, ceramic membranes, metallic membranes and facilitated transport membranes. The main problem with this technology is the inefficient separation from gas mixtures with low CO_2 concentration, such as flue gas of a coal-fired power plant. [16].

1.2.3.2. Adsorption

Unlike chemical absorption process, this method uses solid sorbent rather than a liquid absorbent. The main mechanism is CO_2 adsorption on the surface of the adsorbent [16]. The regeneration process happens either by pressure decrease (as in pressure swing adsorption, PSA), or temperature increase (as in temperature swing adsorption, TSA). The efficiency of PSA is about 85%. In PSA method, CO_2 is adsorbed at high pressure on the surface of the sorbent. Then, sorbent is regenerated at low pressure which results with the release of CO_2. In TSA, the sorbent is regenerated by rising the temperature by using steam or hot air. The purity of CO_2 is higher than 95% for both PSA and TSA, although the duration needed for regeneration for the sorbent is longer with TSA. The sorbents should have higher surface area and higher regeneration ability. The major sorbents are activated carbon, alumina, molecular sieves, lithium zirconate, calcium oxides, zeolites and hydro-talcites [16].

1.2.3.3. Cryogenic Separation

Cryogenic gas separation method requires distillation at low temperatures and high pressures. The desublimation of flue gas occurs at temperatures between -135 °C and -100 °C. Solidified CO_2 is then separated from the other components. Afterwards, CO_2 is compressed to a high pressure of 100-200 atm pressure. This method has an efficiency of 90-95% and yet there is only one disadvantage of this process. Cryogenic separation is an "energy intensive" process because high amount of energy is required to reach such low temperatures and high pressures [10,16].

1.2.3.4. Microbial Separation

Lately, microalgae have been growing its recognition among several productive biological systems for capturing CO_2. Capturing efficiencies of CO_2 seem to be as high as 90%, so it is a promising method. Possible strategies for CO_2 capture and sequestration by exploiting microalgae is still discussed in literature. The dominant form of CO_2 dissolved in water is "bicarbonate" at moderate temperatures (below 30 ºC) and pH's ($\geq$ pH 7). Algae have active bicarbonate pumps and thus, they can concentrate bicarbonate in the cell. Subsequently, the bicarbonate is dehydrated. The resulting carbon-dioxide is captured via Calvin-cycle activity [18].

1.2.3.5. Physical Absorption

It is a well-known technology. It consists of one gas-liquid contactor for absorption and a series of ash tanks for solvent regeneration. The contactor works at high pressure. When the solvent is passed through the low-pressure ash drum, it is regenerated and CO_2 coming from the flue gas is captured. Physical absorption is a very simple process since there are no chemical reactions that occur between the solvent and the gas. Regeneration of solvent may be possible by lowering the pressure, passing the inert gas through the solvent or using thermal regeneration. Temperature is raised to separate CO_2 in thermal regeneration. Physical absorption favors taking place at low temperature and high pressure [10,19].

1.2.3.6. Chemical Absorption

Chemical absorption is the most commonly employed method for the separation of CO_2. It has been used in the industry for capture and separation of CO_2 since 1930's. In chemical absorption, flue gas has to be passed through the absorption column. Aqueous alkaline solvents, such as amine solutions, absorb CO_2 inside the absorption column. In the stripper (desorber), the absorbed CO_2 is removed from the aqueous alkaline solvent and a stream of pure CO_2 is obtained that can be stored for future utilization. The regenerated solvent is sent back to the absorber and the cycle is repeated.

Stripping column requires high amount of thermal energy to heat the solvent for releasing CO_2. Because of that, solvent is passed through a heater before it is sent to the stripper. Electrical energy is used to compress the flue gas before entering the absorption column, to compress the CO_2 for the purpose of storage or to transfer it by pumps and blowers [3,10].

In this thesis study, absorption and stripping operations are to be performed using amine molecules, such as MEA and PZ. In that regard, aqueous amine absorption/stripping is explained in the next section.

1.3. Aqueous Amine Absorption/Stripping

Absorption/stripping with aqueous amines is one of the most mature technologies in the industry. It is used to capture emissions of CO_2 from coal-fired power plants. As a

tail-end process, it is quite advantageous because it can be added on to a power plant that is already in operation. The flow diagram of an open loop process with amine absorption/stripping system is shown in Figure 1.10.

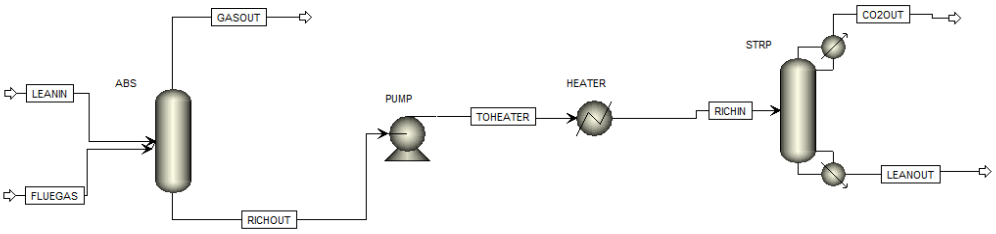

Figure 1.10 Open loop (single pass) flow diagram for absorption/stripping with aqueous amines

This mature technology exploits an aqueous amine solvent (MEA/PZ) which counter currently interacts with the flue gas in a packed absorber column (ABS in Figure 1.10). The CO_2 in the flue gas exothermically reacts with the amine which significantly reduces the CO_2 concentration in the gas stream (GASOUT in Figure 1.10) exiting the absorber.

The rich solvent stream called “RICHOUT” loaded with CO_2 exits the column from the bottom. As “RICHOUT” leaves the absorber, it is fed to the pump to increase its pressure. Thus, outlet stream of the pump is heated across a heater and then sent to the stripper (STRP in Figure 1.10). For the amine-CO_2 reaction to reverse itself and liberate/release CO_2, the temperature of the stripping unit must be maintained at sufficiently high level. In the closed loop version of the process (not shown in Figure 1.10), the lean amine stream, “LEANOUT”, exiting the stripper from the bottom is cooled by the cross exchanger and recycled back to the absorption column to capture more CO_2. The concentrated CO_2 stream which leaves the stripper may be compressed into a supercritical form so that it can be pumped to its destination and it can be used for various purposes, such as enhanced oil recovery. The major technological drawback behind the implementation of aqueous amine absorption or stripping on power plants is cost. Prices of electricity would increase about 80% for coal-fired power plants which perform CO_2 capture [1]. Almost 80% of that price increase is related to capture and compression of CO_2 while the remaining 20% is based on sequestration [1]. In numerous efforts to reduce the cost and increase the efficiency of carbon-dioxide capture, alternative amine solvents are examined.

The benchmark solvent has been 30 wt% monoethanolamine (MEA) for years in amine scrubbing processes. MEA has proven itself for this application [20]. Several specifications justify its use, such as the rapid kinetics [21]. However, its high regeneration energy combined with the large solvent circulation rates leads to high energy consumptions.

In addition to this, CO_2-MEA mixtures are highly corrosive and degrade quickly [21]. These are the certain drawbacks regarding its use and the basic reasons behind new sorbent research. As an alternative, piperazine (PZ) is used in this thesis because it has a higher absorption and desorption rate of CO_2, better thermodynamic properties, greater capacity for CO_2 absorption and more energy efficient as written in literature [1,22–26].

1.3.1. Modeling of Mass Transfer in Liquid Boundary Layer

The steady state diffusion of a species due to a concentration gradient in the liquid phase is governed by Equation 1 which is obtained in rectangular coordinates. In this equation, N_{CO2} represents the flux of CO_2, and x represents the distance in the liquid phase [27].

$$\frac{\partial N_{CO2}}{\partial x} = 0 \qquad \text{Eqn. 1}$$

The flux of CO_2 can be calculated using Equation 2 in which ${k_l}^0$ represents the mass transfer coefficient, $[CO_2]_i$ represents the CO_2 concentration at the interface and $[CO_2]_{bulk}$ represents the CO_2 concentration in the bulk gas mixture.

$$N_{CO_2} = {k_l}^0([CO_2]_i - [CO_2]_{bulk}) \qquad \text{Eqn. 2}$$

To model the mass transfer phenomena taking place at the gas-liquid interface, different theories have been developed. The main theories on mass transfer are penetration theory, film theory, surface renewal theory and Eddy diffusivity theory. Among these, film theory and Eddy diffusivity theory are generally employed.

These are both steady state theories, this is why there are no time dependent variables in the models. However, penetration theory and surface renewal theory are both unsteady state theories which will not be introduced here [27]. Details of packed column model rate-based model and the related assumptions are expressed in Appendix B section of thesis.

1.3.2. Film Theory

Both the liquids and gas phases are divided into two distinct regions, which are namely bulk region and film region, according to the film theory developed by Lewis and Whitman [28]. The assumption of film theory states that the concentrations are allowed to change only in the film region, whereas the concentrations in the bulk gas and liquid are constant. A schematic representation of (remove double) film theory is shown in Figure 1.11.

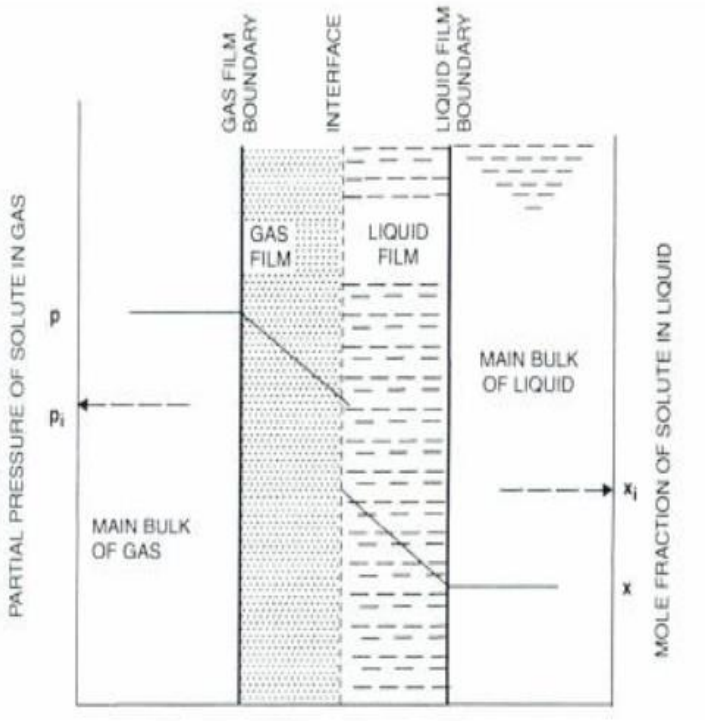

Figure 1.11 Schematic representation of film theory [27]

Film theory combines Eq. 1 and Eq. 2 with the Fick's law to estimate the mass transfer coefficient which will be proportional to the diffusion coefficient [28]. The film theory is so far the simplest model that explains the CO_2 absorption by amines, such as MEA or PZ.

1.3.3. Selection of Equipment/Column

Absorption process requires the generation of an extended area of liquid surface to contact with a gas phase under mass transfer condition. Such thing can be accomplished by three different ways which are tray columns, packed columns and spray contactors.

This three equipment are different in terms of the performance of absorption and stripping operations. In Table 1.1, there is a simplified guideline for the selection of most commonly used types of equipment for gas absorption. Material and energy balances of absorber for the liquid and gas phase are given in Appendix C of thesis.

Table 1.1 Selection guide of absorbers and strippers [29]

	Tray Columns		Packed Columns (Random)	Spray Contactors
	Perforated	Bubble Cap		
Low liquid rate	D	A	C	D
Medium liquid rate	A	C	B	C
High liquid rate	B	C	A	A
Difficult separation (many stages)	A	B	A	D
Easy separation (one stage)	C	C	B	A
Foaming system	B	C	A	C
Corrosive fluids	B	C	A	A
Solids present	B	D	C	A
Low ΔP	C	D	B	A
High turndown ratio	C	A	B	D
Versatility (can be changed)	C	C	A	D
Multiple feed & drawoff points	B	A	C	C

Key: A, best selection; B, usually suitable; C, evaluate before specifying; D, generally not applicable.

In this thesis, we will take advantage of packed columns. For that reason, we will provide a brief information about the packed towers. The advantages of packed column are listed below [30]:

- Lower pressure drop.
- Columns with small diameter are possible.
- Foaming systems can be handled.
- The construction of the system is easy.
- Corrosive material can be handled.
- There is a better mass transfer than that in the spray column.
- There is a reduced back mixing compared to spray column.
- Increased efficiency of separation for the same column height.

However, there are also some disadvantages of using packed columns:

- There are some problems when working with high viscosity liquids and extremely high gas and liquid flow rates.

- There may be channeling which must be avoided by redistributing liquid.

1.3.3.1. Packed Column

Packed columns are also called continuous-contact columns because of the way the vapor and the liquid contact. It is a vertical pressure vessel which is filled with packing material. The flow of gas is upwards and the flow of liquid is downwards through the bed. Liquid has a tendency to wet the surface of the packing material and the vapor passes through this wetted surface. This contact provides a mass transfer according to the equilibrium or kinetic mechanism. Packing material offers a large surface area for this liquid-gas contact without causing excessive pressure drop across a packed section. Otherwise, a higher pressure drop means a higher energy requirement and a higher cost at the end. Packing material should be chemically inert to contacting gas and liquid streams [31].

Packed column structure could change in terms of the packing material. There are random packing and structured packing options. The column may be filled with randomly dumped packing material or with structured packing section which are arranged in a special manner. The randomly packing material can be steel, ceramic or plastic different in terms of the geometric design. Some examples of structured packing can be given as woven wire gauze, plastic gauze or sheet metal. Figure 1.12 shows a packed column which includes a random packing material, mist eliminator, support plate and liquid distributor.

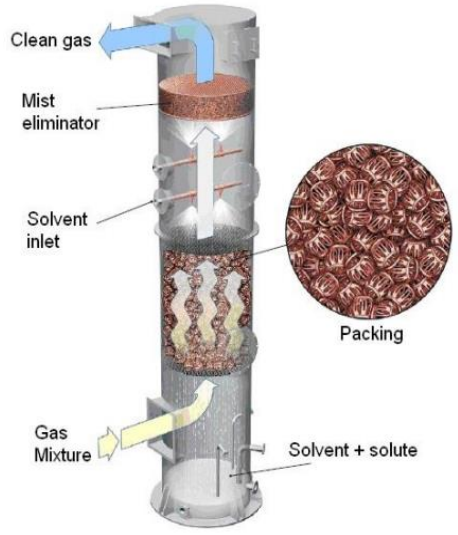

Figure 1.12 Typical packed bed absorption column [32]

In order to condense the vaporized liquid streams, mist eliminators are employed. In Figure 1.13, at the left side, there is a mesh mist eliminator and at the right side, there is a vane mist eliminator.

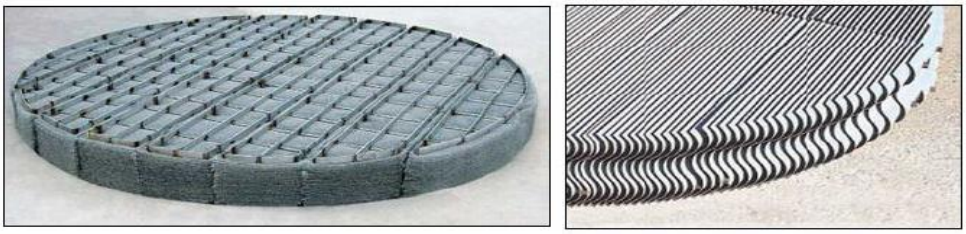

Figure 1.13 Mist eliminators [33]

In the column there are also support plates that hold the packing materials in place. In Figure 1.14, two types of support plates are shown.

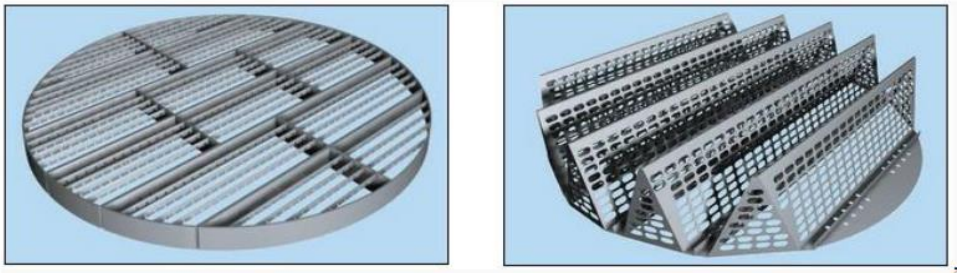

Figure 1.14 Support plates [33]

There are also distributors which prevent channeling inside the packed columns and some of them are shown in Figure 1.15. Liquid stream flows through these distributors.

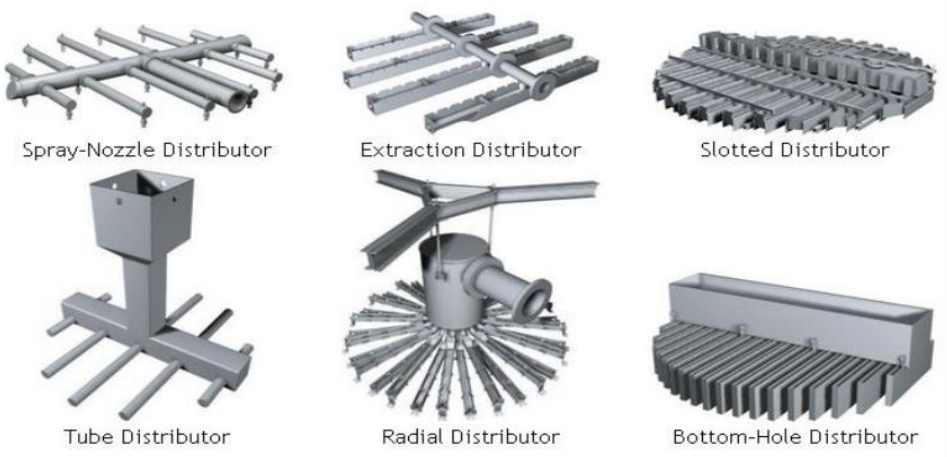

Figure 1.15 Distributor types [33]

1.3.3.2. Types of Packing

There are lots of different packing types in order to provide contact between two phases; however, in general, the types of packing can be categorized as *random* or *structured.* In random packing, the individual pieces do not have any specific arrangement and they are just dumped into a containing shell. The most common random packings widely used in the industry are Raschig rings, Pall rings, Intalox saddles and Berl saddles. All of them are shown in Figure 1.16. When Raschig rings and Berl saddles become useless after a certain time in a column, they are replaced with Pall rings and Intalox saddles since they are more economical than other two types [34].

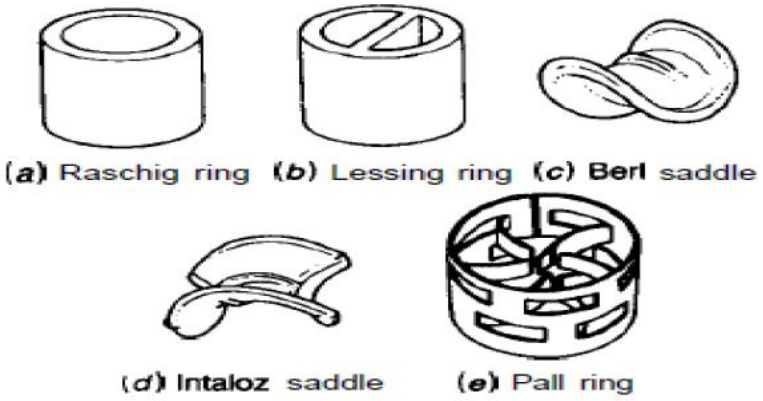

Figure 1.16 Representative drawings of the most common random packings [34]

Raschig rings are hollow cylinders that the outer diameter and height are equal. They are constructed from cheap and light inert materials like porcelain, carbon etc. Ceramic, plastic, metal alloys, steel or clay materials are also used to make Raschig rings. They are available in the sizes between ¼ in to 3 in, or more. If pieces of Raschig rings are dropped into an open shell directly, some breakages can occur due to their fragility. In order to prevent this, sometimes, the empty tower is first filled with water and then the packing material is filled into the water-filled tower.

Pall rings, which have the same form as Raschig rings, are made of plastic or metal. They are open cylinders whose diameter and height are equal. Sizes are available in between 5/8 in and 3 in, or more.

Saddle-shaped packings like Intalox saddles and Berl saddles, are made from plastics, chemical stoneware or a metal that is suitable for shaping. They are available in

the sizes of ¼ in to 2 in. Since they have interlocking structure, they cause less side thrusts than Raschig rings so that they can provide more active surface.

The packing with the solid cross web is called as cross-partition rings which are used as a *structured packing* in common. Their size changes between 3-6 in. Structured packings, which are shown in Figure 1.17, cause to a lower pressure drop compared to random packings for the same fluid capacities. Structured packings are not the best choice in terms of cost. In addition to higher initial purchase cost than random packing, structured packing also requires an extra installation labor cost. Most common nominal size of structured packing is 3 in [34,35].

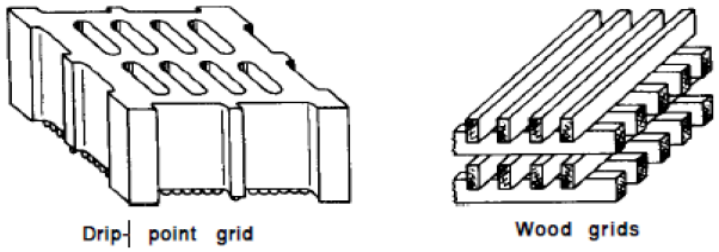

Figure 1.17 Structured packings [35]

1.3.3.3. The Common Material Types of Packing

The common materials which are used to make tower packings are given below:

- **Ceramic Packing**

Ceramic surface of the ceramic packing can provide extremely thin film and can provide greater mixture of liquid vapor [36]. It also causes low pressure drop. Additionally, since surface of ceramic packing can keep liquid hold-up to minimum and promotes wetting, the risk of overheat and coke formation can be minimized. The ceramic packings are preferable for the processes that require high temperature and chemical corrosion resistance.

- **Plastic Packing**

The plastic packings are inexpensive and they are used successfully to increase the tower capacity and efficiency. In many applications, one can observe lots of process advantages of plastic packings. Since plastic packings are not as bulk as ceramic ones, they provide greater capacity with lower pressure drop. They are used in corrosive

application with low to moderate operating temperature. If the temperature allows, plastic packings are better choice than ceramic or metal ones because they are less expensive [36].

- **Metal Packing**

Metal packing improves separation efficiency. The other advantages are high capacity, low pressure drop, cold and heat resistance and longevity [36]. Therefore, metal packings are preferable in refinery fractionators, distillation towers, absorption and stripping applications where high capacity and numerous stages are required.

1.3.3.4. Hydraulic Design Inside the Column

There are some criteria that should be satisfied in designing contacting stages inside the column [37,38]:

- A favorable vapor-liquid contact.
- A liquid holdup that is sufficient for a favorable mass transfer with a high separation efficiency.
- Flooding, pressure drop and entrainment should be kept within adequate limits.

Stage design procedure is generally performed by a trial-and-error approach which consists of a rough stage layout, control of the key performance factors (section packed height, column diameter, etc.), and revision of the design until a satisfactory design is achieved. Hydraulic calculations on Aspen Plus are post-convergence calculations [38]. Fundamentals of gas absorption including HTU, NTU and HETP calculations are given in Appendix A section of thesis.

1.3.3.4.1. Column Diameter

For both trays and packing, section diameter calculation is based on maximum liquid volume flow rate. For packed type columns, diameter calculation is based on an 80% flooding limit approach to maximum capacity [38]. Generally, small diameters are chosen for design. Also, column diameter determination is related to the pressure drop analysis across the packed bed.

1.3.3.4.2. Entrainment, Flooding and Weeping

Vapor flow rate can cause entrainment and flooding if too high and weeping if too low [39]. In Figure 1.18. one can observe, under what conditions entrainment, flooding or

weeping occur in column. In the case of low vapor flow rate, weeping occurs and liquid flows through the stages without a sufficient contact between gas and liquid. In case of high vapor flow rate, flooding will likely to occur and liquid come leave the column without flowing down inside the column, again hindering mass transfer between gas and liquid. That is, high gas velocity can reduce stage efficiency because of the fact that contact time between the phases is reduced. The optimal vapor flow rate is somewhere in between the cases of flooding and weeping. In packed columns, vapor velocity is generally limited to 80% of flooding velocity.

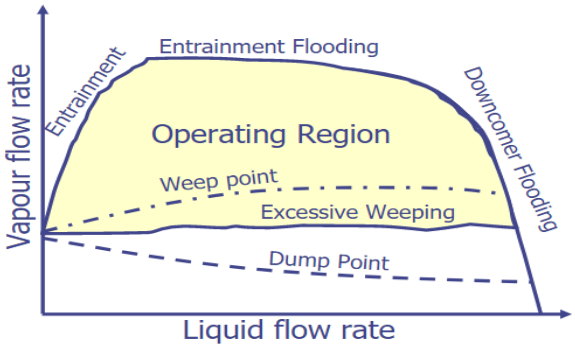

Figure 1.18 Vapor flow rate versus liquid flow rate inside the column [40]

1.3.3.4.3. Pressure Drop

The pressure drop over the stages is an essential design consideration. There are two main reasons behind the pressure loss which are flow of vapor through the packing and the static head of liquid on the stages. So, in design and simulation of packed columns, pressure drop should be taken into consideration. For packed columns, Aspen-Wallis correlation is used as default to represent the pressure drop of a designed separation column in Aspen Plus [38]. It is a homogenous model which is based on a differential volume control. Also, determination of column diameter is related to the pressure drop analysis across the packed bed.

1.4. General Amine Chemistry

1.4.1. Solvents

Aqueous solutions of alkanolamines and sterically hindered amines have been widely employed as solvents in gas treating processes for the removal of the acidic

components, such as CO_2 and H_2S. The alkanolamines are characterized by the existence of the hydroxyl group (-OH) and the amino group ($-NH_2$). They are organic derivatives of ammonia. The presence of the (-OH) group decreases the amine vapor pressure and increases its solubility in water, while the ($-NH_2$) group provides the required reactivity with acid gases to lead the absorption of them [41].

As shown in Figure 1.19, alkanolamines are categorized as primary, secondary, or tertiary based on the number of carbon atoms directly bonded to the nitrogen atom. Primary amines only have one carbon bonded to the nitrogen and secondary amines have two carbon atoms bonded to the nitrogen whereas tertiary amines have 3 carbon atoms bonded to the nitrogen, as their names imply [42]. Sterically hindered amines represent either a primary amine, when it is attached to a tertiary carbon or a secondary amine, when it is attached to at least one secondary or tertiary carbon [43].

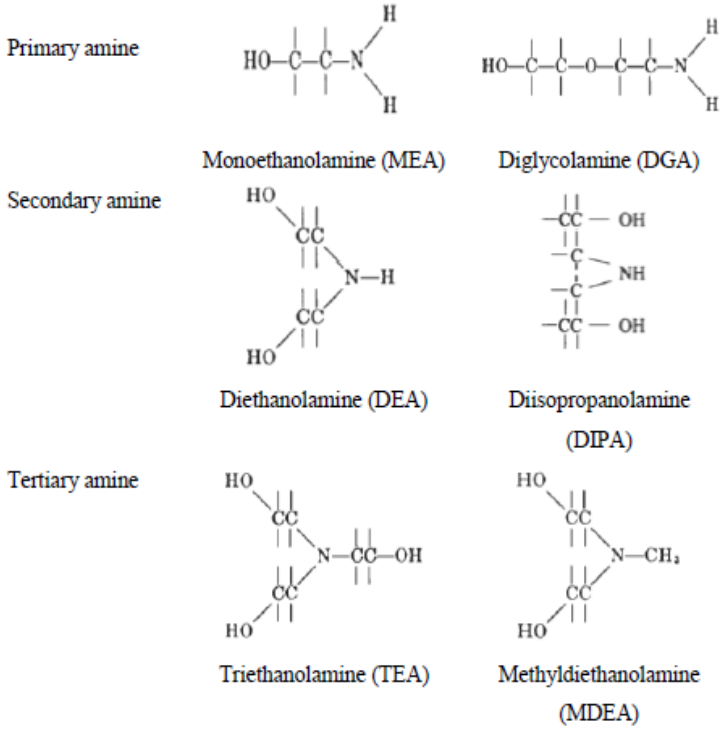

Figure 1.19 Molecular structures of alkanolamine [41]

The amines should have the following properties to be employed in chemical applications [21]:

- High capacity of CO_2.
- High rate of absorption.

- Low vapor pressure.
- Low viscosity.
- Inexpensive.
- Non-corrosive.
- No degradation at operating conditions.
- Non-toxic.
- Non-hazardous.

The industrial standard for amine-based CO_2 capture is 30 wt% monoethanolamine (MEA) for years in amine scrubbing processes, as mentioned before [20]. As an alternative for monoethanolamine (MEA), piperazine (PZ) is studied in this thesis. The reason behind this is that aqueous piperazine has been displayed as a new promising solvent for post-combustion capture technology [44].

1.4.2. MEA-CO_2-H_2O and PZ-CO_2-H_2O Equilibrium Systems

The logic behind the ionic reactions and vapor-liquid equilibrium in single solute systems are explained in this section. As shown in Figure 1.20, the weak electrolyte distributes itself in water between the vapor and liquid phases at a certain temperature and pressure (To be thorough, there is actually no "electrolyte" with ionic groups present in the vapor phase. We use the term "electrolyte" for the species in the vapor phase to indicate that it is the same species from which the electrolyte presented in the liquid phase).

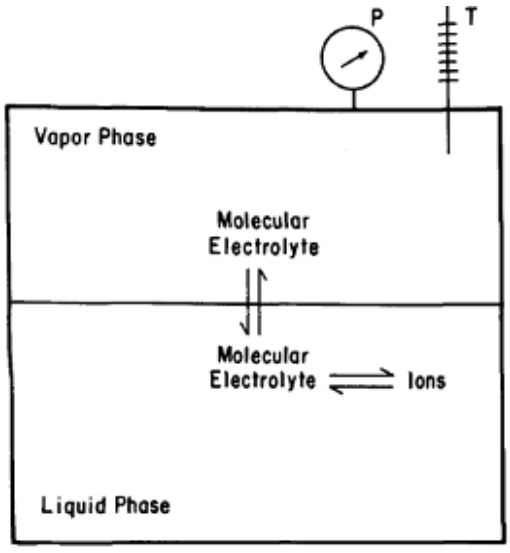

Figure 1.20 Vapor-liquid equilibrium in a single-solute system [45]

At very low concentrations, phase equilibrium between gas and liquid is primarily determined by Henry's Constant and the molality of the solute (vertical phase equilibrium). Molality of ionic solute in the liquid phase, in turn, is highly influenced by the chemical dissociation equilibrium, characterized by a dissociation constant (horizontal phase equilibrium) [45].

The complex mechanism of CO_2 absorption of MEA is shown in Figure 1.21. As can be seen, each MEA molecule can form adducts with 1 CO_2 molecule. The mechanism consists of the zwitterion formation mechanism in (a), the single step mechanism in (b) and the carbamic acid reaction mechanism in (c) [46]. CO_2 approaches MEA in order to form a zwitterionic adduct of MEA^+COO^- which is an intermediate used for the formation of carbamate [47].

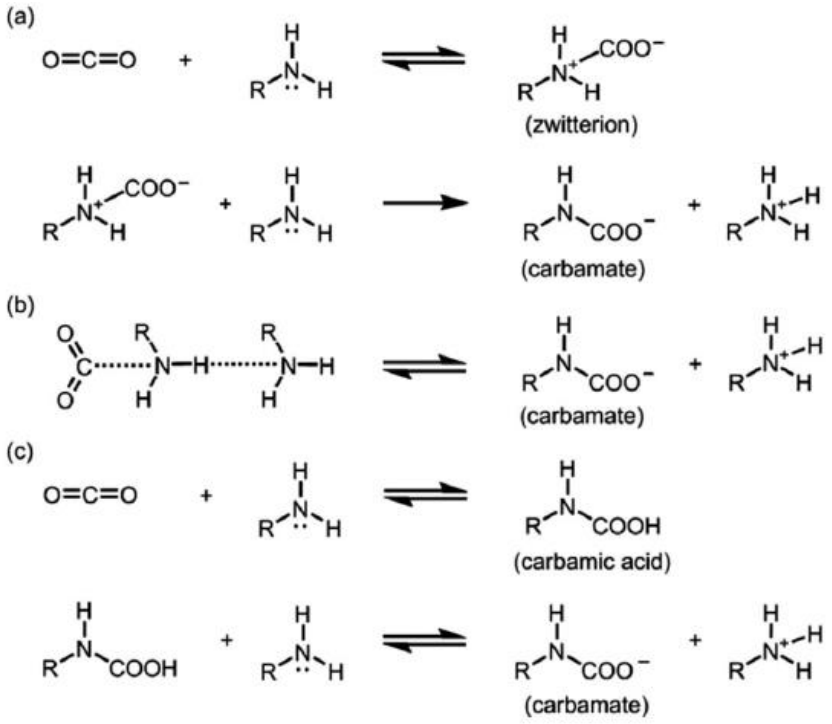

Figure 1.21 Complex reaction mechanism of MEA/CO_2 [46]

As mentioned above, MEA has been benchmark solvent for amine scrubbing. The chemical absorption of CO_2 in aqueous solutions of MEA can be expressed by considering the following species: water, neutral MEA, carbon dioxide (CO_2), the ionic species hydronium cation (H_3O^+), hydroxide ion (OH^-), bicarbonate anion (HCO_3^-), carbonate anion (CO_3^{-2}), protonated MEA ($MEAH^+$) and MEA carbamate ($MEACOO^-$). The set of MEA reactions in water in presence of CO_2 are listed as [48,49,58,50–57]:

$$2H_2O \leftrightarrow H_3O^+ + OH^- \quad (1)$$

$$CO_2 + 2H_2O \leftrightarrow HCO_3^- + H_3O^+ \quad (2)$$

$$H_2O + HCO_3^- \leftrightarrow CO_3^{-2} + H_3O^+ \quad (3)$$

$$MEAH^+ + H_2O \leftrightarrow MEA + H_3O^+ \quad (4)$$

$$MEACOO^- + H_2O \leftrightarrow MEA + HCO_3^- \quad (5)$$

The CO_2 binding mechanism of PZ is shown in Figure 1.22. As can be seen, each PZ molecule can form adducts with 2 CO_2 molecules. Since protonated piperazine might not directly react with CO_2, its protonation is unlikely to happen and indicated by X [59].

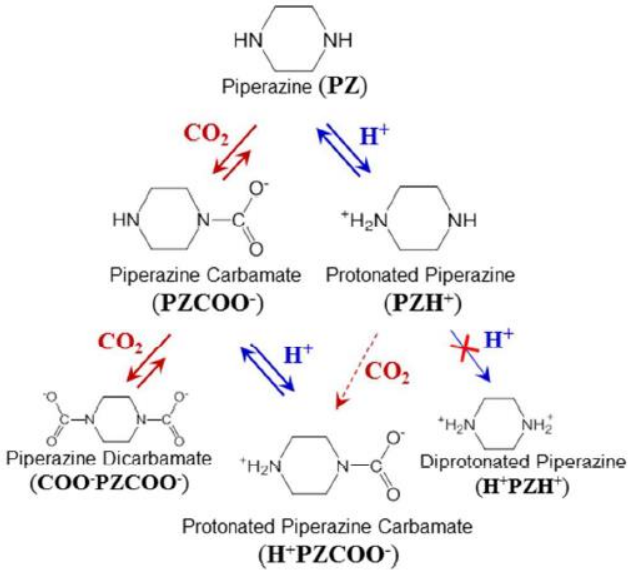

Figure 1.22 Reaction mechanism for absorption of CO_2 into aqueous PZ solution [59]

Promising solvent piperazine (PZ) reacts two times with the absorbed CO_2 and it produces anions and cations in the liquid phase apart from the ones produced by the dissociation of water. In order to thermodynamically describe the process, chemical equilibrium reactions should be considered when dealing with amine scrubbing systems. The chemical absorption of CO_2 in aqueous solutions of PZ can be explained by considering the following species: water, neutral PZ, carbon dioxide (CO_2), the ionic species hydronium cation (H_3O^+), hydroxide ion (OH^-), bicarbonate anion (HCO_3^-), carbonate anion (CO_3^{-2}), protonated PZ (PZH^+), PZ carbamate ($PZCOO^-$), PZ dicarbamate ($PZ(COO^-)_2$) and protonated PZ carbamate ($HPZCOO$). The set of piperazine reactions are [1,54,68–71,60–67]:

$$2H_2O \leftrightarrow H_3O^+ + OH^- \quad (1)$$

$$CO_2 + 2H_2O \leftrightarrow HCO_3^- + H_3O^+ \quad (2)$$

$$H_2O + HCO_3^- \leftrightarrow CO_3^{-2} + H_3O^+ \quad (3)$$

$$PZH^+ + H_2O \leftrightarrow PZ + H_3O^+ \quad (4)$$

$$PZ + CO_2 + H_2O \leftrightarrow PZCOO^- + H_3O^+ \quad (5)$$

$$HPZCOO + H_2O \leftrightarrow PZCOO^- + H_3O^+ \quad (6)$$

$$PZCOO^- + CO_2 + H_2O \leftrightarrow PZ(COO^-)_2 + H_3O^+ \quad (7)$$

The system comprises of solvent species of PZ and H_2O, molecular acid gas species and the ions, that are not considered by vapor-liquid equilibrium (VLE), as illustrated in Figure 1.21. Details of solution chemistry is expressed in Appendix D. section of thesis.

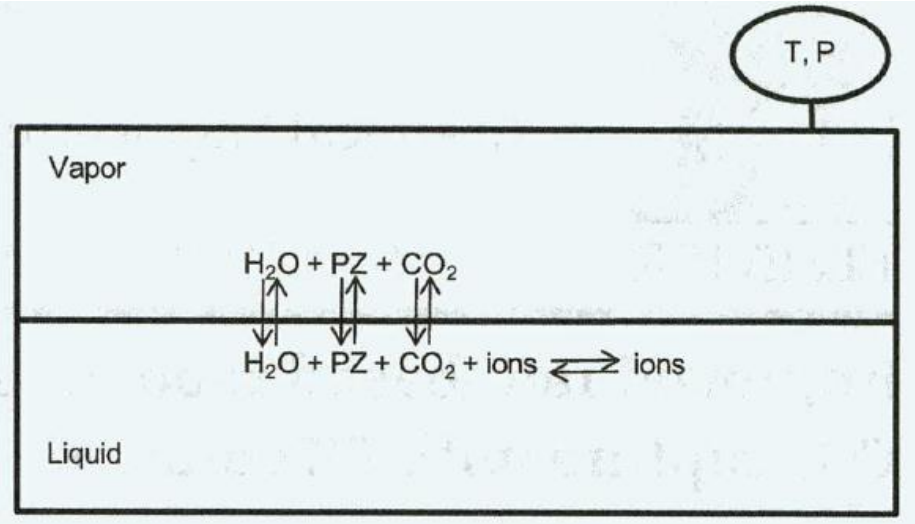

Figure 1.23 Vapor-liquid equilibrium (VLE) in a closed system in the existence of aqueous piperazine solution and acid gases [61]

System is highly non-ideal due to the existence of ions in liquid phase. The values of kinetic parameters related to species ought to be chosen carefully from literature under normal circumstances. Nevertheless, default parameters in Aspen Plus have been implemented in this study. To model the system, the chemical equilibrium constants are calculated by Aspen Plus considering the following Equation 3 (T in K and A, B, C, and D are species-specific constants) [61]:

$$lnK_j = A_j + \frac{B_j}{T} + C_j lnT + D_j T \qquad \text{Eqn. 3}$$

1.5. Aspen Plus as a Simulation Tool

This section of introduction is divided into four parts which are "Component Handling", "Electrolyte Equation of State (EOS)", "Reaction Handling" and "The Aspen Plus® RadFrac Model". In process engineering, Aspen Plus® software by Aspen Technology is one of the most utilized process modeling and simulation tool. It is suitable to use both at an industrial and academic level [72].

Aspen Plus provides the ability to model a wide spectrum of processes, from separation columns to various reactors (CSTR, PFR, Batch) and also contains all of the auxiliary equipment typically used in a chemical plant, such as heaters, coolers, heat exchangers, mixers, valves, pumps, compressors and pipelines.

Aspen Plus has an extremely large set of physical properties in its database. Components' properties are retrieved from different databases like NIST and DECHEMA. As mentioned above, the post-combustion CO_2 capture by aqueous amine solutions requires a reactive absorption-stripping process. These processes are typically modeled by using RadFrac™ model of Aspen Plus® software. Under "The Aspen Plus RadFrac™ Model" section, the model is expressed in terms of [72]:

- Mode of equilibrium stages
- Rate-based mode
- Film modeling-Resistances-Film Discretization
- Fluid dynamics

All items in the list support and complete each other. It is not mathematically required to write the model equations in Aspen Plus®. In fact, each block includes the mass and energy balances which are responsible for characterizing each unit operation. As a rule, an Aspen Plus® simulation is built in two separate environments:

1. Properties
2. Simulation

First step is the definition of components and then, the proper methods are selected for the assessment of thermodynamic properties in the "Properties" environment. In the

"Simulation" environment, the streams, the equipment, and the major parameters of the model are representatively placed in a flowsheet. Equipment and all the streams are chosen from model palette.

1.5.1. Component Handling

All the ionic reactions are handled by Aspen Plus. Under normal circumstances, related databanks from Aspen Plus database are selected and then pure components and their specifications are retrieved. However, in default examples, there is no need to do so. True components including all ions are already given at Components-Specifications table.

1.5.2. Electrolyte Equation of State

As soon as the components are defined, proper equation of state is specified to evaluate the thermodynamic properties. A model must be chosen because of the strong non-ideal character of the liquid phase due to the presence of ions. There are two main equation of state in Aspen Plus that can handle electrolyte chemistry: ELEC-NRTL and ENRTL-RK. Most of the studies in the literature was found to use ELEC-NRTL as the equation of state of choice because of its higher accuracy in experimental validation [56,73–78]. For this purpose, the ELEC-NRTL model was used in this study. After the desired thermodynamic model is introduced, Aspen Plus® retrieves the rest of the parameters by default from the database which means Aspen Plus is ready to jump into the simulation environment.

1.5.3. Reaction Handling

Due to the reactive nature of CO_2 capture process, the set of reactions need to be specified under the tab of "Chemistry-Reactions". The reactions regarding MEA or PZ should be specified for reaction handling. In numerous works published on post-combustion CO_2 capture, reactions are involved. Both MEA and PZ related reactions are accessible from Aspen Plus database after defining components on electrolyte wizard. Five main equilibrium reactions occur with MEA and seven main equilibrium reactions occur with PZ solvent. These equilibrium reactions are shown in Figure 1.22 and Figure 1.23.

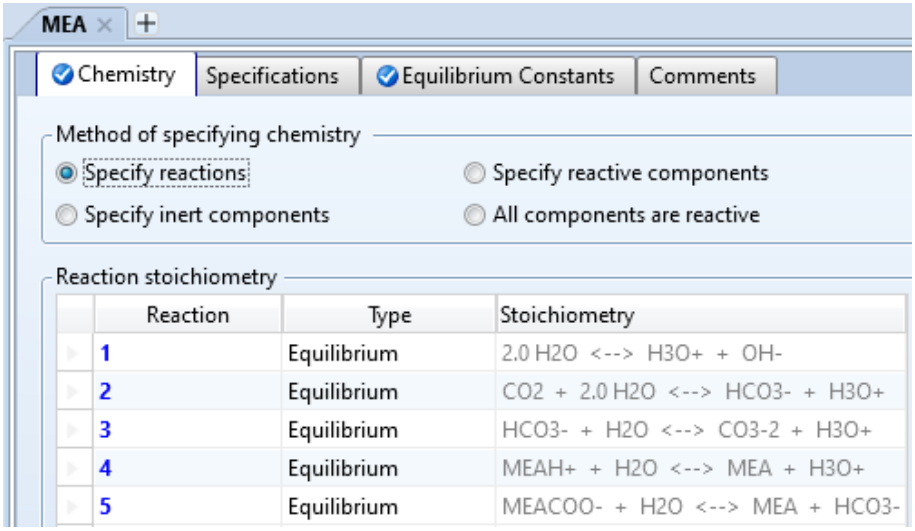

Figure 1.24 Equilibrium reactions of MEA-CO_2-H_2O system in Aspen Plus

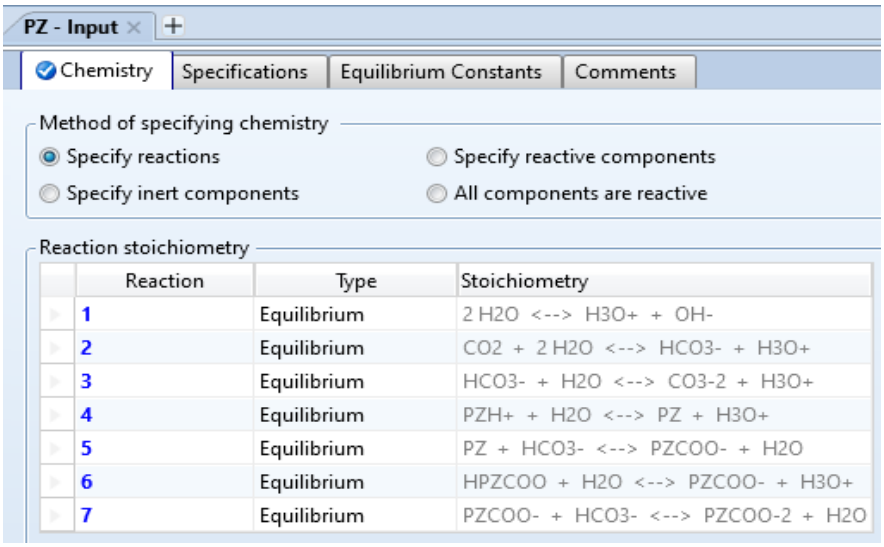

Figure 1.25 Equilibrium reactions of PZ-CO_2-H_2O system in Aspen Plus

Aspen Plus Software presents two methods for the calculation of equilibrium constants as a function of absolute temperature T:

- **Standard Gibbs free-energy change:** The following rigorous equation is used to find the equilibrium constant (Equation. 4):

$$K_{eq} = exp\left(\frac{-\Delta G^0}{RT}\right) \qquad \text{Eqn. 4}$$

where the ΔG^0 values are retrieved from the database of Aspen Plus.

- **Parameter-based correlation:** The following equation is used to find the equilibrium constant (Equation. 5):

$$ln\left(K_{eq}\right) = A + \frac{B}{T} + Cln(T) + DT \quad \text{Eqn. 5}$$

where the A, B, C and D coefficients can be retrieved from several articles.

Since parameter-based and standard methods matched each other so closely, Aspen Properties® database is used to find equilibrium constant. The expression built in Aspen Plus® for kinetic reactions is the power law. Kinetic constants calculated by the Arrhenius equation are given in Equation. 6:

$$k = k^0\left(-\frac{E_a}{RT}\right) \quad \text{Eqn. 6}$$

Particularly, the kinetic parameters concerning MEA were taken from Errico et al (2016) and Pinsent et al (1956) [79,80]. While for PZ, parameters are taken from Pinsent et al (1956), Bishnoi and Rochelle (2002) and Samanta and Bandyopadhyay (2009) [68,81].

1.5.4. The Aspen Plus® RadFrac™ Model

In order to model absorption and stripping columns, RadFrac™ blocks are chosen from the model palette because reactions occur inside the columns. Without axial dispersion, reactive absorption and stripping columns are typically modeled as ideal plug-flow from fluid dynamics point of view. Particularly, the RadFrac™ model usage is based on the plug-flow estimation as a series of CSTRs. For modeling such columns, one requirement is to verify if the column behavior is similar to that of an ideal plug-flow. In the RadFrac™ model, two different approaches can be used to model multistage separation equipment: the rate-based mode and the equilibrium stages mode. In both modes, the column height is discretized into certain stages or segments. Calculation type of the RadFrac™ columns is generally chosen as rate-based (non-equilibrium) in the literature because mass transfer rate limitations are taken into consideration in this model [72].

1.5.4.1. Equilibrium Stages Mode

In cases where the thermodynamic equilibrium is established quickly between liquid and vapor phases, the streams leaving each stage could be treated in equilibrium mode. When the equilibrium mode is used, one can achieve the maximum efficiency by implementing a single theoretical stage. However, the effect of column parameters, such as type of packing and packed bed amount, cannot be calculated in the equilibrium mode.

Apart from that, some processes do not reach the equilibrium quickly and mass transfer rates should be considered. In these cases, activation of the rate-based model becomes necessary [82].

1.5.4.2. Rate-based Mode

Most CO_2 capture processes are away from the phase equilibrium condition because of mass transfer limitations. Thus, for modeling reactive absorption and stripping of CO_2 with MEA or PZ, the most widely used approach is the rate-based one [72,73,83].

Based on the film theory by Lewis and Whitman [28], rate-based mode takes the limitations regarding mass transfer into account. Rate-based approach can be used to describe the processes taking place in both the absorber and the stripper in detail. Thanks to RadFrac™ unit operation model, both tray and packed columns can be modeled via rate-based mode [82].

A schematic representation of the rate-based simulation based on mass transfer calculations for CO_2 absorption is given in Figure 1.24. Both the liquid and gas phases are divided into distinct regions, separated by an interface. These are named bulk region and film region. The material and the energy balances are different for each region. Ideal CSTR balance equations are used for the bulk zone [84]. While; for the interphase transfer, material and the energy transport, the rigorous Maxwell-Stefan approach is used [85].

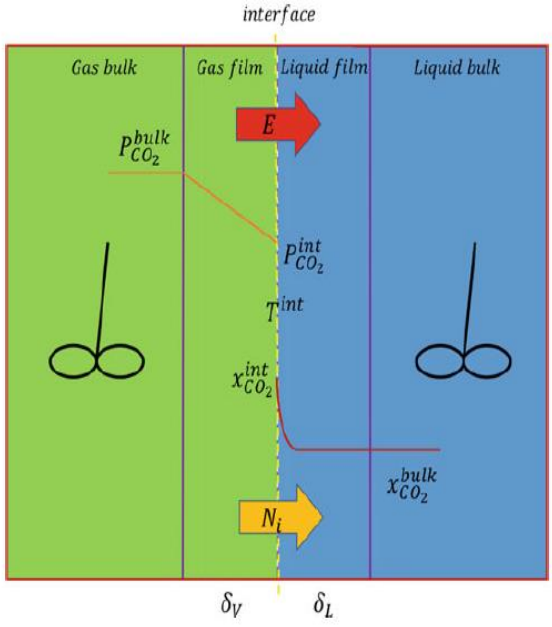

Figure 1.26 Schematic representation of mass transfer by the absorption [72]

In order to describe the two regions; rate-based mode, options and different parameters must be set-up. The selection of rate-based approach on Aspen Plus during absorber design is shown in Figure 1.25.

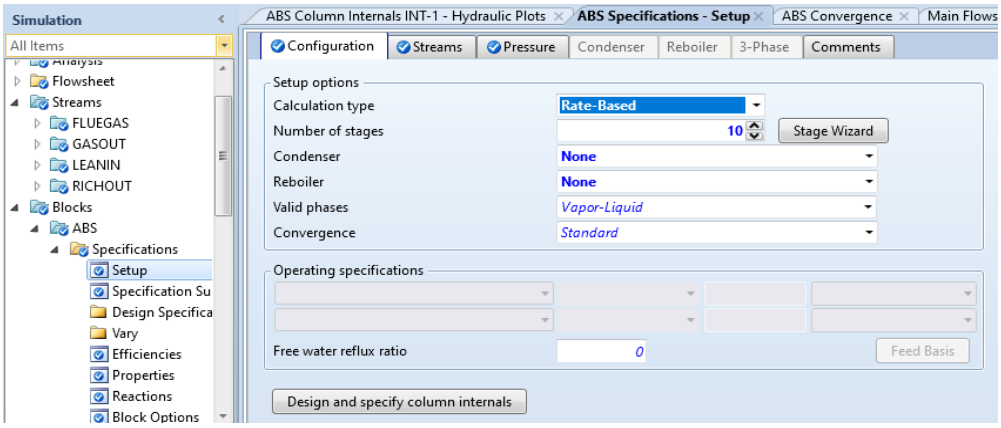

Figure 1.27 Selection of rate-based approach in Aspen Plus during absorber design

1.5.4.3. Film Modeling-Resistances-Liquid Film Discretization

In Figure 1.24, the profiles observed in these two films are dependent on the CO_2 mole fraction in the absorber. Since there are no reactions in the gas phase, a linear profile is observed in the gas phase. After solvent (liquid) absorbs carbon-dioxide, it readily reacts with MEA/PZ. Because of that, a highly non-linear profile is observed in the liquid film.

To effectively express the different behaviors of the two films, there are various options available in the rate-based mode to justify the specific resistances of each phase [72]. Liquid film must be discretized due to fast reactions. Since no reaction occurs in gaseous phase, the resistance to diffusion of materials is the only item considered. Specifically, “Consider Film” option is used for the gaseous phase and “Discretize Film” option is used for the liquid phase. Discretization points for liquid film is generally set as 5 and in the literature [65].

1.5.4.4. Analysis of the Fluid Dynamics

In the absence of axial dispersion, absorption and stripping columns are typically modeled as ideal plug-flow in terms of fluid dynamics. Particularly, the RadFrac™ model is based on the plug-flow estimation as a series of CSTRs. The backmixing and the axial

diffusion/dispersion due to counter-current flow are the two processes that can cause deviation of fluid dynamics behavior of columns from the ideal one [72,86–90].

While analyzing fluid dynamics in simulation environment, simulation is run and converged first. Hydraulic plots are checked to see if there is flooding or weeping inside the column. Improvements can be made on column to get better results in terms of fluid dynamics. A sample hydraulic plot of a stripper column is shown in Figure 1.28.

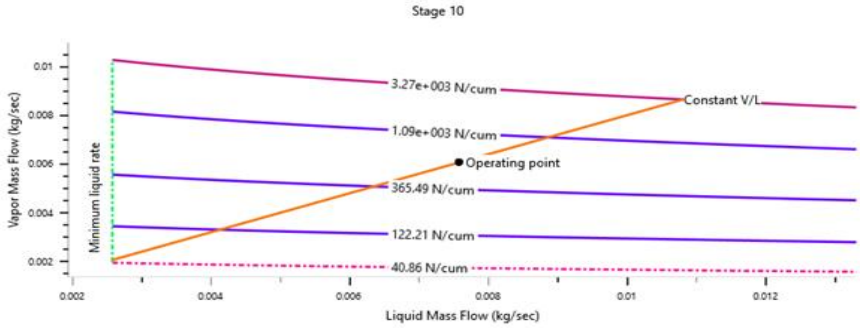

Figure 1.28 A sample hydraulic plot of a stripper column in Aspen Plus

1.6. Aim of This Thesis

The aim of this thesis is to design a laboratory scale CO_2 capture system. In order to design these systems effectively and efficiently on an industrial scale, an actively working laboratory-scale process is essential. Therefore, a carbon-dioxide capture system is designed and simulated by utilizing packed columns and taking advantage of chemical absorption in Aspen Plus environment for a laboratory scale CO_2 capture process. Commonly used MEA (monoethanolamine) and PZ (piperazine) are mainly compared in terms of their capture rate, absorption efficiencies and energy efficiencies.

1.7. Outline of This Thesis

This thesis study is composed of five chapters which are organized as follows. In chapter 1, titled “Introduction”, background on global warming, greenhouse gases, CO_2 levels in the atmosphere, brief overview of CO_2 capture systems, aqueous amine absorption/stripping, selection of column, general amine chemistry, Aspen Plus as a simulation and objectives of the thesis are presented. Chapter 2, titled “Literature Survey”, presents what has been done on literature so far. Chapter 3, titled “Materials and Methods” presents the basic simulation details, simulation environment and different

process flowsheet configurations. Chapter 4, titled “Results and Discussion” presents all the obtained simulation results including absorber design, open loop design and closed loop design. Conclusion and recommendations are provided in chapter 5.

CHAPTER 2

LITERATURE SURVEY

2.1. Literature Survey Criteria

There are several experimental and theoretical studies carried out on CO_2 capture in the literature. Major review articles discussing these studies are published by Leung et al. (2014) , Boot-Handford et al. (2014), Yang et al. (2008), Mikkelsen et al. (2009), and MacDowell et al. (2010) [16,22,91–93]. There is a vast literature regarding CO_2 processes, and in order to carry out this thesis study in a focused manner, a set of criteria has been established to narrow down the literature survey. In this chapter, only the articles that meet all of the following criteria are discussed:

- Aspen Plus simulation is present.
- Laboratory scale experiments are done.
- Chemical absorption solvents, such as amines, are used.
- Packed columns are used.

After the articles are collected from the literature, the articles were then classified based on the type of solvent. In the next sections, studies on MEA, PZ, NH_3 and the other chemical absorption solvents are examined.

2.2. Literature Studies on CO_2 Capture Carried out Using Chemical Absorption in Laboratory Scale Packed Bed Columns and Simulated with Aspen Plus

The solvents used in the collected articles are MEA, PZ, NH_3 and NH_3/PZ blend, respectively. In the sections below, studies regarding each type of the solvent is examined in detail.

2.2.1. CO_2 Capture Studies Using MEA

In the first study, Plaza, Wagener and Rochelle at the University of Texas at Austin studied modeling of CO_2 capture with aqueous MEA solutions. A new model was proposed using a pilot plant run with 35 wt% of MEA which is equal to 9 m [73].

In the pilot plant experiments, there was an inlet gas with a molar flow rate of 34572 (mol/hr) at 25.1 °C. CO_2 mole fraction of flue gas is 0.119. The lean feed stream at 39.9 °C which was sent into absorber from top of the column while the inlet gas stream was sent into the column from the bottom. Rich loading of lean stream was 0.48 (mol CO_2/mol MEA). CO_2 removal ratio via absorption was found as 60%.

Process flow diagram of the pilot plant is given in Figure 2.1. Packed type absorber column with a height of 6.10 m and a diameter of 0.43 m was used in the pilot plant. For the packing of absorber, Flexipac 1Y was chosen as the packing material and 12 equal stages were used in the column. Specifications of the stripper column were the same with the absorber column. This study utilized pilot plant data and proposed a model using Aspen Plus [73].

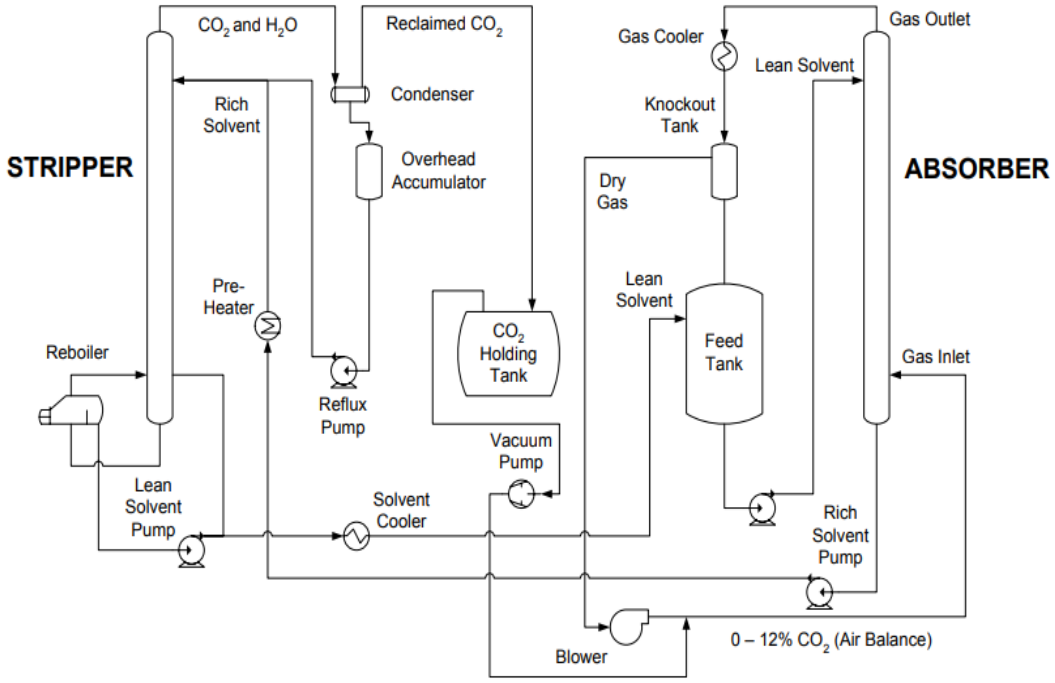

Figure 2.1 Process flow diagram of pilot plant [94]

Aspen Plus simulations assumed that equilibrium reactions take place in the stripper. The thermodynamic model of ELEC-NRTL was used. The reactions on the MEA-CO_2-H_2O system were handled by using different studies on literature such as Aboudheir et al (2002), Hilliard et al (2008) and Rochelle et al (2001) [70,95,96]. The RadFrac block was chosen because there were reactions taking place inside the columns. Both absorption and stripping units were run at rate-based mode. There were no hydrodynamic

studies of these columns throughout the article. To model stripper column, a 3-stage flash was configured on flowsheet. A counter-current heat exchanger was used to preheat the rich stream before entering into stripper column. Higher stripping temperatures yielded the higher selectivity of CO_2. Additionally, the performance of stripping unit was tried to be enhanced via case studies and optimizations [73].

In the study of Nakagaki and co-workers, experimental evaluation of concentration and temperature effects on heat of dissociation of CO_2 loaded 30 wt% MEA solution in strippers was carried out [74]. A small-scale apparatus consisting of an absorption column and a stripping unit were used in the experiments. Capture and recovery of CO_2 was performed using these columns. Schematic of the experimental apparatus is given in Figure 2.2.

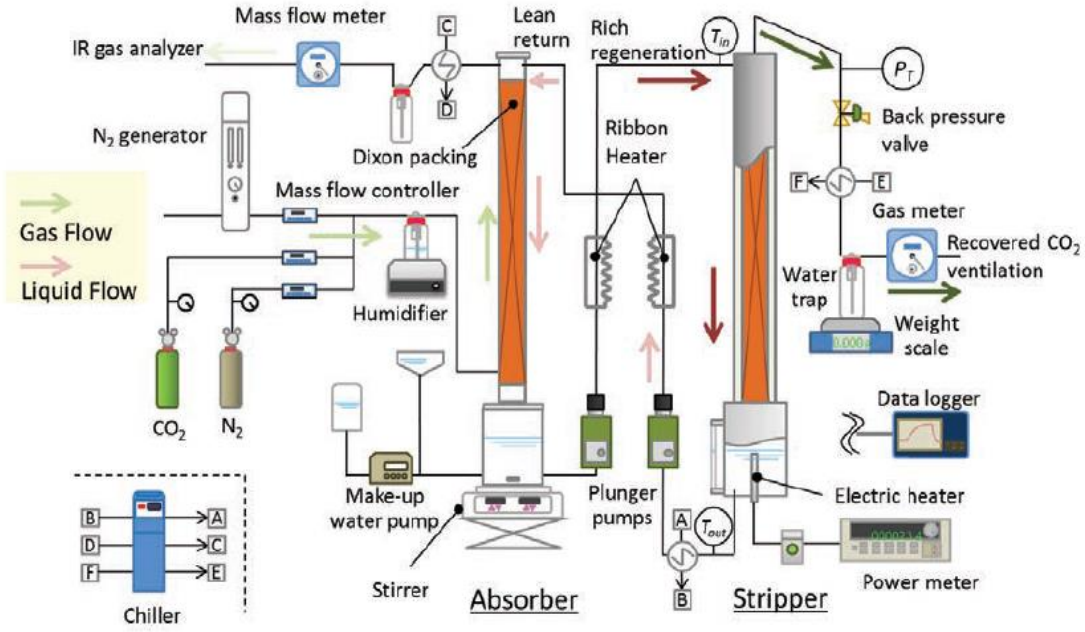

Figure 2.2 Schematic of experimental apparatus from [74]

A cylindrical tube with 30 mm inner diameter and with the Dixon type packing material was designed as an absorber column. The stripper column was found to recover 10 kg/day of CO_2. Inlet gas was a mixture of CO_2 at 0.15 bar partial pressure in N_2. Inlet gas stream went into column from the bottom while the lean solution went into the absorber from top of the column with a stable L/G ratio of 4.0 or 6.0 L/m^3. A cylindrical chamber thermally insulated by vacuum insulation with 29.4 mm inner diameter was designed to be stripper column. A lean solution loaded with carbon dioxide was pumped into the stripping unit at a constant temperature and flow rate. The regenerated solution

was taken from the bottom, and a mixture of CO_2, steam and negligible amount of amine vapor were taken from top of the column. The temperature of absorber column was set as 40 °C. The amine solution had the same temperature value as the absorption unit. Lean and rich loading of amine solution were 0.108 and 0.467 mol CO_2/mol amine, respectively. Heater was designed to heat the inlet stream to the stripper up to 80 °C with no pressure change.

Aspen Plus offers default examples which are embedded into its graphical user interface. For the simulation in the study, the flowsheet shown in Figure 2.3 is used along with MEA-CO_2-H_2O equilibrium system from Aspen Plus' database. In order to simulate inlet gas, 15% CO_2 concentration in N_2 is selected. As a benchmark solvent, 30 wt% MEA solution was preferred to remove acid gases.

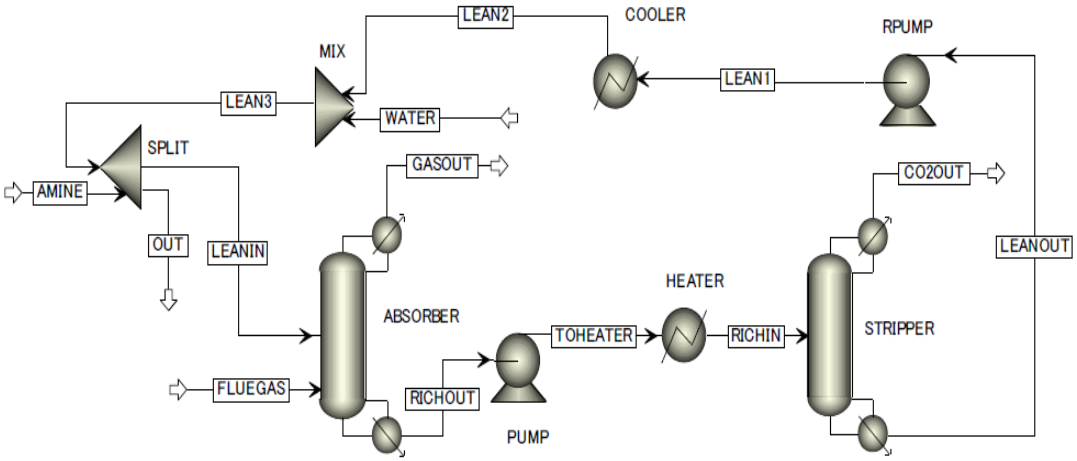

Figure 2.3 PFD of small scale apparatus built on Aspen Plus [74]

Rate-based mode and RadFrac columns were employed for this CO_2 capture system. The ELEC-NRTL equation of state was chosen for liquid and ENRTL-RK EOS was chosen for vapor in the simulation. Packed type absorber and stripper columns were used at the heights of 1.5 and 1.1 m, and diameters of 0.04 and 0.03 m, respectively. Flow of gas and liquid occurs counter-currently inside the columns. Dixon packing with a 3 mm diameter was used as a packing material. There were not any hydrodynamic studies of these columns inside the article. Simulation results were compared with the experimental ones. By changing some thermodynamic parameters, modifications were done on the results of lean and rich loadings of CO_2 and improvements have been seen [74].

In the study of Thiels and co-workers, CO_2 absorption by using 30 wt% MEA solution in rotating packed bed (RPB) absorber and packed bed (PB) absorption column was modeled and designed [78]. Experiments with packed bed column and rotating packed bed absorbers were performed at different loadings of lean carbon dioxide in MEA solution and the results were compared. They were then modeled and simulated by the Aspen Advanced Custom Modeler (ACM). The validated model with Aspen Plus was then utilized to design an improved absorber for further absorption/stripping processes.

Experiments with the packed setups were performed at different design specifications. All specifications of feed streams are summarized in the Table 2.1 below.

Table 2.1 Operating conditions of feed streams [78]

Set-up	**Packed Column**	**RPB**
Inlet temperature (°C)	25 (Gas); 50 (Liquid)	-
Gas flow (L/min)	5	5-60
Inlet gas CO_2 fraction (mol%)	10	10
Liquid flow (L/min)	0.1	0.1
Liquid MEA fraction (mol%)	11.2	11.2
MEA concentration (wt%)	30	3.37482
Lean loading of CO_2 (mol CO_2/mol amine)	0.365-0.444	0.0; 0.157; 0.249; 0.380; 0.442

Rotating packed bed was studied experimentally by changing its lean loadings as given in the table above. Also, outlet CO_2 concentrations data were obtained to see absorption efficiency. Main specifications related to column size and packing are given in the Table 2.2.

Table 2.2 Specifications of experimental absorption units (PB and RPB) [78]

Set-up	**Packed Column**	**RPB**
Packing Type	Plastic 6 mm Raschig rings	Stainless wire mesh
Diameter (m)	0.025	0.125-Outer Diameter; 0.025 Inner Diameter
Packing Height (m)	0.6	0.023

A simulation environment on Aspen ACM was created for RPB absorbers because rotating one was found to remove more CO_2 out of the inlet gas than packed column. The equilibrium constants of liquid phase equilibrium reactions were taken from Rochelle et al. (1989) and the kinetic data were taken from Aboudheir et al. (2003) [97,98]. Under all process conditions, there were good agreements between simulated and experimental CO_2 removal.

Columns were simulated using rate-based mode. The RadFrac block was chosen because reactions take place inside the columns. All the simulations were performed by using random packings. Sulzer 125Y packing was used for packed column and stainless wire mesh packing at (700 rpm; 1000 rpm; 1600 rpm rotor speeds) was used for RPB [78]. Flue gas specifications used on Aspen Plus simulations is listed in Table 2.3 below. Process flow diagram of experimental or model was not illustrated in the article. Only a different arrangement of columns was shared and visualized [78].

Table 2.3 Simulating conditions of FLUEGAS stream [78]

Mass flow (kg/hr)	240
Inlet temperature (^{0}C)	50
Pressure (atm)	1.24
Composition (vol%)	
N_2	73.1
CO_2	14.8
H_2O	6.8
O_2	5.3

Furthermore, both absorber types were examined hydrodynamically. A 60% flooding limit flooding factor was chosen. To achieve 90% acid gas removal, flooding was taken into consideration and examined in detail in this article by using different rotating speeds. Lean and rich loadings of carbon dioxide and arrangement of columns in simulation environment were the main studied parameters throughout the article [78].

In Kalatjari et al. (2019), simulation, experimental and thermodynamic modeling of a dynamic pilot plant for the capture of CO_2 by using MEA solution at various

temperatures and concentrations was studied [56]. Additionally, four different equations of states were used to thermodynamically model and to simulate the pilot plant data. At the end, experimental results of total energy consumptions for regeneration in the desorber column were compared with the present models.

Schematized flow diagram of pilot plant is shown in Figure 2.4. A counter-current flow of gas and liquid streams was performed. The lean feed stream (MEA) was sent into the absorber from top of the column while the inlet gas stream was sent into column from the bottom. The solution rich in CO_2 exited from the bottom of absorber column, heated up in a heat exchanger and then fed into the desorber column. CO_2 captured at the top of desorber column was saturated with water. In order to strip off CO_2 from stripping unit, hot vapor was used [56]. CO_2 captured from the top of desorber column was saturated with water. The water vapor was cooled inside the condenser and then removed via condensate separator. The vapor condensed was refluxed to the desorber unit by utilizing a condensate reflux pump.

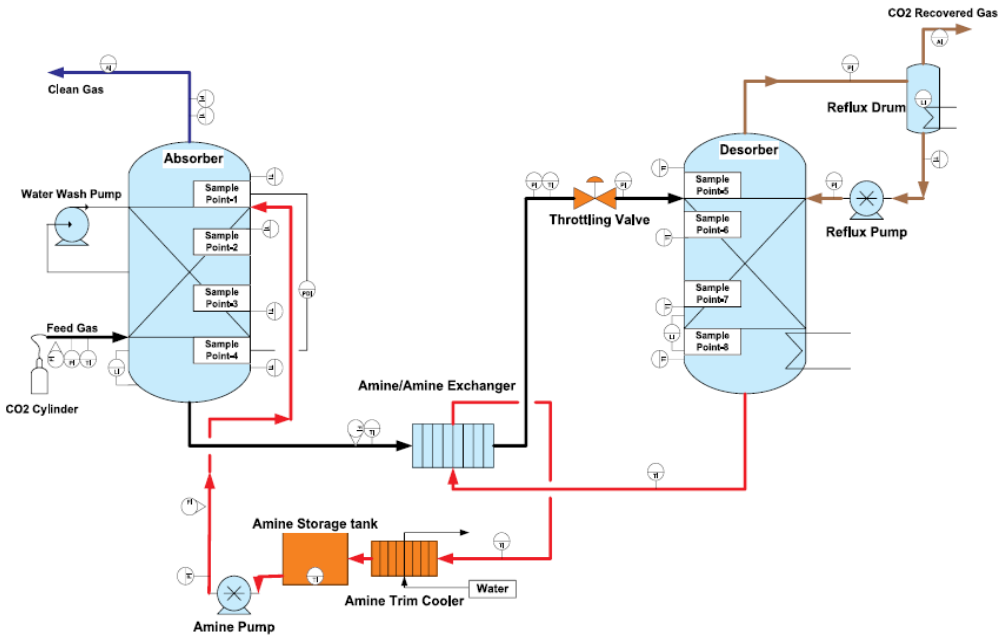

Figure 2.4 Schematized flow diagram of pilot plant [56]

The lean solution coming from the bottom of stripping unit was cooled in a heat exchanger and then it was pumped to the top of absorber, thus, lean solution was recycled. In experimental part of study, there were two different inlet gas compositions (rich CO_2 feed > 99 mol% at 2.1 bar g, 22-30 kg/hr flow rate and lean CO_2 feed approximately 5 mol% at 2.1 bar g, 77-80 kg/hr flow rate).

The experiments were performed at 1.8 bar g at different concentrations of MEA (27, 29 wt% for rich feed of CO_2 and 25, 28, 30, 33 wt% for lean feed of CO_2) within the range of 25 to 80 °C in the absorber and 70 to 120 °C in the stripper. Specifications of these two columns are given in the Table 2.4 below.

The purpose of building simulations was to investigate different parameters such as pressure, temperature, MEA concentration, flow rate of solvent (MEA and the water), the concentration of CO_2 at the outlet of stripper, loadings (rich and lean), partial pressure of CO_2, circulation rate and energy consumption of stripper. Simulations and their inlet specifications were also within the ranges of pilot plant. There were four different methods used for thermodynamic modeling of pilot plant [56]:

1. ELEC-NRTL Bishnoi
2. Default ELEC-NRTL by Aspen Plus
3. Gabriel's Approach
4. ELEC-NRTL Regressed-DRS by Aspen Plus

Table 2.4 Column specifications of pilot plant [56]

Column	**Absorber**	**Stripper**
Packing Type	Structural Flexipac	Structural Flexipac
# of stages	7	7
Diameter (m)	0.25	0.25
Packing Height (m)	1.9	1.9

There were five equilibrium reactions in the system of MEA-CO_2-H_2O and reaction kinetics were taken from Hikita et al., (1977) and Pinsent et al., (1956) [80,99]. In order to treat the non-idealities of gas phase, SRK equation of state-EOS was employed besides the ELEC-NRTL Bishnoi thermodynamic model in the liquid phase [56]. Both absorption and stripping units were simulated in rate-based mode. There were no hydrodynamic studies throughout the article. At the end, among many parameters, loading of gas and regeneration energy were the most important factors in terms of cost and environment. Gabriel's approach gave the better results such as (partial pressure of CO_2, gas loading of CO_2, and compositions). Simulations using Gabriel's approach were the most compatible with the data of pilot plant in terms of overall energy consumption [56].

2.2.2. CO_2 Capture Studies Using PZ

In the study of Plaza and Rochelle in 2011, at the University of Texas at Austin, CO_2 capture results taken from pilot plant were modeled by using aqueous piperazine (PZ) [100]. This pilot plant was built in the University of Texas at Austin and therefore, it helped Plaza, Dugas, Rochelle and their co-workers to publish many articles related to post combustion CO_2 capture by using aqueous amine solvents.

In the pilot plant, the inlet gas was at 25.1 °C. Most of the specifications were same with the Plaza et al. (2009). CO_2 mole fraction of flue gas was around 0.12. Volumetric flow rate of gas was around 0.165 m^3/s. There are 12 runs repeated with different PZ concentrations (5 m to 9 m), solvent flow rate and lean loadings in the pilot plant. The lean feed stream mixture went into the absorber from top of the column while the inlet gas stream with a mixture of air went into column from the bottom. Rich loadings of lean stream were changed between 0.34 and 0.380 (mol CO_2/mol alkalinity) and the lean loadings were changed between 0.257 and 0.331 (mol CO_2/mol alkalinity). The highest CO_2 removal efficiency among 12 runs was found as 85.9% at 7.46 m PZ and 5.5 L/G ratio. Packed type absorber column with a height of 6.10 m and a diameter of 0.427 m was used in this pilot plant. For the packing of absorber, Mellapak 2X was chosen [100].

Aspen Plus reconciliation model was based on the PZ-CO_2-H_2O system and its equilibrium reactions. Lean amine feed consisted of a mixture of PZ, CO_2 and H_2O. To generate the inlet gas conditions carbon dioxide, nitrogen, oxygen and water were mixed. To adjust the experimental data and results to close energy and mass balances and match CO_2 removal, parameter estimation tool of Aspen was used. While designing the wetted wall column on Aspen, rate-based mode was activated. Thus, a RadFrac block was chosen for separation and the reactions were taken into consideration. Thermodynamic properties were taken from Frailie et al. (2010) [101]. Specifications of gas and liquid streams were taken from Dugas's experimental data (2009) which were also used to calculate kinetic constants [23]. 30 stages were used to simulate the packed absorption column. Actually, the performance of the absorption unit was tried to be improved in terms of removal efficiency. L/G ratio, intercooling a heat stream into the middle of column, liquid temperature and loadings were the main parameters in this study [100]. For example, 8 m PZ at 4.2 L/G ratio (mol L/mol G) resulted with 90% removal and for the 4.4 L/G ratio at 8 m PZ (mol L/mol G) resulted with 80% removal. So, determining a specific L/G ratio

was significant. There were no hydrodynamic studies of these columns throughout the article.

In the study of Zhang and co-workers (2017), the pilot plant that consisted of an absorption column used for capturing CO_2 with aqueous PZ was modeled [44]. An advanced flash stripper was built into the pilot plant campaign in the University of Texas at Austin.

Concentration of solvent, lean loading, concentration of CO_2 in inlet gas, flow rate of gas stream, L/G ratio and intercooling configurations were tested in the pilot plant. 5 m of PZ showed better performance due to increased mass transfer rates than 8 m one. Also, it increased the number of transfer units and decreased the heat duty of the stripper column which was seen after performance analysis. Figure 2.5 shows the process flow diagram of the pilot plant. The synthetic flue gas was a mixture of dry air, pure make up stream of CO_2 and the pure CO_2 stream coming from the top of stripper [44].

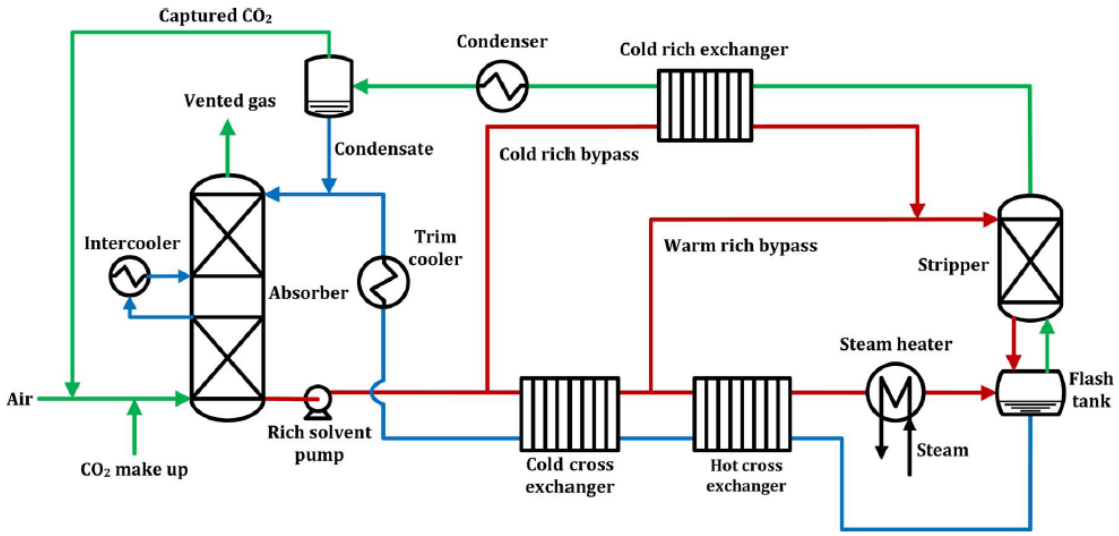

Figure 2.5 Pilot plant of absorber/stripper configuration [44]

Table 2.5 summarizes the characteristics and operating specifications of absorber in the pilot plant campaign. The stripper column had a random Raschig Super-Ring No. 0.3 packing type. The lean stream coming out of stripper was recycled back to the absorber after passing through 2 heat exchangers and a trim cooler [44]. With some developments on intercooling in absorber, removal efficiencies were increased over 90%.

The experimental data was then validated in Aspen Plus by using rate based rigorous absorber model. The ELEC-NRTL equation of state was chosen for this example file. An independent model was built for the PZ-CO_2-H_2O equilibrium system including

enthalpy, Gibbs free energy, heat capacity and activity coefficient type of parameters. Rate expressions were retrieved from wetted wall column experimental data. Rate based mode and RadFrac columns on the basis of reactions occurring inside the columns were activated for this CO_2 capture system. Hydraulic plots of columns were not given in the article.

Table 2.5 Characteristics and operating specifications of absorption column in pilot plant [44]

	Absorber
Packing type	Stainless and Structured Raschig Super-Pak (RSP-250)
Inner diameter (m)	0.43
Packing height (m)	6.10 (2 bed x 3.05)
Solvent (PZ)	
Concentration (*m*)	5, 8
Mass flow rate (kg/hr)	1720-3540
Lean loading (mol CO_2/mol alkalinity)	0.18-0.26
Inlet Gas	
CO_2 (mol%)	6, 12
H_2O (mol%)	1-2
Mass flow rate (kg/hr)	710-1050

Gao et al. (2019) demonstrated 99% CO_2 removal by the scrubbing of amine from the flue gas of coal at the University of Texas at Austin [102]. This post combustion capture campaign was conducted by employing the advanced flash stripper configuration with 5 m piperazine. Molality of PZ was changed between 4.1 and 5.9. 12 m of absorber column was packed and removal efficiency between 90 and 99% was tried to be achieved. Especially, 20% increase in solvent rate had an effect on the jump of CO_2 removal from 90 % to 99%. At the same time, rich loading value declined from 0.40 to 0.38 (mol CO_2/mol alkalinity) which did not practically change the cost of energy for regeneration at high removal. Process flow diagram pilot solvent test unit consisting of an absorber and the configuration of advanced flash stripper is given in Figure 2.6.

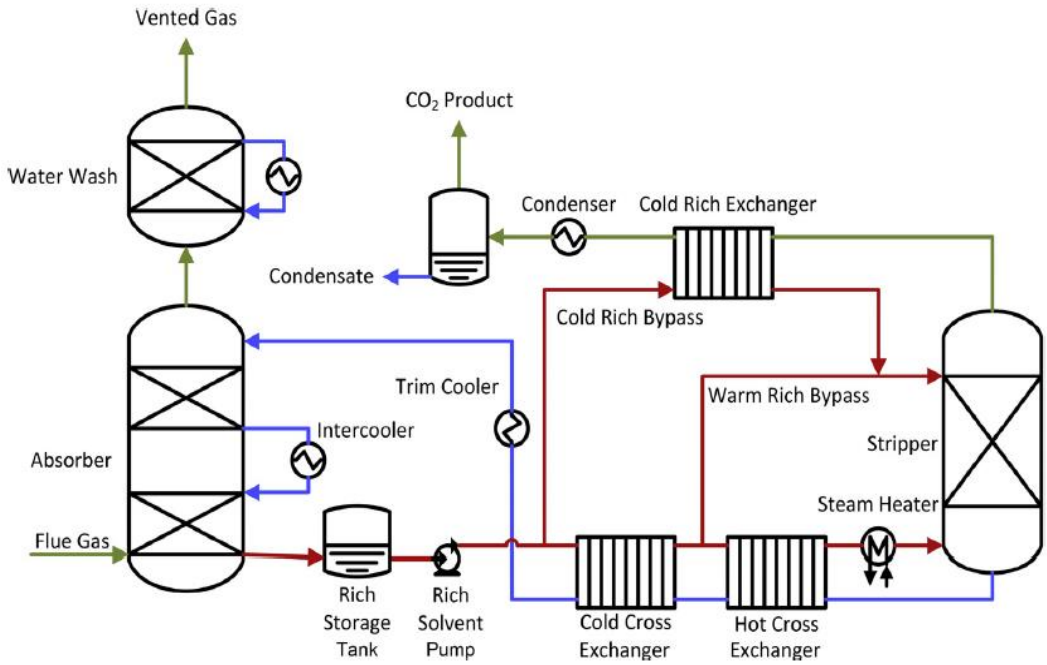

Figure 2.6 Process flow diagram of pilot test unit [102]

This plant focused on post combustion capture just as this thesis study. The flue gas obtained from coal-fired boiler was first cooled to get rid of its moisture and then fed into the bottom of absorption column which had 3 sections of 6 m Sulzer Mellapak 252Y structured type of packing. However, as it is seen in the table only two sections were used. Characteristics of columns in pilot plant are summarized in the Table 2.6 below.

Table 2.6 Column characteristics of pilot plant [102]

Set-up	**Absorber**	**Stripper**
Packing Type	M252Y	RSR #0.5, #0.7
Inner Diameter (m)	0.66	-
Packing Height (m)	2 x 6.10	2 x 2

Lean solvent entered absorption column from the top and contacted with the flue gas. To control its water content and to remove the amine entrained, flue gas depleted in CO_2 was fed into a water wash column before being discharged to the atmosphere [102]. The liquid and the vapor were then separated in the stripper and the lean solvent was recycled back to the absorber. 2 m of stripping unit had RSR #0.5 and the rest 2 m of stripping unit had RSR #0.7 random packings. Throughout the study on this pilot plant, 68 runs were

performed. Operating conditions of absorption and stripping columns are given in the Table 2.7 below.

Table 2.7 Operating conditions of columns in pilot plant [102]

	Absorber	**Stripper**
Gas inlet temperature (^{0}C)	36.6-62.1	-
Solvent inlet temperature (^{0}C)	31.75-49.75	-
Inlet gas CO_2 fraction (mol % dry)	10.6-12.3	-
Mass flow rate of inlet gas (kg/s)	0.46-0.66	-
Mass flow rate of solvent (kg/s)	1.38-2.90	-
L/G (kg/kg)	2.9-4.8	-
Lean loading of CO_2 (mol CO_2/mol amine)	0.199-0.268	-
Rich loading of CO_2 (mol CO_2/mol amine)	0.358-0.378	-
CO_2 removal	83.1%-99.1%	-
Stripper T (^{0}C)	-	134.25-150
Stripper P (bar)	-	5.51-7.36

To evaluate the performance of pilot test unit (especially the absorber and stripper), a rigorous process was modeled on Aspen Plus by 36 different parametric tests. Performances of both columns (especially the removal efficiency) were assessed and tried to be developed by playing with some parameters such as loadings, inlet solvent temperatures, inlet gas temperatures and mass flow rates of these streams [102]. The ELEC-NRTL equation of state was chosen for the simulations. Data collected from wetted wall column was used to model reaction rate with Arrhenius equation. Rate based mode and RadFrac columns were employed for this CO_2 capture system. Hydraulic plots of columns were not given in the article. Due to the advanced flash stripper, heat duty of the process did not increase more than 5% even at higher CO_2 removal rates. In the end, carbon dioxide capture at 99% removal rate from coal fired flue gas by PZ solution with a reasonable cost was found to be feasible.

2.2.3. CO_2 Capture Studies Using NH_3

Niu and co-workers (2012) constructed a laboratory scale pilot plant and operated it to study CO_2 removal by aqueous solutions of NH_3. The pilot plant consisted of two absorbers connected to a stripper. Gas mixtures were separated either partially or completely. Temperature profiles, removal efficiencies, CO_2 loadings and their effects were obtained from the 19 runs of the pilot plant [75].

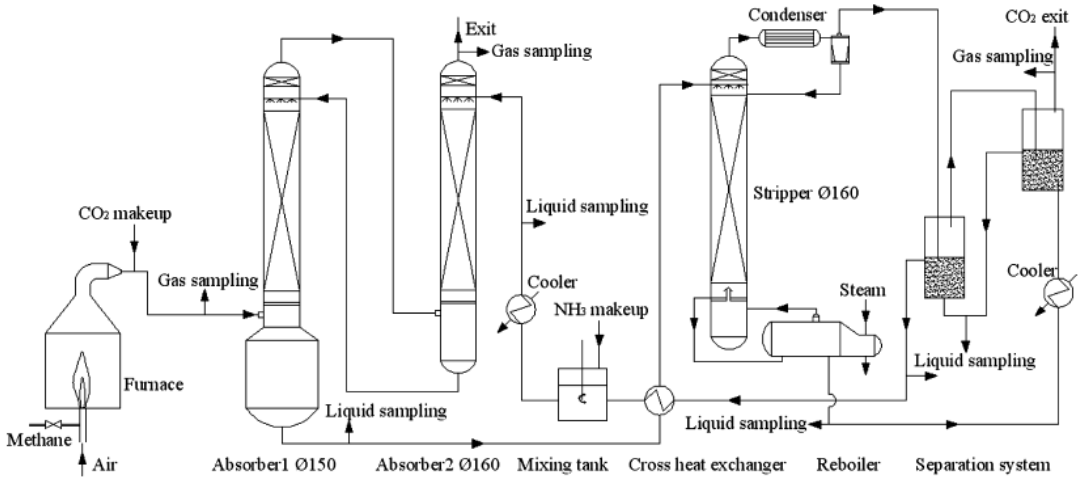

Figure 2.7 Process flow diagram of laboratory pilot plant [75]

Process flow diagram of laboratory pilot plant is given in Figure 2.7. All the columns are made of stainless steel. The packing height of absorber #1 and #2 were determined as 1.47 m. The packing height of absorption column #2 could be varied within 1.47 m which let researchers to examine the effect of packing height on removal of CO_2. The flue gas stream consisted of a mixture of air and CO_2. Inlet gas stream entered the column (#1) from the bottom. The two absorbers could be run in parallel or in series. Flow of gas and liquid counter currently interact with each other in the absorption column. Characteristics of absorber columns are given in the Table 2.8.

Table 2.8 Characteristics of absorption columns in pilot plant [75]

	Absorber #1	**Absorber #2**
Packing type	Metal wire gauze structured	Metal wire gauze structured
Inner diameter (m)	0.15	0.16
Packing height (m)	1.47	1.47

Loss of ammonia at the top of the stripper was tried to be reduced thanks to the high pressure of the column. As the time passed by, high pressure in desorber led to the precipitation of some solids [75]. It could have caused shutdown of pilot plant because of blockage of condenser and reflux pipes. To solve this problem, gas mixture of NH_3 and CO_2 were adopted in this pilot plant study.

Pressure of stripping unit was preferred close to the 1 atm and the pressure of absorber was set to exactly 1 atm, respectively. As the pressure decreases, temperature of reboiler also decreased. Thus, blockage and precipitation problems were solved. Operation was then simplified and conducted separately for absorber and stripper columns. Some of the operating conditions of absorption columns are given in the Table 2.9.

Table 2.9 Operating conditions of absorption column in pilot plant [75]

	Absorber
Gas inlet temperature to absorber #1 (^{0}C)	17.7-138.0
Solvent inlet temperature to absorber #2 (^{0}C)	18.0-29.0
Inlet gas CO_2 fraction (v/v %)	6.9-15.7
Flow rate of inlet gas (m^3/s)	9.0-16.0
Flow rate of solvent (L/h)	60-180
NH_3 concentration (wt%)	7.6-8.5
Lean loading of CO_2 (mol/mol)	0-0.397
Rich loading of CO_2 (mol/mol)	0.084-0.482

Rate based mode and RadFrac distillation module were employed in Aspen Plus to simulate this CO_2 capture system. The results obtained from rate-based simulation were in good agreement with the pilot plant data. The ELEC-NRTL equation of state (EOS) was chosen for this simulation. By using this EOS, enthalpies, equilibrium vapor pressures, entropy and speciation of solutions were predicted. Chemical equilibrium was assumed for the NH_3-CO_2-H_2O system. For the calculation of vapor properties NRTL-RK was used and ELEC-NRTL method was utilized for the calculation of liquid

properties. Equilibrium and kinetic data were taken from literature. Some optimizations were applied to the simulation system. Temperature profiles, removal efficiencies and CO_2 loadings were tried to be optimized by changing packing height of absorption unit, ammonia concentration of lean stream, liquid temperature and gas flow rate parameters [75]. Hydraulic plots of columns were not given in the article.

Liu et al. (2015) studied rate-based model simulations of CO_2 absorption on Aspen Plus by using aqueous NH_3. These simulations were examined using pilot plant and experimental data in the literature. Transfer condition factor, reaction condition factor, kinetic parameters and mass transfer coefficients in the rate-based model affected the results ultimately [76]. All the results showed that reconciliation of simulation data with different operating conditions was significant before the detailed optimization and design on Aspen Plus. Laboratory scale apparatus of absorption column is given in Figure 2.8.

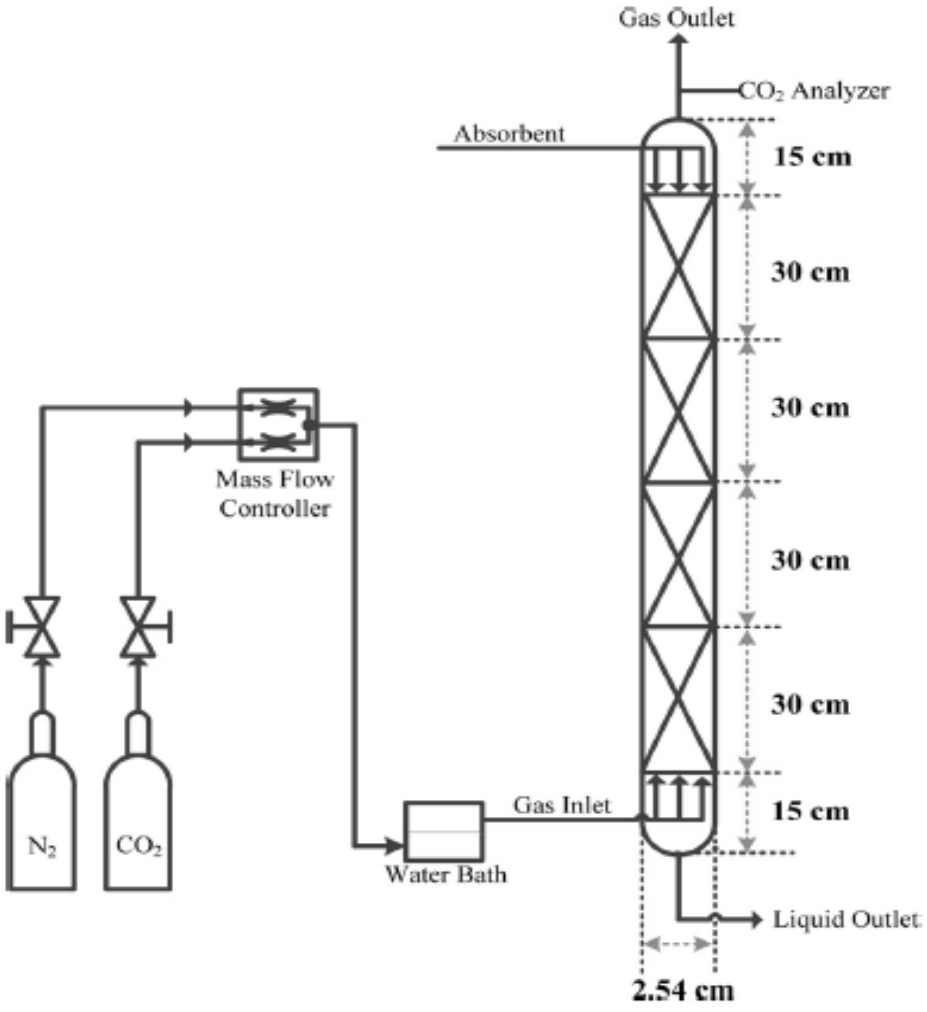

Figure 2.8 Laboratory scale apparatus of absorption column [76]

Some characteristics of absorber column are given in the Table 2.10. The inlet gas stream was passed through a water bath and it consisted of a mixture of pure CO_2 and N_2. From a 29.7 wt% aqueous NH_3, two dilute solutions were prepared (3 and 7 wt%).

Table 2.10 Characteristics of absorption column in pilot plant [76]

	Absorber
Packing type	Ceramic Raschig rings
Internal diameter (m)	0.0254
Packing height (m)	0.3

The lean feed entered from top of the column. Based on laboratory experiments, some graphs were plotted such as CO_2 removal rate versus packing height and CO_2 removal efficiency versus packing height.

Main operating conditions during simulations were 4 L/min gas flow rate, 0.15 mole fraction of CO_2, 3 wt% NH_3 concentration. 6 mm Raschig ring was used as a type of packing. Since there was a film resistance in both phases, removal efficiency could not be predicted as 100%. An absorption model was tried to be developed by using laboratory and literature data in the article. Rate-based mode was employed in Aspen Plus to simulate this CO_2 capture system. The equilibrium model of this multi-stage distillation column system assumed that liquid and vapor phases leaving any stage were in thermodynamic equilibrium with each other [76]. The ELEC-NRTL equation of state was chosen for this simulation. By using this EOS, thermodynamic properties such as viscosity, diffusivity and thermal conductivity were predicted. Chemical equilibrium was assumed for the NH_3-CO_2-H_2O system. Kinetic data was obtained by Pinsent et al. (1956) and embedded into Aspen Plus. After fitting experimental data to simulation data, 3 wt% of aqueous NH_3 was used and which caused reactor and transfer condition factors to be found as 0.25 and 0.75, respectively. Rate-based model, film resistance, flow model, reaction and transfer condition factors were the main parameters that were changed to optimize the system [76]. Hydraulic plots of columns were not given in the article.

In the study of Qi and Wang (2017), rate-based modeling and laboratory study on the absorption of both CO_2 and SO_2 in packed column by using aqueous NH_3 was studied [77]. This new process was called combined capture process.

In the experimental part of the study, main operating parameters such as CO_2 and SO_2 concentrations, loadings of CO_2 and SO_2, L/G ratio and temperature of absorption process and their effects on the volatilization of NH_3 and absorption of CO_2 were identified. As a result of experiments, 5 wt% aqueous NH_3 solvent (at the lean loading of 0.2 mol CO_2/mol NH_3 and lean loading of 0.1 mol SO_2/mol NH_3) was used to achieve the absorption efficiency over 85%. Process flow diagram of up-to-date combined capture process is given in Figure 2.9.

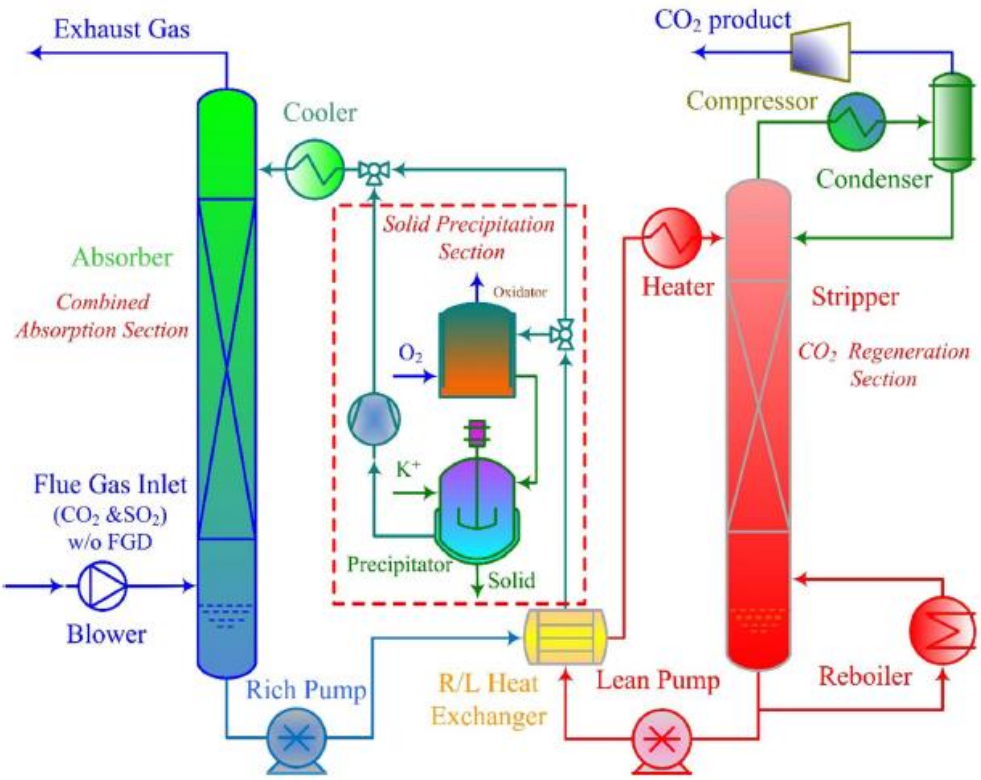

Figure 2.9 Process flow diagram of up-to-date combined capture process [77]

The lean solvent was a CO_2 and SO_2 loaded NH_3. A stainless-steel packed absorber column was used in the experiments. Inlet gas stream was pre-heated in water bath and entered to the bottom of the column [77].

Table 2.11 Characteristics of absorption column in pilot plant [77]

	Absorber
Packing type	Dixon rings
Internal diameter (m)	0.06
Packing height (m)	1

Lean feed and inlet gas counter currently contacted each other during this separation process. Some packing characteristics of absorber column are in the Table 2.11. The operating conditions of absorber column are given in the Table 2.12 below.

Table 2.12 Operating conditions of absorption column in pilot plant [77]

	Absorber
Absorber temperature (^{0}C)	20-50
Column Pressure (bar)	1.5
SO_2 concentration (ppm)	96-2578
Inlet gas CO_2 fraction (v/v %)	1.9-14.2
L/G ratio (L/m^3)	2.6-20.1
Liquid phase SO_2 loading	0-0.3
Liquid phase CO_2 loading	0-0.4
NH_3 concentration (wt%)	5

Rate based mode and RadFrac module were activated in Aspen Plus to simulate this combined capture system. The results of experimental plant data were validated with the rate-based simulation. The ELEC-NRTL equation of state was chosen for this simulation file. Chemical equilibrium was assumed for the NH_3-CO_2-H_2O system. For the calculation of vapor properties SRK was used, and ELEC-NRTL method was utilized for the calculation of liquid properties. Equilibrium and kinetic data were taken from literature and physical properties were taken from the database of Aspen Plus. Modeling on Aspen Plus indicated that loading of SO_2 provided similar effects compared to the loading of CO_2 in terms of mass transfer, heat of CO_2 absorption and the efficiency of absorption [77]. However, loading of SO_2 showed lower volatilization of ammonia compared to the CO_2 one. By changing with parameters, removal efficiencies were tried to be increased. Valuable contributions were provided to the literature due to combined absorption studies. Hydraulic plots of columns were not given in the article.

2.2.4. CO_2 Capture Using Other Solvents

In this subsection of literature survey, there is only one article that tries to fit experimental and simulation results. Yu et al (2016) worked on rate-based simulations and experimental studies of absorption of CO_2 by using NH_3/PZ blend solutions which is

a potential promoter for absorption of CO_2 [103]. This study basically analyzed the effects of concentration of NH_3 and PZ, temperature of absorption process, CO_2 loading of lean solution and flow rate of solution on the performance of NH_3/PZ blend solution for the capture of CO_2. After adding PZ to aqueous NH_3, the rate of absorption of CO_2 was enhanced and CO_2 removal efficiency became comparable to that of MEA-based processes. Unfortunately, adding PZ raised the temperature along the column and increased the free NH_3 concentration in the solution. Thus, a high amount of NH_3 was lost from the absorption column. Schematic flow diagram of experimental setup is given in Figure 2.10.

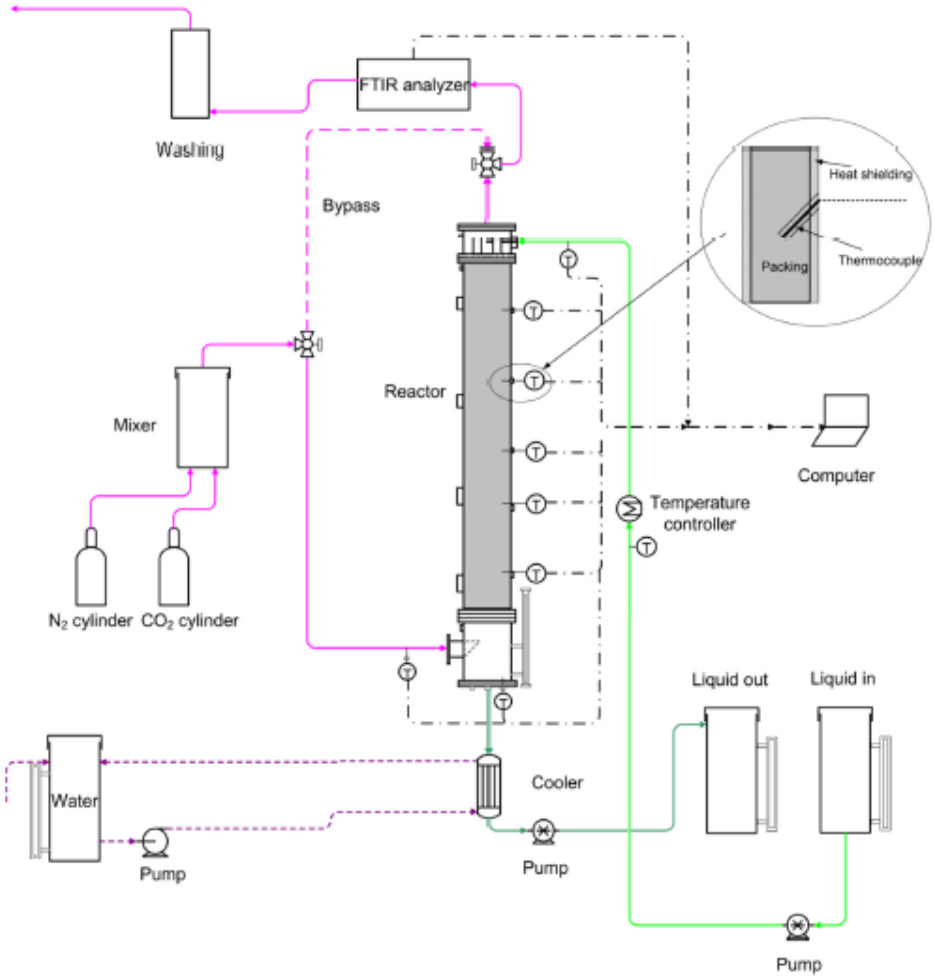

Figure 2.10 Schematic flow diagram of experimental setup [103]

Some packing related specifications of absorber column are shared in Table 2.13. CO_2 was absorbed into the blend solution. The temperature of inlet gas and lean solution were controlled by water baths and was measured at the inlet to the absorber column. During experiments, 16 runs were performed.

Table 2.13 Characteristics of absorption column in experimental setup [103]

	Absorber
Packing type	2.5 mm Dixon rings
Internal diameter (m)	0.06
Packing height (m)	1

Operating conditions used in the setup were summarized in the Table 2.14. Some operating conditions like loading or inlet gas concentration were held constant.

Table 2.14 Operating conditions used in the experimental setup [103]

	Absorber
NH_3 concentration (wt%)	2.87-8.76
PZ concentration (wt%)	0-6.96
CO_2 loading (mol CO_2/mol NH_3)	0.198-0.201
Liquid flow rate (L/h)	2-4.4
Liquid temperature (^{0}C)	10.2-24.8
Gas flow rate (L/min)	19.15
Gas temperature (^{0}C)	24.6-25.4
Inlet gas CO_2 concentration (%)	10.04

Rate-based mode was activated in Aspen Plus to simulate this capture system. The results of experimental plant data were validated with the rate-based simulation. 10 equilibrium reactions were considered for the NH_3-PZ-CO_2-H_2O system. For the calculation of vapor properties RK method was used and ELEC-NRTL method was utilized for the calculation of liquid properties [103]. Equilibrium data, kinetic data and some transport properties were taken from literature and physical properties were taken from the database of Aspen Plus. In the end, experimental data were compared with the Aspen Plus simulation results in terms of ammonia concentration at the outlet, temperature along the column and removal efficiency. Hydraulic plots of columns were not given in the article. However, determining a specific L/G ratio in the column was too important for the process design because it would lead flooding if it were high.

2.3. Lessons Learned from the Literature

From the chapter of literature survey, the following items are learned:

- Packed column types are generally used in absorption processes. However, there are also plate/tray types of separation columns.
- Most of the time, random packing was used in these processes. Types of random packing are classified with respect to their structure such as Raschig ring, Pall ring, cascade ring and Berl saddle. Structured packings were not preferred much. The reason behind is that they are difficult to obtain and not cost effective.
- There are two main equation of states in Aspen Plus that can handle electrolyte chemistry: ELEC-NRTL and ENRTL-RK. ENRTL-RK is the less used thermodynamic method. Most of the studies in the literature were observed to use ELEC-NRTL as their choice because of its higher accuracy in experimental validation. For this purpose, we used the ELEC-NRTL model in this study.
- Some studies in the literature used the default reaction chemistry in the Aspen database. However, mostly researchers used the kinetic data taken from literature. Some articles created their own reaction models by fitting their simulation results to their experimental data on Aspen Plus.
- Columns are modeled by using RadFrac columns since there are reactions occurring inside the columns.
- In most studies, rate-based mode was activated. Equilibrium mode is not generally used. Calculation type of the RadFrac columns is chosen as rate-based (non-equilibrium) because mass transfer rate limitations are taken into consideration in this model. An important reason that the equilibrium mode was not preferred is that the effect of column parameters related to packing cannot be calculated in the equilibrium mode, as explained in the introduction chapter. Also, the assumption of intimate contact between the liquid and gaseous phases is not enough to work with equilibrium mode. Mass transfer phenomena and thus rate-based calculations matter here [72].
- Some studies examined the hydraulics of the columns (absorber and the stripper). Thanks to Aspen Plus, one could generate hydraulic plots of the liquid and vapor streams in the column. L/G ratio is an important aspect of column hydraulics.

Hydraulic plots are visualized to see if there is flooding or weeping inside the column.

In the light of what is learned from the “Literature Survey”, the “Materials and Methods” chapter expresses details behind the studies performed in this thesis.

CHAPTER 3

MATERIALS AND METHODS

3.1. General

The chapter covers summary of computational methods used in this thesis study. Computational simulations were carried out using Aspen Plus V10 software. This chapter is organized as follows.

In section 3.2, basic Aspen Plus simulation details are shared. In the subsections, solvent reactions, components and electrolyte equation of states used in these simulations are given in detail.

In section 3.3, details of the simulation environment are shared. In the subsections, flue gas and amine solvent specifications, main target of simulation, column type and column sizing used in these simulations are given in detail.

In section 3.4, process flowsheet configurations are shared. In the subsections, absorber design, open loop (single pass) process design and closed loop (recycle) process design simulations are given in detail. Calculations are mainly divided into three parts:

- Absorber design
- Open loop design
- Closed loop design

3.2. Basic Aspen Plus Simulation Details

In this section, simulation approaches used in absorber design, open loop studies, and closed loop studies are explained.

3.2.1. Solvent Reactions

Either reactions between components may be created on Aspen using Electrolyte Wizard or default examples which are embedded into graphical user interface of Aspen

can be used to simulate equilibrium reactions between ions. At first trials, the electrolyte wizard was used for defining automatic chemistry generation. Base components, hydrogen ion type, possible salt types and global property method etc. were introduced inside the electrolyte simulation. It is given up because Aspen's control panel, where the simulation is run, showed some warnings related to the lack of parameters. In this study, built-in reaction sets for both MEA-CO_2-H_2O and PZ-CO_2-H_2O equilibrium systems present in default Aspen Plus examples are used. The related set of reactions are given in introduction chapter. Equilibrium constants for reversible reactions and rate constants for irreversible reactions are already embedded into Aspen Plus default examples. Therefore, there is no need to redefine them.

3.2.2. Components

Under normal circumstances, related databanks from Aspen database are selected and then pure components and their specifications are retrieved [72]. However, in default examples, there is no need to do so. True components including all ions are already given at Components-Specifications table. Apparent components used with monoethanolamine solvent are MEA (C_2H_7NO), H_2O, CO_2, N_2, O_2 and CO. For piperazine, apparent components are PZ ($C_4H_{10}N_2$), H_2O, CO_2, N_2, O_2 and CO.

There is no reaction occurring in the gas phase. However, in the liquid phase, ionic reactions of MEA-CO_2-H_2O and PZ-CO_2-H_2O systems take place. As a result of these reactions, various ionic components are formed. List of components including MEA-based reactions is shown in Figure 3.1 below. Also, list of components including PZ-based reactions is illustrated in Figure 3.2 below.

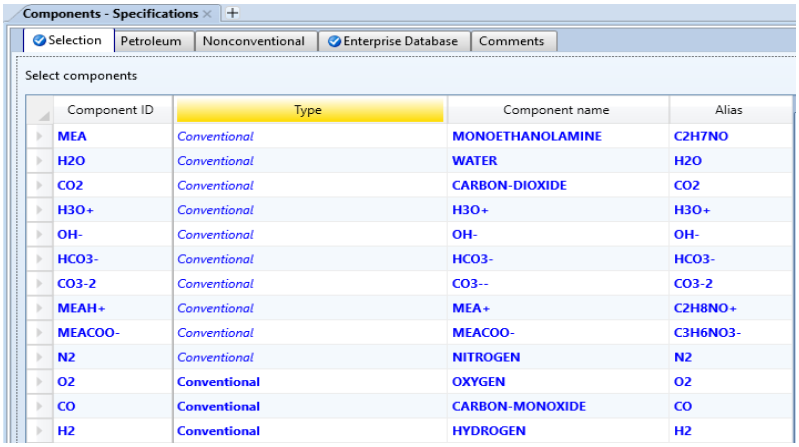

Component ID	Type	Component name	Alias
MEA	Conventional	MONOETHANOLAMINE	C2H7NO
H2O	Conventional	WATER	H2O
CO2	Conventional	CARBON-DIOXIDE	CO2
H3O+	Conventional	H3O+	H3O+
OH-	Conventional	OH-	OH-
HCO3-	Conventional	HCO3-	HCO3-
CO3-2	Conventional	CO3--	CO3-2
MEAH+	Conventional	MEA+	C2H8NO+
MEACOO-	Conventional	MEACOO-	C3H6NO3-
N2	Conventional	NITROGEN	N2
O2	Conventional	OXYGEN	O2
CO	Conventional	CARBON-MONOXIDE	CO
H2	Conventional	HYDROGEN	H2

Figure 3.1 List of components formed by MEA-CO_2-H_2O reactions in the Aspen Plus

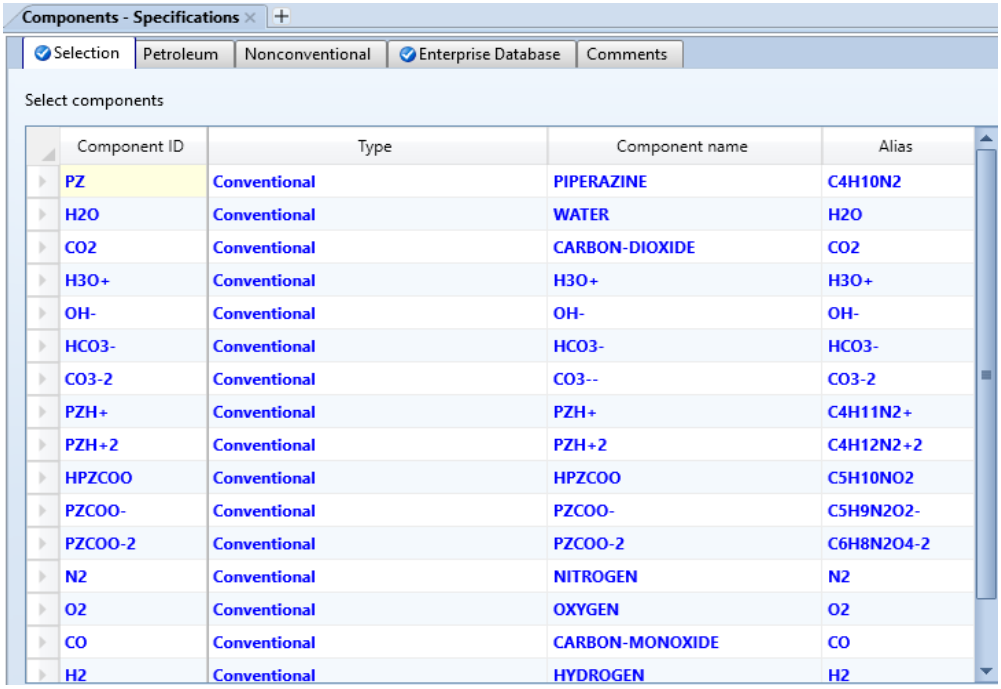

Component ID	Type	Component name	Alias
PZ	Conventional	PIPERAZINE	C4H10N2
H2O	Conventional	WATER	H2O
CO2	Conventional	CARBON-DIOXIDE	CO2
H3O+	Conventional	H3O+	H3O+
OH-	Conventional	OH-	OH-
HCO3-	Conventional	HCO3-	HCO3-
CO3-2	Conventional	CO3--	CO3-2
PZH+	Conventional	PZH+	C4H11N2+
PZH+2	Conventional	PZH+2	C4H12N2+2
HPZCOO	Conventional	HPZCOO	C5H10NO2
PZCOO-	Conventional	PZCOO-	C5H9N2O2-
PZCOO-2	Conventional	PZCOO-2	C6H8N2O4-2
N2	Conventional	NITROGEN	N2
O2	Conventional	OXYGEN	O2
CO	Conventional	CARBON-MONOXIDE	CO
H2	Conventional	HYDROGEN	H2

Figure 3.2 List of components formed by PZ-CO_2-H_2O reactions in the Aspen Plus

Components are handled by two main approaches in Aspen Plus. Apparent component approach basically means to deal with base components. These components are considered undissociated. In the case of true component approach, the dissociation of the components is taken into account. Once the option is activated just like in this thesis study, Aspen Plus gathers all the apparent (base) components with their ions as shown in both figures above.

3.2.3. Electrolyte Equation of State

As soon as the components are defined, a suitable equation of state is specified in order to evaluate their thermodynamic properties. A proper thermodynamic model needs to be chosen because of the highly non-ideal behavior of the liquid phase due to presence of ions. For this purpose, the ELEC-NRTL model was used in this study. According to several studies in the literature, electrolyte nonrandom-two-liquid (NRTL) is highly sophisticated and thermodynamically rigorous model [97,104,105]. Along with the ELEC-NRTL, ENRTL-Redlich Kwong could be used in the literature [76,77,103]. ENRTL-RK is the coupled version of ELEC-NRTL and Redlich Kwong equation of states. It is generally used for the calculation of the non-idealities of the vapor phase. Method name setup window in Aspen Plus is shown in Figure 3.3 below.

After the thermodynamic model is selected, Aspen Plus® automatically obtains the rest of the required parameters from its vast database which means Aspen is ready to jump into the simulation environment.

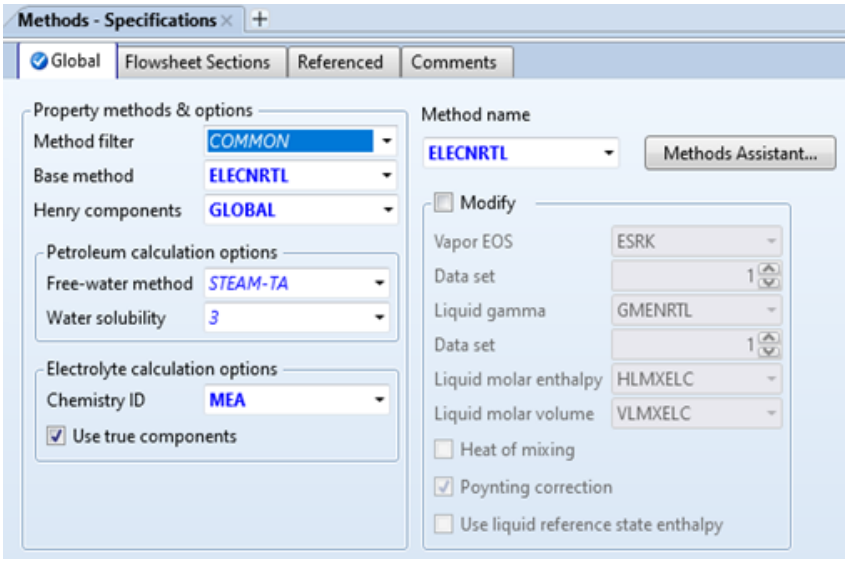

Figure 3.3 Thermodynamic method name set-up window

3.3. Simulation Environment

In this section, phase of designing simulation environment is explained. All stream types and equipment are selected from model palette and added to main flowsheet.

3.3.1. Flue gas and Amine Solvent Specifications

In the beginning, an absorber column is designed. There is a flue gas that needs to be processed. It is most likely coming from fossil-fuel fired power plants. Especially, carbon-dioxide inside the flue gas must be eliminated by a solvent. Flue gas stream is at 25 ^{o}C including mixture of 15% CO_2 and 85% N_2 by mole fraction. The flue gas is fed into absorber column from the bottom stage (10th stage) with a volumetric flowrate of 1.5 L/min. Initially, pressure is set to 1.5 bar. To observe the effects of increasing inlet gas pressure, four different pressure values (1.5 bar, 2 bar, 3 bar, 4 bar) are tried.

A lean amine solvent at 40 ^{o}C and 1.7 bar (with no CO_2 concentration) is fed into the top of absorption column. Molar flow rate of aqueous solvent is selected as 0.479241 mol/min MEA or PZ, and 3.37482 mol/min H_2O. Both inlet streams are named according

to their main specifications. Inlet gas stream is named as FLUEGAS and lean amine solvent stream is named as LEANIN. While studying on open loop, specifications of LEANIN stream does not change. However, composition of LEANIN stream changes in closed loop (Even, the stream's name is changed to TORECYC after recycling back to absorber column, as explained later in this chapter). Specifications of feed streams did not change with respect to amine solvent. Main specifications of FLUEGAS and LEANIN streams are summarized in Table 3.1.

Table 3.1 Main specifications of feed streams

	FLUEGAS	**LEANIN**
Temperature (^{0}C)	25	40
Pressure (bar)	1.5 ,2, 3, 4	1.7
Volume flow (L/min)	1.5	-
Mole fraction		
CO_2	0.15	-
N_2	0.85	-
Mole flow (mol/min)		
MEA/PZ	-	0.479241
H_2O	-	3.37482

3.3.2. Simulation Target

The main target of these open loop and closed loop simulations is to capture 90% of CO_2 inside FLUEGAS stream. It means that 90 % mole purity is desired at the gas phase outlet stream (CO2OUT stream, as we will see later in the chapter) of stripper.

3.3.3. Column Type

Throughout the simulations, packed column is preferred. Both absorption and stripping units are designed this way. The advantages of using packed column taken from introduction section, selection of equipment/column, are listed below [30]:

- For corrosive liquids like MEA, a packed column is usually a cheaper option than the equivalent plate column.
- Lower pressure drop compared to a plate column is possible.

- The liquid hold-up is lower than a plate column because toxic or flammable liquids should be stored or kept as small as possible in terms of safety issues.
- Columns with small diameter are possible.
- More suitable for handling foaming systems.
- The construction of the system is easy.
- Better mass transfer than the spray column.
- Increased efficiency of separation for the same column height.

Raschig ring packing type is used for both columns. They can be made of inert materials which are cheap and light, like porcelain, carbon, ceramic, plastic, metal alloys, steel or clay.

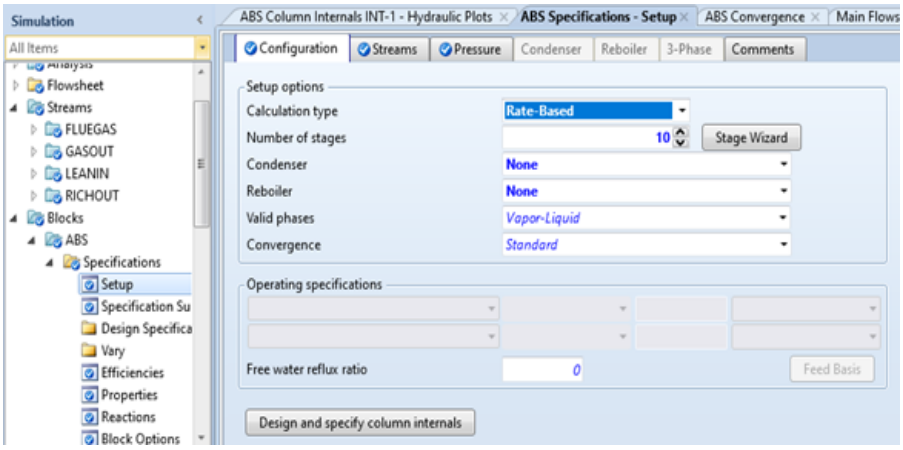

Figure 3.4 Selection of rate-based mode during absorber design

In order to model absorption and stripping columns, RadFrac blocks are chosen from the model palette because reactions occur inside the columns. Without axial dispersion, reactive absorption and stripping columns are typically modeled as ideal plug-flow in terms of fluid dynamics [72]. Introduction chapter gives detailed information related to fluid dynamics inside the column. Calculation type of the RadFrac columns is chosen as rate-based (non-equilibrium) because mass transfer rate limitations are taken into consideration in this model. Selection of rate-based mode during absorber column design is given in Figure 3.4.

3.3.4. Column Sizing

One of the advantages of packing column is working with small diameter columns [30]. First, a first-guess column diameter value is given under column internals tab.

Simulation is run and converged. Hydraulic plots are visualized to see if there is flooding or weeping inside the column. The diameter is then automatically calculated using Aspen Plus. A suitable pressure drop method is selected to provide a proper correlation for flooding point correlation [106].

Packed height of columns is not automatically calculated. However, it is chosen as a result of calculations. CO_2 mole fraction in the CO_2 rich stream leaving the absorber with respect to packed height of absorber column is studied to find the best packed height. Since an experimental study will be carried out in the future, a realistic value is specified for height of the stripper.

3.4. Process Flowsheet Configurations

Different process flow configurations are created on Aspen Plus. These are single absorber design, open loop design and closed loop design.

3.4.1. Absorber Design

Absorber column is the place where the electrolyte CO_2 capture reactions take place. FLUEGAS and LEANIN streams are sent to column and it is accepted as the beginning of process. Main objective behind designing an absorption column is to efficiently capture CO_2 within FLUEGAS. CO_2 removal efficiency of absorber column is calculated as more than 90% for both MEA and PZ solutions. There is not any design specification embedded into absorption unit. Schematic of absorber column is given in Figure 3.5 below.

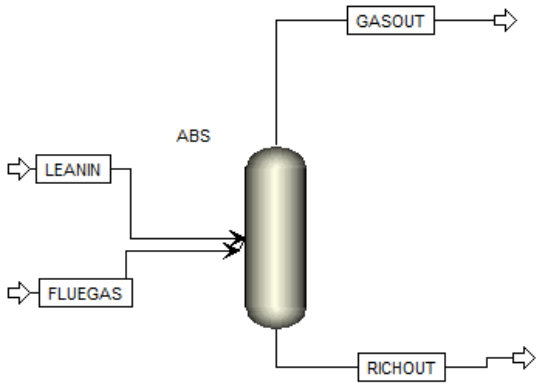

Figure 3.5 Simulated absorber column with its inlet and outlet streams

The feed streams are FLUEGAS, consisting of CO_2 and N_2, and the LEANIN, containing aqueous MEA or PZ solutions. Both feed streams' specifications are given in Table 3.1. The lean amine solution is fed to the column from the top while the flue gas is fed to the column at the bottom. Most of the CO_2 inside the flue gas was chemically absorbed and the remaining portion of gas called "GASOUT" left the absorber column from the top. The rich solvent stream called "RICHOUT" loaded with CO_2 left the column from the bottom.

For the absorption process, packed column is used. Packing material is chosen as ceramic Raschig rings by Norton. Specifically, they are cheap and easy to handle as told before in column type section above. Specifications of the absorber column is summarized in the Table 3.2.

Table 3.2 Specifications for absorber column

	Absorber (RadFrac)
Calculation Type	Rate-based
Number of Stages	10
Condenser	None
Reboiler	None
Packing	0.25-IN OR 6-MM Ceramic by Norton
Packing Type	Raschig
Section Diameter (m)	0.015
Section Packed Height (m)	0.6
Mass transfer coefficient method	Onda-68
Interfacial Area Correction Factor	1.2
Interfacial Area Method	Onda-68
Heat Transfer Coefficient Method	Chilton and Colburn
Film Resistance Options	Discretize film for liquid Consider film for vapor
Discretization Points for Liquid Film	5

Top stage pressure of absorber column is set as 1 atm. The absorber column consists of 10 stages with no condenser and no reboiler. Inside column internals panel, update pressure drop from top stage is marked. RadFrac is used to model the absorber. Mass-transfer calculations require rate-based types of calculations. To converge rate-

based calculations, maximum number of iterations are chosen as 50 with a convergence tolerance of 10^{-5}. Always after the simulation is converged, hydraulic plots of columns should be controlled to not to face with weeping or flooding. Basic design specifications of stripper column are given in the next open loop and closed loop sections.

3.4.2. Open Loop Process Design

Figure 3.6 shows the open loop process used in the simulations. The process starts with an absorber column (ABS) to which FLUEGAS and LEANIN streams are fed. FLUEGAS enters the column from the bottom and LEANIN is fed into the column from the top. Chemical absorption using MEA and PZ solvents occurs inside the absorber column. Product streams are named GASOUT and RICHOUT. The treated gas stream GASOUT exits from the top of the absorber. The rich solvent stream RICHOUT loaded with CO_2 leaves from the bottom. As RICHOUT stream leaves the absorber, it is fed to the pump (PUMP) to increase its pressure. The pump is chosen from model palette-pressure changers tab. Pump outlet is specified to increase pressure by 20 psia. RICHOUT stream is pressurized via pump and outlet stream of the pump is named as TOHEATER.

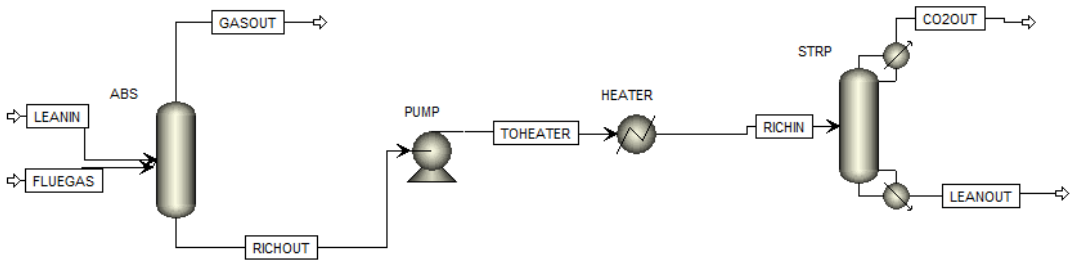

Figure 3.6 Process flowsheet of open loop study

The TOHEATER leaves the pump at 43.0362 ºC and is fed into a heat exchanger (HEATER) where its temperature is increased to 81.2 ºC. The stream leaving the heat exchanger is named as RICHIN. There is no pressure change.

The stripper column (STRP) is modeled with RadFrac and the rate-based calculation type is chosen. This rate-based model is basically used for multi-stage separation operations. Rigorous calculations are applied. It consists of 20 stages including partial-vapor condenser and kettle type reboiler. Vapor-liquid is chosen as valid phase for

separation process. RICHIN stream is considered as a feed and introduced into the 2nd stage of stripper. The first stage belongs to partial-vapor condenser. Top stage pressure of column is set as 1 atm.

For the separation, packed type stripping unit is preferred. The packing material is chosen as ceramic Raschig ring provided by Norton. 0.25-in or 6-mm packing dimension is defined. The critical point behind this is not to struggle with flooding and weeping in any of these columns. As mentioned earlier, right after simulations are converged hydraulic plots are controlled to see whether they are troubled or not. Critically, 80% flooding velocity approach used for hydraulic calculations. To converge rate-based calculations, maximum number of iterations are increased to 60 with a convergence tolerance of 10^{-5}.

The reaction of CO_2 and amine reverses because of pressure and temperature conditions in the stripper. Product streams of stripper are named as CO2OUT and LEANOUT. A concentrated CO_2 stream, CO2OUT, is obtained at the top. Mole fraction of CO_2 in CO2OUT stream is targeted to be 0.9 in the design specifications. The hot lean solvent, LEANOUT, leaves the column at 104.198 ºC and it is not recycled back.

Basic design specifications of stripper column are given in Table 3.3 below. The stripper is modeled with RadFrac and rate-based calculation type is chosen.

Table 3.3 Specifications of stripper column built into open loop

	STRIPPER (RadFrac) for open loop
Calculation Type	Rate-based
Number of Stages	20
Condenser	Partial-Vapor
Reboiler	Kettle
Mass Reflux Rate (kg/hr)	5
Packing	0.25-IN OR 6-MM Ceramic by Norton
Packing Type	Raschig
Section Diameter (m)	0.1
Section Packed Height (m)	2.1

(cont. on next page)

Table 3.3 (cont.)

Mass transfer coefficient method	Onda-68
Interfacial Area Correction Factor	1.0
Interfacial Area Method	Onda-68
Heat Transfer Coefficient Method	Chilton and Colburn
Film Resistance Options	Discretize film for liquid Consider film for vapor
Discretization Points for Liquid Film	5

There are two different design specifications in open loop calculations built inside stripping unit. One of them is related to "CO2OUT" stream's mole purity and the other one is related to stage temperature. To set the mole purity at 90%, distillate to feed ratio is changed between 10^{-5} and 1. In order to obtain the first stage temperature of stripper at 45 ^{o}C (318 K), reflux rate is changed between 0.0001 kg/s and 0.0075 kg/s. The related results to stripper column are obtained from single pass design in the light of these constraints and those are given in the results chapter.

3.4.3. Closed Loop Process Design

Flow diagram of closed loop (recycle) is given in Figure 3.7. The process starts with FLUEGAS stream entering the absorber unit (ABS). FLUEGAS enters the column from the bottom and LEANIN is fed into the column from the top. The treated gas, GASOUT, exits from the top of the absorber. The rich solvent stream, RICHOUT, loaded with CO_2 leaves from the bottom. As soon as the RICHOUT leaves the absorber, it is fed to the pump (PUMP1). The pressure increase is chosen as 20 psia, again. Main specifications of feed streams entering absorber are given in section 3.3.1.

RICHOUT stream exiting absorption unit is pumped into cross heat exchanger (HEX). TOHEATER stream enters heat exchanger at approximately 43 ^{o}C and its temperature is increased to 81.2 ^{o}C. There is no pressure change. Design calculation mode is activated with shortcut model selection. Counter-current flow type heat exchanger is used in the recycle process. TOHEATER stream is heated and LEANOUT stream is cooled counter-currently.

Recycle process is built on open loop study. First inputs are replaced with results taken from LEANOUT stream. Therefore, heat exchanger is put instead of heater. The hot lean solvent is cooled by cold stream outlet temperature specified heat exchanger. At the same time, heated stream is prepared to fed into stripper (STRP).

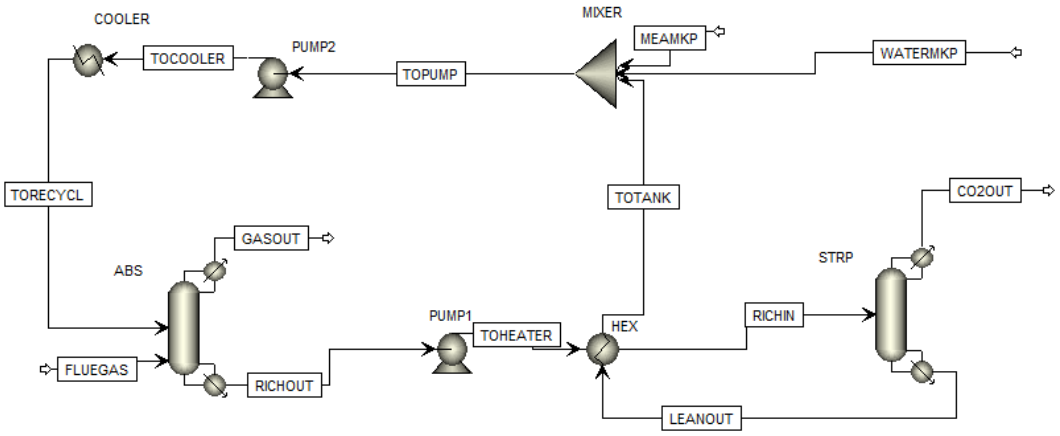

Figure 3.7 Process flowsheet of closed loop study

The rich solvent stream RICHIN is sent to stripper column. Most of the information provided in section 3.4.2 (open loop) is valid for closed loop process design until the bottom product of stripper. Operating specifications of stripper are initial-guess values. An example of it is shown in Figure 3.8. Reflux rate is specified as 5 kg/hr and distillate to feed ratio is given as 0.081. In open loop studies, reflux rate is initially guessed as 1 kg/hr. This situation made a big difference between the results.

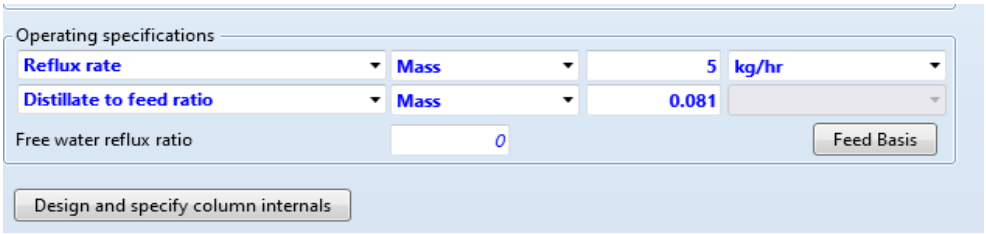

Figure 3.8 Operating specifications of stripping unit in closed loop process

A concentrated CO_2 stream, CO2OUT, is obtained at the top. Mole purity of CO2OUT stream is targeted to be 0.9 on design specifications. The hot lean solvent, LEANOUT, goes out of the column at approximately 103-104 ^{o}C and it is recycled back.

After cooling, TOTANK stream transports lean solvent into the MIXER block. Two make-up streams are embedded into flowsheet here which are “MEAMKP/PZMKP”

and “WATERMKP”. As an initial guess, mass flow rate of water make-up is determined as 0.025 kg/hr at 60 ^{0}C and 1.2 bar. The mass flowrate of amine make-up is initially given as 0.0001 kg/hr at 60 ^{0}C and 1.2 bar. The converged flow rates of water and MEA make-up are calculated using balance operators. The mixture stream (TOPUMP) is sent to another pump (PUMP2). 1.7 bar discharge pressure is set as pump outlet. Finally, passing through the cooler unit, mixture is cooled back to 40 ^{o}C. At the exit of the cooler, stream is named as TORECYLE and it is sent back to the absorber column. Except its temperature and pressure, its composition becomes totally different from initial LEANIN stream.

Basic design specifications of stripper column are given in the Table 3.4.

Table 3.4 Specifications of stripper column built into the closed loop process

	STRIPPER (RadFrac) for closed loop
Calculation Type	Rate-based
Number of Stages	20
Condenser	Partial-Vapor
Reboiler	Kettle
Mass Reflux Rate (kg/hr)	5
Packing	0.25-IN OR 6-MM Ceramic by Norton
Packing Type	Raschig
Section Diameter (m)	0.085
Section Packed Height (m)	2.1
Mass transfer coefficient method	Onda-68
Interfacial Area Correction Factor	1.0
Interfacial Area Method	Onda-68
Heat Transfer Coefficient Method	Chilton and Colburn
Film Resistance Options	Discretize film for liquid Consider film for vapor
Discretization Points for Liquid Film	5

This time, there is only one design specification built inside stripping unit in the closed loop process as opposed to two design specifications in the open loop process. It is related to CO2OUT stream’s mole purity. To set the mole purity at 90%, distillate to

feed ratio is changed between 10^{-5} and 1. Here, mass reflux rate is kept constant at 5 kg/hr because it is not a variable of design specification.

Originally, reflux rate and distillate to feed ratio are written as an initial guess under stripper column setup panel. However, mass distillate to feed ratio is used as design specification variable to find CO2OUT stream's mole purity. Both MEA and PZ solutions are compared in detail. The loop starts from absorber column and ends with absorber column as well. This is how the recycle is obtained. The related results to stripper column are obtained from closed loop design in the light of these constraints and those are given in the results chapter.

CHAPTER 4

RESULTS AND DISCUSSION

4.1. General

This thesis study investigates the design and simulation of laboratory-scale post-combustion CO_2 capture process using Aspen Plus software. The chapter consists of three main simulation studies using monoethanolamine (MEA) and piperazine (PZ) solutions. Chemical absorption process including an absorber design, open loop studies including an absorber and a stripper, and closed loop (recycle) studies in Aspen Plus are investigated comparingly using these two chemical sorbents.

The simulations were carried out by changing inlet gas stream's (FLUEGAS) pressure to 1.5 bar, 2 bar, 3 bar and 4 bar. In the light of the results of these simulations, constraints such as CO_2 loading, temperature, pressure, molality, packing type of absorber, column packed height and column diameter were determined. CO_2 capture rate of absorber, absorption efficiency of absorber and the energy requirement of stripper column are also calculated and compared for MEA and PZ solutions. The simulation conditions and constraints are selected in a practical and realistic manner so that the simulation results might then be used to construct a laboratory-scale apparatus where the CO_2 capture will experimentally be performed and studied using the selected amines.

This chapter is organized as follows. In section 4.2, first, the validation of the specification of the ionic components are performed in Aspen Plus and compared with the literature results. In section 4.3, the results regarding the absorber design are presented and the CO_2 loading, temperature of LEANIN stream, column diameter, height of column and molality of amine solutions are determined. In section 4.4, the open loop (single pass) process design results are depicted. In section 4.5, the closed loop (recycle) design results are presented.

4.2. Speciation Validation of Species

The speciation of ionic species in the liquid phase gives information about the concentration profile of each species at certain loadings of CO_2 in the solvent. To study the speciation of CO_2-MEA-H_2O system, ELEC-NRTL thermodynamic model is used in Aspen Plus. Absorption simulation of CO_2 into aqueous MEA was carried out at 40 ˚C with 0.33 M MEA solution.

Distribution of species was evaluated with increasing amount of molar flow rate of CO_2 to attain higher CO_2 loading. In Figure 4.1, the concentrations of MEA, $MEACOO^-$, HCO_3^- and $MEAH^+$ were represented along with amount of CO_2 loaded, and the results obtained in this study are compared with an experimental literature study. As seen, simulation results in this study and experimental results in the literature study are in good agreement. As CO_2 loading is increased, the concentration of neutral MEA decreases since MEA turns into various ionic species. The concentration of $MEAH^+$ (protonated MEA) increases with CO_2 loading. Concentration of HCO_3^- gradually increases as more CO_2 is absorbed in system. $MEACOO^-$ (MEA carbamate) concentration increases until CO_2 loading is around 0.5 and then decreases. $MEACOO^-$ decomposes to generate HCO_3^- and MEA at higher loadings.

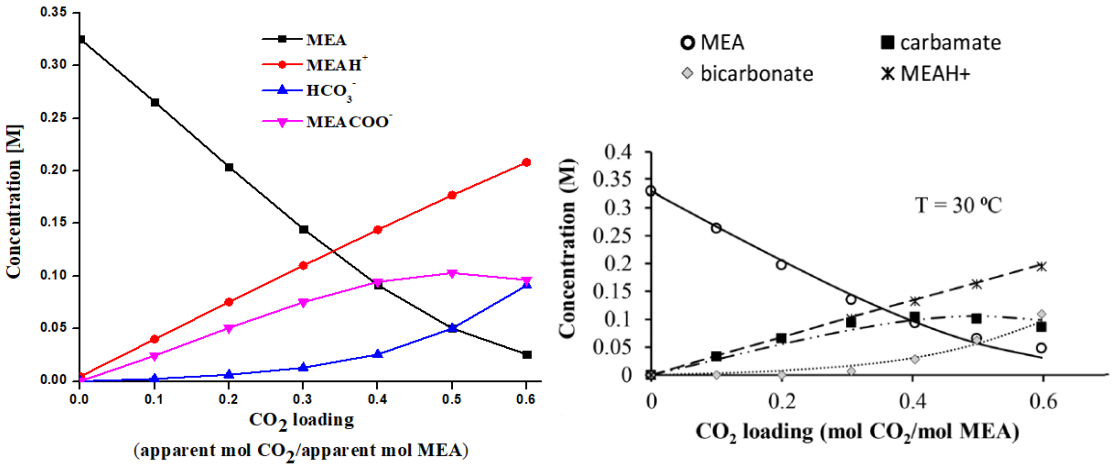

Figure 4.1 Speciation validation of a 0.33 M MEA solution (left: obtained from simulations at 40 ˚C, right: obtained from literature at 30 ˚C) [107]

Speciation validation study of PZ-H_2O-CO_2 system is also performed within the ELEC-NRTL framework. Absorption simulation of CO_2 into aqueous PZ was carried out

at 40 °C with 0.6 M concentration of PZ solution. Distribution of species was evaluated with increasing amount of molar flow rate of CO_2 to attain higher CO_2 loading. In Figure 4.2, the concentrations of PZ, HPZCOO, CO_2, HCO_3^-, $PZCOO^-$, $PZ(COO^-)_2$ and PZH^+ were represented along with amount of CO_2 loaded, and the simulation results are put side by side by an experimental result from a literature study. As seen, the simulation results are in good agreement with the experimental study in the literature.

As CO_2 loading is increased, the neutral PZ concentration was observed to decrease since PZ reacts to form various ionic species. The concentration of CO_2 is almost zero up to a CO_2 loading of 1 since all CO_2 system can be chemically absorbed up by aqueous PZ solution up to a CO_2 loading of 1. Beyond CO_2 loading of 1, it is seen that CO_2 concentration increases as the solution cannot absorb CO_2 further. Concentrations of protonated PZ carbamate (H^+PZCOO^-) and HCO_3^- gradually increase as more CO_2 is absorbed in system. Concentration of PZH^+ reaches a maximum around a CO_2 loading of 0.6, then decreases with CO_2 loading. $PZ(COO^-)_2$ (piperazine dicarbamate) and $PZCOO^-$ (piperazine carbamate) concentrations reaches a maximum as CO_2 loading is increased, then decreases to zero at around a CO_2 loading of 1.

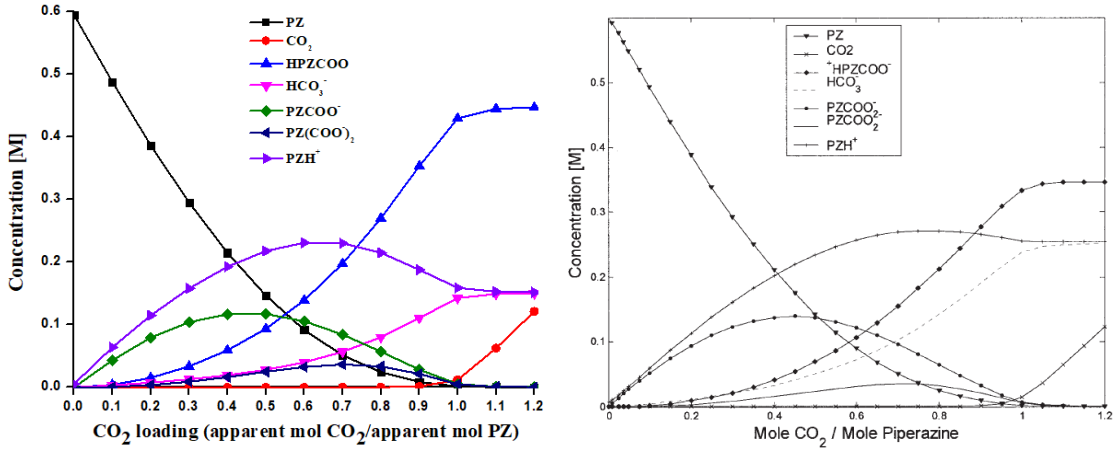

Figure 4.2 Speciation validation of a 0.6 M PZ solution at 40 °C (left: obtained from simulations, right: obtained from literature) [71]

4.3. Absorber Design

In this section, process design, calculations and their results related to absorber design are presented.

4.3.1. CO_2 Loading

LEANIN stream goes into absorber from top of the column while the FLUEGAS stream goes into column from the last stage (bottom). The FLUEGAS consists of CO_2 (15% mol) and N_2 (85% mol) gases. To simulate inlet gas, a literature standard of 1.5 bar pressure and 25 °C temperature is used. LEANIN stream consists of H_2O (3.37482 mol/min) and MEA or PZ (0.479241 mol/min). It has a pressure of 1.7 bar and a temperature of 40 °C. 1.7 bar value is chosen for LEANIN stream because that pressure value is found to be the minimum pressure that rate-based calculations in the absorber is possible in the Aspen Plus simulations.

The metric used for assessing the effect of CO_2 loading in amine solutions on absorption performance is selected as the absorption efficiency. The absorption efficiency of the amine solution is calculated from Equation 1 shown below [108]. While calculating the absorption efficiency, apparent mass flow rate values are used.

$$Absorption\ Efficiency = \frac{(CO_2\ Inflow) - (CO_2\ Outflow)}{(CO_2\ Inflow)} \quad \text{Eqn. 1}$$

Figure 4.3 shows the absorption efficiency versus CO_2 loading in MEA solution at different FLUEGAS pressures, namely 1.5 bar, 2 bar, 3 bar and 4 bar. CO_2 loading in MEA solution is ranged between 0 and 0.6. In the simulation, CO_2 amount in the LEANIN stream is incrementally increased to scan the CO_2 loading range. Maximum CO_2 loading in LEANIN stream without any vapor phase is found to be 0.62856. Beyond that value, LEANIN stream is observed to become a liquid-vapor mixture (two-phase mixture), thus, CO_2-saturated. Up to the CO_2 loading of ca. 0.3, the absorption efficiency is almost 1 for all FLUEGAS pressures. For all FLUEGAS pressures, the absorption efficiency decreases after some CO_2 loading. As the pressure increases, absorption efficiency decreases at an earlier CO_2 loading. For example, at 4 bar FLUEGAS pressure, absorption efficiency starts to decrease at 0.3 CO_2 loading, and at 1.5 bar FLUEGAS pressure, absorption efficiency starts to decrease at 0.4 CO_2 loading.

Absorption efficiency versus CO_2 loading in PZ solution at 1.5 bar, 2 bar, 3 bar and 4 bar is illustrated in the Figure 4.4. CO_2 loading is changed between 0 and 0.9 to calculate the efficiency. Maximum loading for PZ without turning into the vapor is 0.9456.

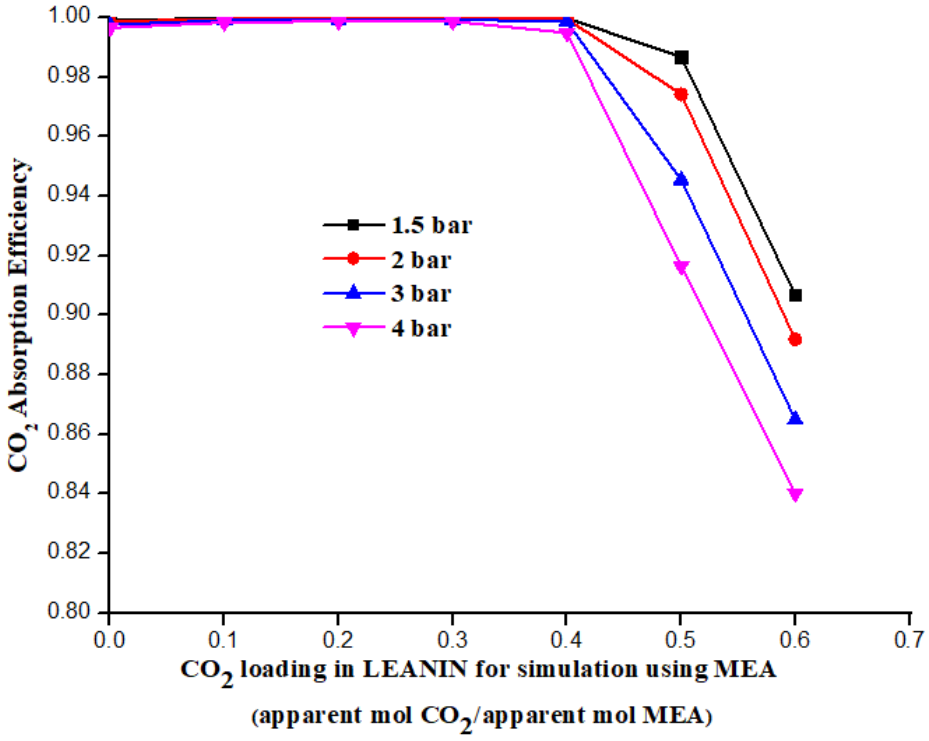

Figure 4.3 Absorption efficiency versus CO_2 loading in MEA solution for 1.5 bar, 2 bar, 3 bar and 4 bar FLUEGAS pressures

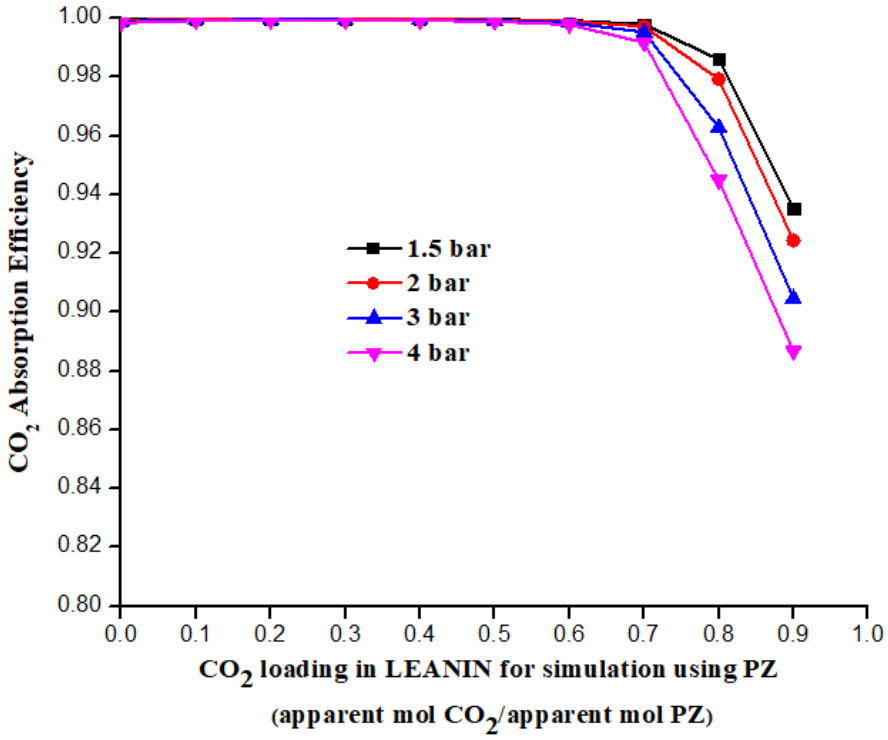

Figure 4.4 Absorption efficiency versus CO_2 loading in PZ solution for 1.5 bar, 2 bar, 3 bar and 4 bar FLUEGAS pressures

Beyond that value, LEANIN becomes a liquid-vapor mixture (two phase mixture), thus, CO_2-saturated. One should note that the maximum CO_2 loading value in PZ solution is larger than that in MEA solution (0.9456 in PZ solution vs. 0.62856 in MEA solution). Another result is that up to the CO_2 loading of ca. 0.5, the absorption efficiency is almost 1 for all FLUEGAS pressures. This behavior is similar to that observed with MEA solution. However, with PZ solution, the limit of CO_2 loading was observed to be higher than that of MEA solution (0.5 CO_2 loading in PZ solution vs. 0.3 CO_2 loading in MEA solution). These two results show the ability of PZ solution to absorb a higher amount of CO_2 compared to MEA solution under the same amine concentrations. Apart from that, for all FLUEGAS pressures, the absorption efficiency decreases after some CO_2 loading, as seen in MEA solution. As the pressure increases, absorption efficiency decreases at an earlier CO_2 loading. For example, at 4 bar FLUEGAS pressure, absorption efficiency starts to decrease at 0.5 CO_2 loading, and at 1.5 bar FLUEGAS pressure, absorption efficiency starts to decrease at 0.7 CO_2 loading.

Comparing the MEA solution and PZ solution results in terms of absorption efficiency, it is seen that the maximum absorption efficiencies are obtained at lower CO_2 loadings, as low as zero CO_2 loading. From these two graphs, it is understood that it is not required to add CO_2 into the LEANIN stream. If MEA and PZ solvents are compared, CO_2 absorption efficiency of PZ solution is found to be higher than that of MEA solution. As a practical outcome, it is chosen to use zero CO_2 loading in LEANIN stream for both MEA and PZ solutions in the simulations.

4.3.2. LEANIN Temperature

The effect of temperature of LEANIN stream on the CO_2 absorption efficiency is studied for both MEA solution and PZ solution. While keeping the FLUEGAS temperature constant at 25 °C, the LEANIN temperature is changed between 20 °C and 60 °C.Figure 4.5 shows CO_2 absorption efficiency of MEA solution versus LEANIN temperature for different FLUEGAS pressures. For all LEANIN temperatures, the absorption efficiency is found to be very high, almost 1. For all pressures, the absorption efficiency is found to increase a little bit with decreasing FLUEGAS pressure. The increase in absorption efficiency with LEANIN temperature is more pronounced at higher FLUEGAS pressures.

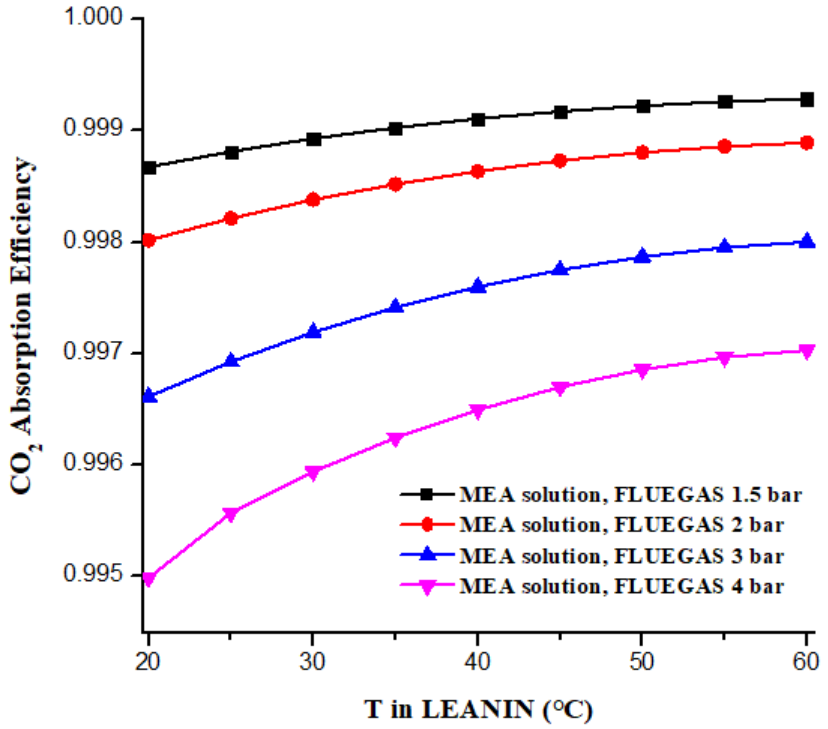

Figure 4.5 Absorption efficiency versus LEANIN temperature in MEA solution for 1.5 bar, 2 bar, 3 bar and 4 bar FLUEGAS pressures

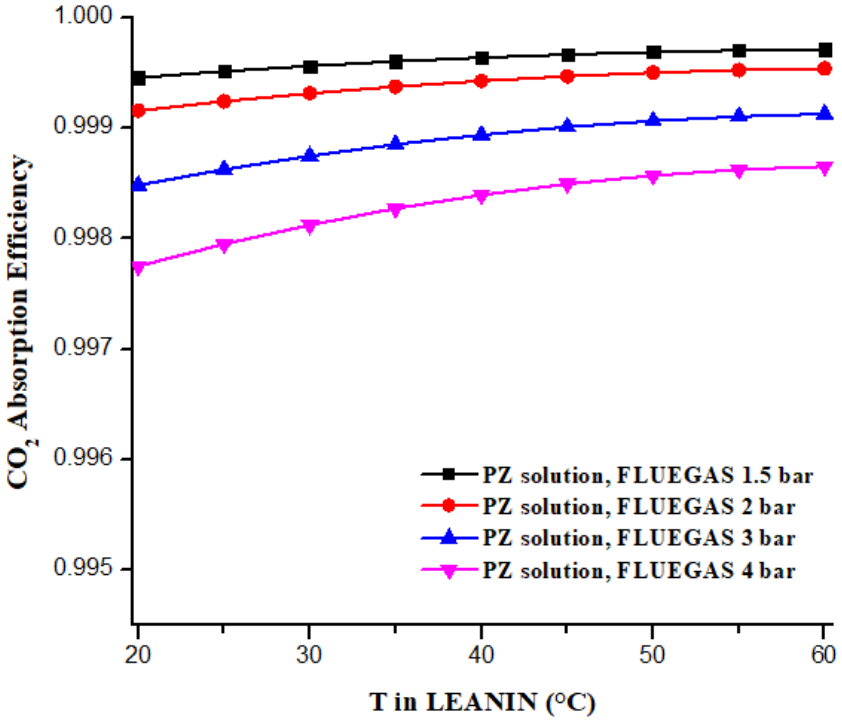

Figure 4.6 Absorption efficiency versus LEANIN temperature in PZ solution for 1.5 bar, 2 bar, 3 bar and 4 bar FLUEGAS pressures

Figure 4.6 shows CO_2 absorption efficiency of PZ solution versus LEANIN temperature for different FLUEGAS pressures. For all LEANIN temperatures, the absorption efficiency is found to be very high, almost 1, a trend which is similar to the one observed with MEA solution. As in MEA solution, for all pressures, the CO_2 absorption efficiency of PZ solution is found to increase a little bit with decreasing FLUEGAS pressure. And again, the increase in absorption efficiency with LEANIN temperature is more pronounced at higher FLUEGAS pressures. Only noticeable difference is that the lowest CO_2 absorption efficiency at 4 bar FLUEGAS pressure is a bit higher in PZ solution compared to MEA solution (ca. 0.998 in PZ solution vs. ca. 0.995 in MEA solution).

Although we see changes in CO_2 absorption efficiency with LEANIN temperatures for both MEA and PZ solutions, the magnitude of change is very small; thus, we can assume that the CO_2 absorption efficiency is almost independent of the LEANIN temperature. As a practical result of these analyses, an intermediate temperature of 40°C is chosen as the temperature of LEANIN stream to be used in the simulations.

4.3.3. Column Diameter and Height

The diameters of the absorber and stripper columns are calculated automatically using Aspen Plus to provide a good hydraulics inside the columns. The diameter of absorption column is obtained as 0.015 m for both open and closed loop simulations.

The height of the absorber column is not automatically calculated in Aspen Plus. In order to decide on the height of the absorber column, the apparent CO_2 mole fraction in RICHOUT stream is monitored for different packed heights. For both MEA solution and PZ solution, packed height of absorber column is changed between 0.1 meter and 1 meter, and the corresponding CO_2 mole fraction in RICHOUT stream is calculated. Also, the variation in CO_2 mole fraction in RICHOUT stream with FLUEGAS pressure is analyzed.

Figure 4.7 shows the apparent CO_2 mole fraction in RICHOUT stream versus packed height using MEA solution. As seen, the apparent CO_2 mole fraction increases up to a packed height, then stays constant with further increase in packed height. The trend is valid for all pressures. Another result is that higher apparent CO_2 mole fractions are observed at higher FLUEGAS pressures.

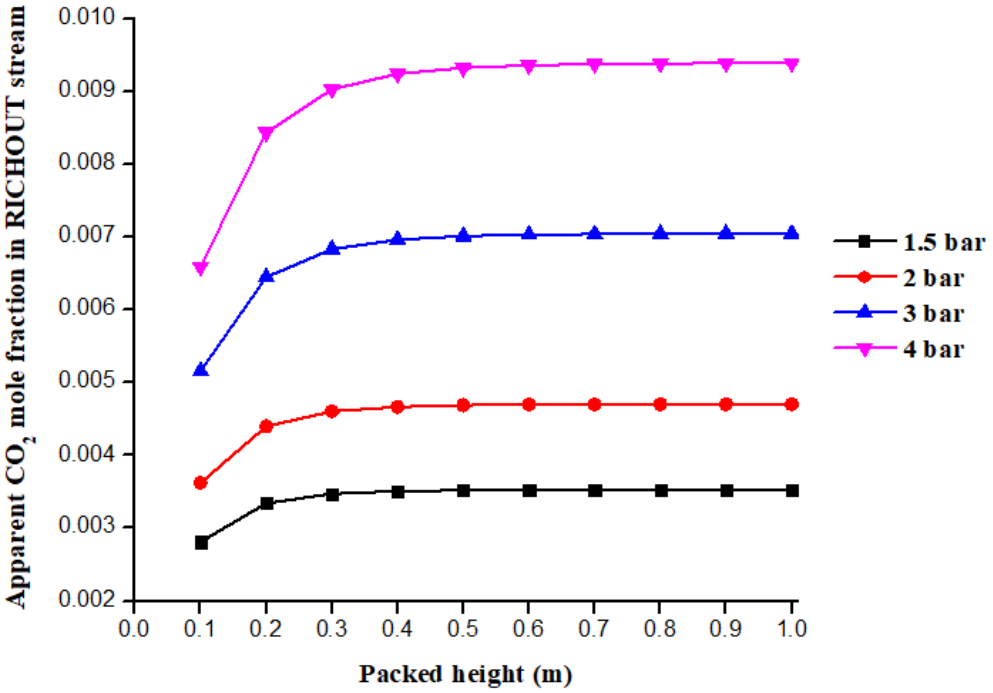

Figure 4.7 Apparent CO_2 mole fraction in RICHOUT stream versus packed height of absorber at 1.5 bar, 2 bar, 3 bar and 4 bar FLUEGAS inlet pressures with MEA solution

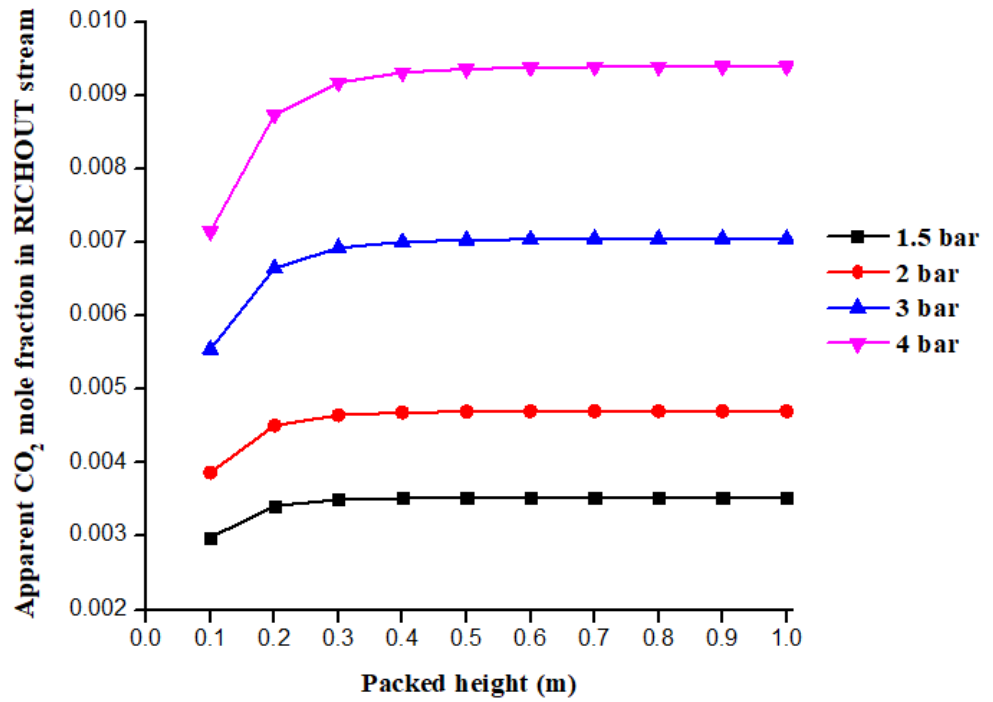

Figure 4.8 Apparent CO_2 mole fraction in RICHOUT stream versus packed height of absorber at 1.5 bar, 2 bar, 3 bar and 4 bar FLUEGAS inlet pressures with PZ solution

Figure 4.8 shows the apparent CO_2 mole fraction in RICHOUT stream versus packed height using PZ solution. Similar to MEA solution, the apparent CO_2 mole fraction increases up to a packed height, then stays constant with further increase in packed height with PZ solution. Again, the trend is valid for all pressures. Also, higher apparent CO_2 mole fractions are observed at higher FLUEGAS pressures, as in MEA solution.

Considering both solutions, PZ solution shows a bit better performance than MEA in terms of capturing CO_2 in RICHOUT stream. Thus, as a practical result of the analysis above, an intermediate value of 0.6 m as the height of the absorber is chosen.

4.3.4. Molality of Amine Solutions

Molality of amines in the amine solutions is an important metric to study. From a reaction rate point of view, it can be predicted higher molal concentration of amine implies higher CO_2 capture rates in the absorber and more efficient separation with absorption [27]. However, this prediction does not take the mass transfer rate into account. The situation can be explained using MEA solution as follows. Currently, approximately 30 wt% MEA is considered as the benchmark solution for aqueous amine absorption/stripping (30 wt% MEA corresponds to 7 m MEA solution where m stands for molality). The improvement coming from a higher concentration of MEA disappears at concentrations higher than 35 wt%, because the viscosity of the solution increases up to a point that the diffusivity of CO_2 in Equation 2 decreases and the mass transfer rates start decreasing as shown in Equation 3 (In Equation 2, D_{CO2} is the diffusivity of CO_2 in gas phase, $D_{CO2,water}$ is the diffusivity of CO_2 in water, μ_{water} is the viscosity of water, $\mu_{solution}$ is the viscosity of water and in Equation 3, N_{CO2} is the flux of CO_2 , $k_{MEA\text{-}CO2}$ is the rate constant of the reaction between MEA and CO_2, $[MEA]_i$ is the concentration of MEA at the interface, P_{CO2},i is partial pressure of CO_2 at the interface, P^*_{CO2},i is the equilibrium vapor pressure of CO_2 at the interface, γ_{CO2} is the activity coefficient of CO_2 and H_{CO2} is the Henry's constant of CO_2) [109].

$$D_{CO_2} = D_{CO_{2,water}} \left(\frac{\mu_{water}}{\mu_{solution}}\right)^{0.545} \quad \text{Eqn. 2}$$

$$N_{CO_2} = \sqrt{k_{MEA-CO2} * [MEA]_i * D_{CO_2}} \frac{(P_{CO_{2,i}} - P^*{}_{CO_{2,i}})}{(\gamma H)_{CO_2}} \quad \text{Eqn. 3}$$

The molalities and corresponding viscosities of amine solutions are shown in Table 4.1-4.2.

Table 4.1 MEA molar flow rate, molality of MEA solution and viscosity of MEA solution where H_2O flow rate is 3.37482 mol/min. Temperature is 40°C and pressure is 1.7 bar (as in LEANIN stream conditions)

MEA Molar Flow Rate (mol/min)	Molality of MEA in solution (mol/kg)	Viscosity of MEA solution (cP)
0	0.000	0.671
0.1	1.645	0.795
0.2	3.290	0.971
0.3	4.934	1.191
0.4	6.579	1.445
0.5	8.224	1.725
0.6	9.869	2.026
0.7	11.513	2.341
0.8	13.158	2.662
0.9	14.803	2.986
1	16.448	3.308

Table 4.2 PZ molar flow rate, molality of PZ solution and viscosity of PZ solution where H_2O flow rate is 3.37482 mol/min. Temperature is 40°C and pressure is 1.7 bar (as in LEANIN stream conditions)

PZ Molar Flow Rate (mol/min)	Molality of PZ in solution (mol/kg)	Viscosity of PZ solution (cP)
0	0.000	0.671
0.1	1.645	0.680
0.2	3.290	0.687
0.3	4.934	0.693
0.4	6.579	0.697
0.5	8.224	0.702

(cont. on next page)

Table 4.2 (cont.)

0.6	9.869	0.705
0.7	11.513	0.708
0.8	13.158	0.711
0.9	14.803	0.713
1	16.448	0.715

The other reason why the process is never operated at concentrations higher than 35 wt% is that MEA becomes highly corrosive when concentrated [27].

We studied the effect of amine solution molality in LEANIN stream on absorbance performance by comparing apparent CO_2 mole fraction in RICHOUT streams at different amine solution molalities. Figure 4.9 shows the apparent CO_2 mole fraction in RICHOUT stream versus MEA molality in LEANIN stream at different FLUEGAS pressures.

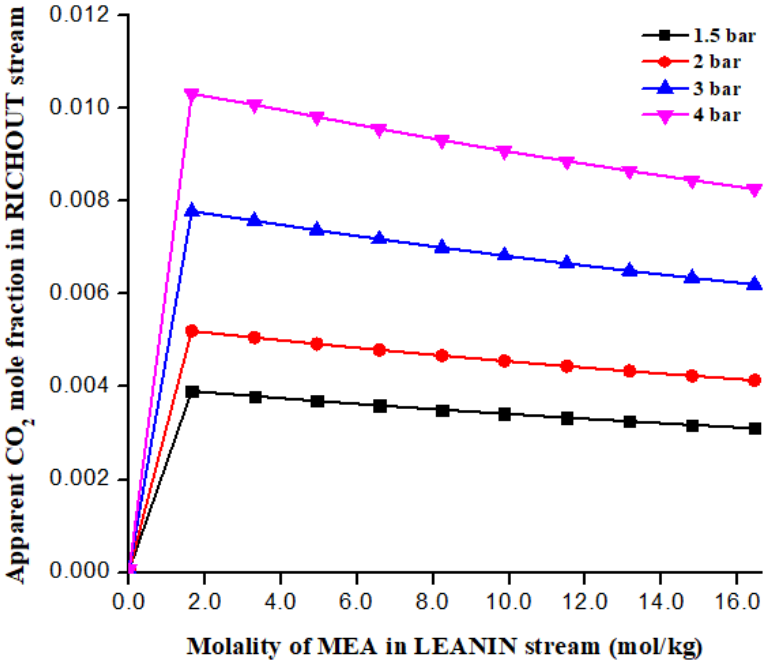

Figure 4.9 Apparent CO_2 mole fraction in RICHOUT stream versus molality of MEA in LEANIN stream at 1.5 bar, 2 bar, 3 bar and 4 bar FLUEGAS pressures

As seen, the apparent CO_2 mole fraction in RICHOUT stream first increases as we introduce the MEA into LEANIN stream, reaches a peak value, then decreases with

increasing MEA solution molality. This is due to increased viscosity of the MEA solution at higher molalities. As the pressure in FLUEGAS increases, higher RICHOUT mole fractions are observed. This trend can be explained by higher physical solubility of CO_2 in MEA solution at higher FLUEGAS pressures. A similar trend is observed for PZ solutions, as shown in Figure 4.10.

LEANIN stream in amine solution simulations consists of only amine (either MEA or PZ) and H_2O. There is not any CO_2 inside of it. MEA or PZ has a molar flow rate of 0.479241 mol/min. H_2O has molar flow rate of 3.37482 mol/min. Apparent mass fraction of MEA in LEANIN stream is 0.325 (32.5 wt% MEA in LEANIN stream). According to analysis of CO_2 diffusion coefficient, corrosive behavior mentioned above, and apparent CO_2 mole fraction in RICHOUT stream, a 32.5 wt% MEA solution used in our simulations is found to be in the safe region of operation. Currently, 40 wt% PZ solution is considered as a benchmark among next-generation solvents for amine scrubbing in the literature (40 wt% PZ corresponds to 8 m PZ solution where m stands for molality) [22,24]. Thus, the selected PZ concentration in LEANIN stream is in accordance with literature.

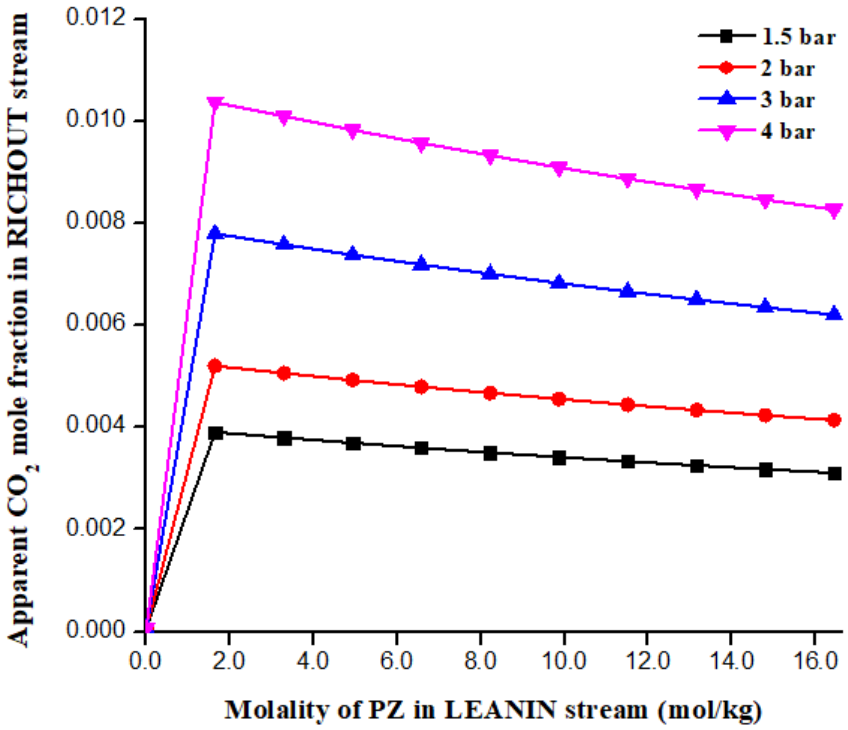

Figure 4.10 Apparent CO_2 mole fraction in RICHOUT stream versus molality of PZ in LEANIN stream at 1.5 bar, 2 bar, 3 bar and 4 bar FLUEGAS pressures

As seen in Figure 4.9 and Figure 4.10, there is a steep increase in the apparent CO_2 mole fraction in RICHOUT stream between 0 m and ca. 2 m for MEA and PZ solutions. In order to resolve this change, simulations were performed between 0 m and 1 m. This analysis might help for understanding the minimum amount of amine that can be used for CO_2 capture in absorber column.

Figure 4.11 shows the apparent CO_2 mole fraction in RICHOUT versus MEA molality in LEANIN stream at different FLUEGAS pressures. As seen, the apparent CO_2 mole fraction in RICHOUT tend to increase with increased MEA molality. For FLUEGAS pressures of 1.5 bar, 2 bar, and 3 bar, the apparent CO_2 mole fraction first increases with MEA molality, then reaches a plateau. For 4 bar FLUEGAS pressure, a continuous increase in apparent CO_2 mole fraction in RICHOUT stream is observed. This might be due to effect of pressure on the physical solubility of MEA.

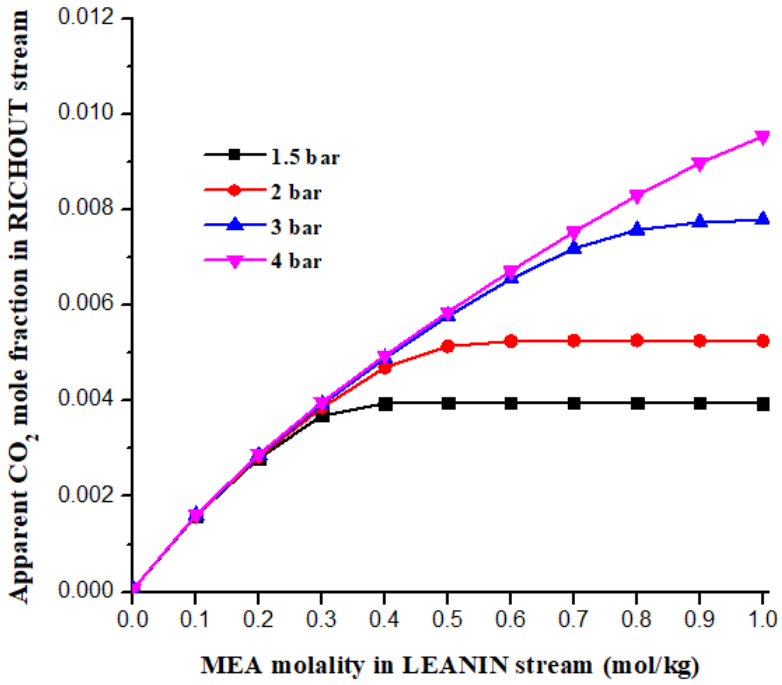

Figure 4.11 Close-up of apparent CO_2 mole fraction in RICHOUT stream versus molality of MEA in LEANIN stream at 1.5 bar, 2 bar, 3 bar and 4 bar FLUEGAS pressures

Figure 4.12 shows the apparent CO_2 mole fraction in RICHOUT versus PZ molality in LEANIN stream at different FLUEGAS pressures. Unlike the MEA case, in PZ case, we see that the apparent CO_2 mole fraction in RICHOUT first increases, then

reaches a plateau with increased MEA molality for all FLUEGAS pressures. Also, the obtained apparent CO_2 mole fractions in RICHOUT stream are higher than that in MEA case. This shows a higher amount of CO_2 absorption is possible using PZ solutions compared to MEA solutions. From the analysis of Figure 4.11 and Figure 4.12, it can be concluded that the minimum amount of amine for CO_2 capture is governed by FLUEGAS pressure.

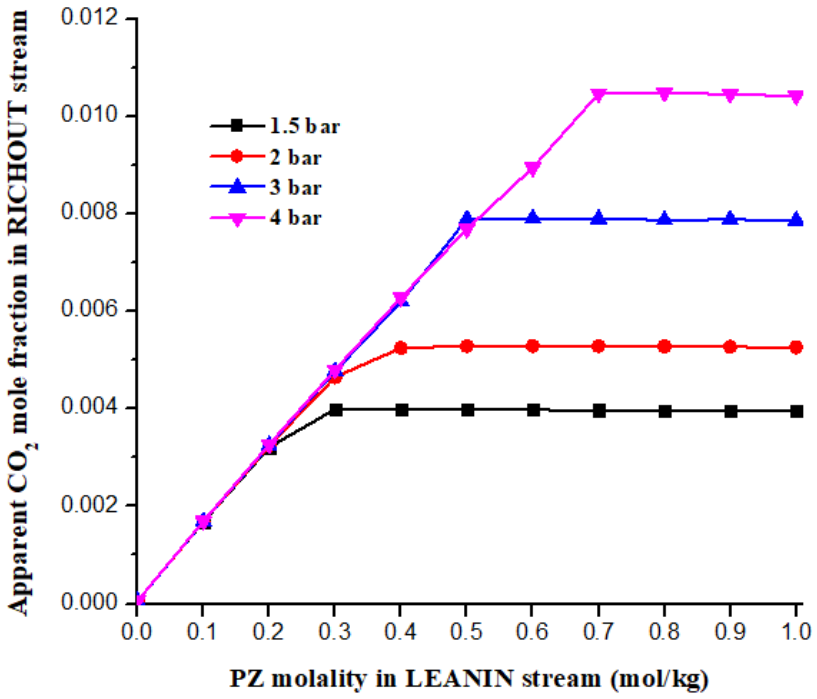

Figure 4.12 Close-up of apparent CO_2 mole fraction in RICHOUT stream versus molality of PZ in LEANIN stream at 1.5 bar, 2 bar, 3 bar and 4 bar FLUEGAS pressures

CO_2 capture rate of MEA and PZ solutions versus amine molality are calculated between 0 m and 1 m as well. Related graphs (Figure E.1 and Figure E.2) and calculations are shown in Appendix E.

4.3.5. CO_2 Reaction Rate inside Absorber Column

The CO_2 absorption rate (also can be called as CO_2 reaction rate or capture rate) along with the temperature and pressure inside the absorber column is investigated to understand the absorption behavior over the stages in the absorber column at different FLUEGAS pressures (Note that there are no actual stages in the absorber (or stripper)

columns since they are both packed columns, and what we call stage here is a theoretical means of discretization of column calculations done by Aspen Plus). The absorber contains 10 stages, as explained in Chapter 3.

Figure 4.13 shows the temperature inside the absorber column and CO_2 reaction rate using MEA solution versus stage (1: top, 10: bottom) of absorber at 1.5 bar, 2 bar, 3 bar and 4 bar FLUEGAS pressures. The CO_2 reaction (absorption) rate as well as the temperature increase towards the bottom of the column (note that the CO_2 reaction rate is negative since it is being consumed in the reaction). This is expected since the bottom stage has the highest concentration of CO_2. It is because CO_2 is fed at the bottom of the absorber column. Also, CO_2 absorption by amines are exothermic reactions explaining the high temperature at the bottom stage. In addition, higher CO_2 absorption rates and higher temperatures are obtained as the FLUEGAS pressure increases. Temperature change is a bit higher in PZ solution. Similar trends are observed for the PZ solution, as shown in Figure 4.14. It is worth to note that the CO_2 absorption rates are higher in PZ solution illustrating that the reaction kinetics is faster with PZ solutions.

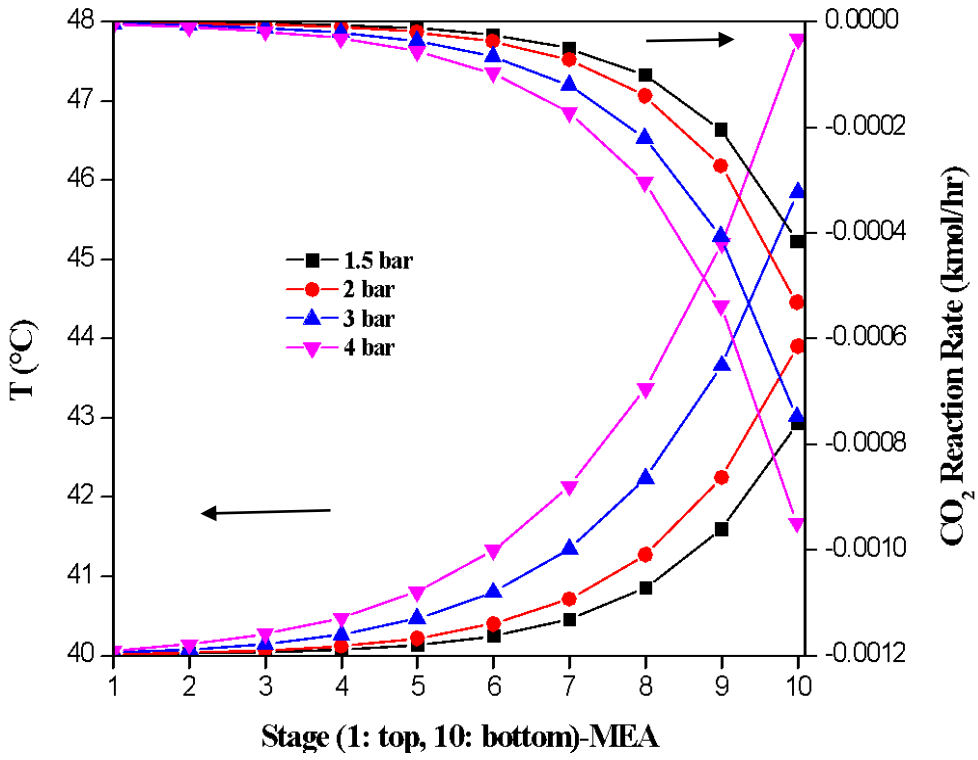

Figure 4.13 Column temperature and CO_2 reaction rate of MEA solution versus stage (1: top, 10: bottom) of absorber at 1.5 bar, 2 bar, 3 bar and 4 bar FLUEGAS pressures

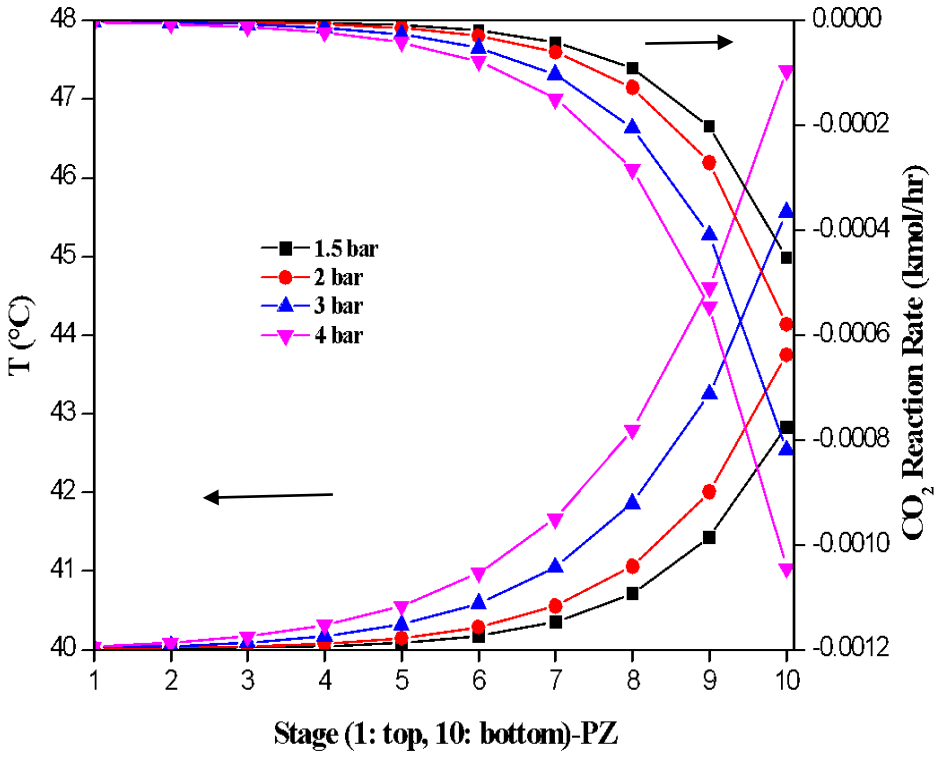

Figure 4.14 Column temperature and CO_2 reaction rate of PZ solution versus stage (1: top, 10: bottom) of absorber at 1.5 bar, 2 bar, 3 bar and 4 bar FLUEGAS pressures

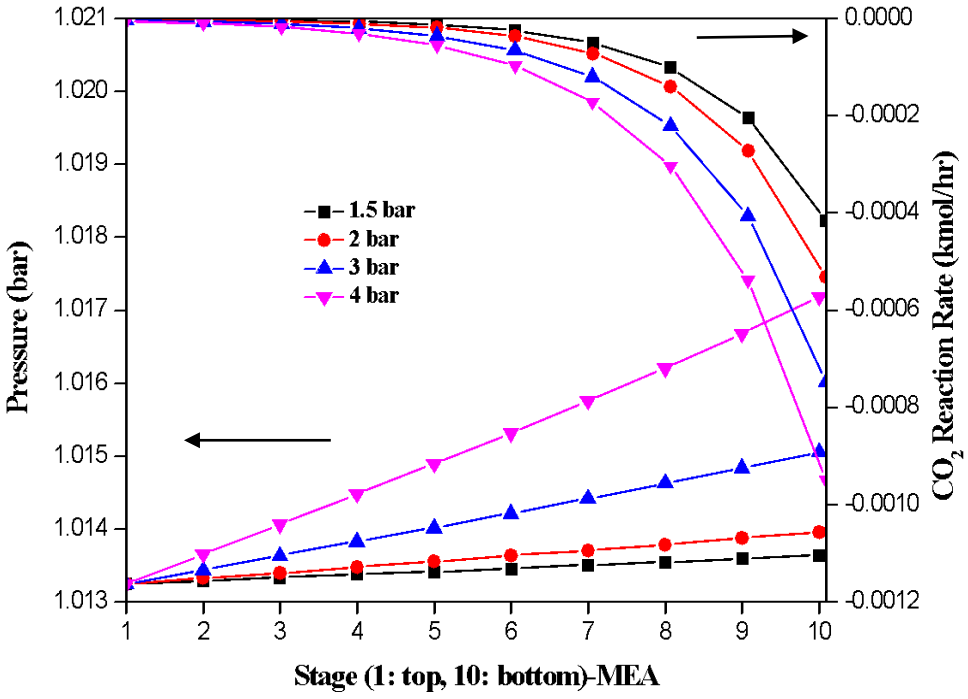

Figure 4.15 Column pressure and CO_2 reaction rate of MEA solution versus stage (1: top, 10: bottom) of absorber at 1.5 bar, 2 bar, 3 bar and 4 bar FLUEGAS pressures

Figure 4.15 shows the column pressure and CO_2 removal rate of MEA solution versus stage (1: top, 10: bottom) of absorber at 1.5 bar, 2 bar, 3 bar and 4 bar FLUEGAS pressures. As it is expected, column pressure and CO_2 reaction rate increases from top to bottom. As seen, pressure profile inside the column is linear. Also, higher CO_2 reaction rates and higher pressures are obtained at higher FLUEGAS pressures. Similar trends are observed for the PZ solution, as shown in Figure 4.16. Again, it is worth to note that the CO_2 absorption rates are higher in PZ solution illustrating that the reaction kinetics is faster with PZ solutions.

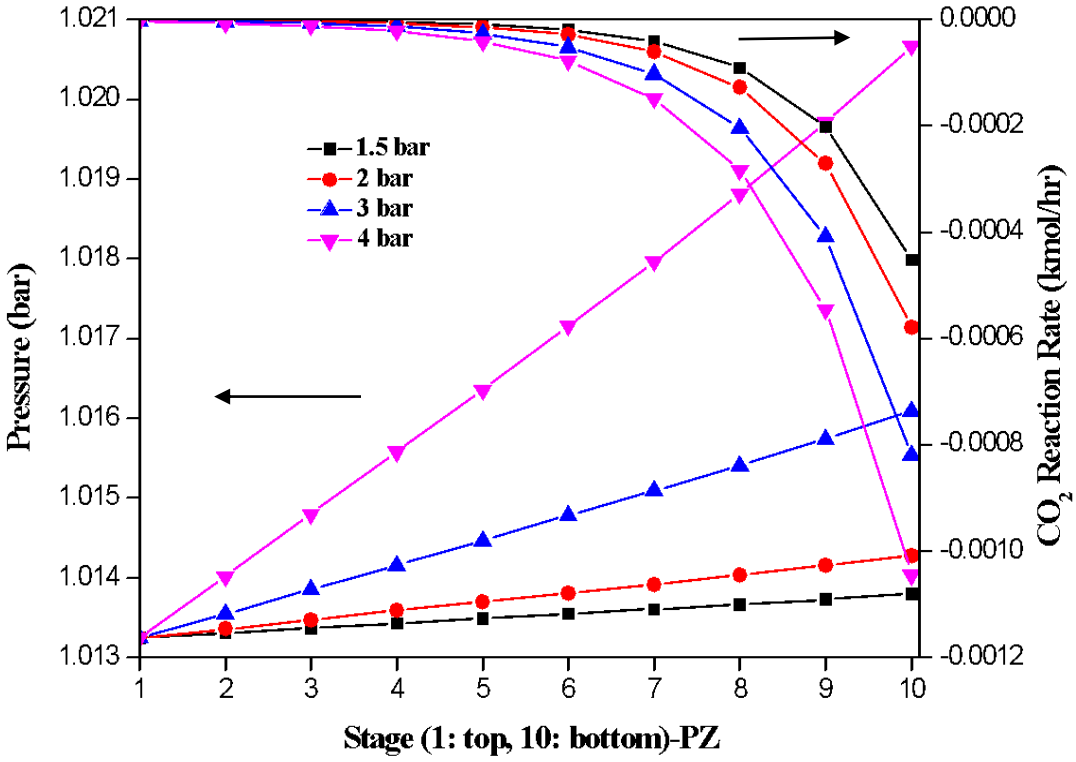

Figure 4.16 Column pressure and CO_2 reaction rate of PZ solution versus stage (1: top, 10: bottom) of absorber at 1.5 bar, 2 bar, 3 bar and 4 bar FLUEGAS pressures

4.3.6. Hydraulic Plots of Absorber Studies

Four representative hydraulic plots of absorber using MEA solution and PZ solution are shown in Figure 4.17 and Figure 4.18, and Figure 4.19 and Figure 4.20, respectively. As seen, the hydraulic plots show good hydrodynamic behavior inside the absorber for the lowest and the highest FLUEGAS pressures. Hydraulic plots for the intermediate pressures for both MEA and PZ solutions are given in Appendix F.

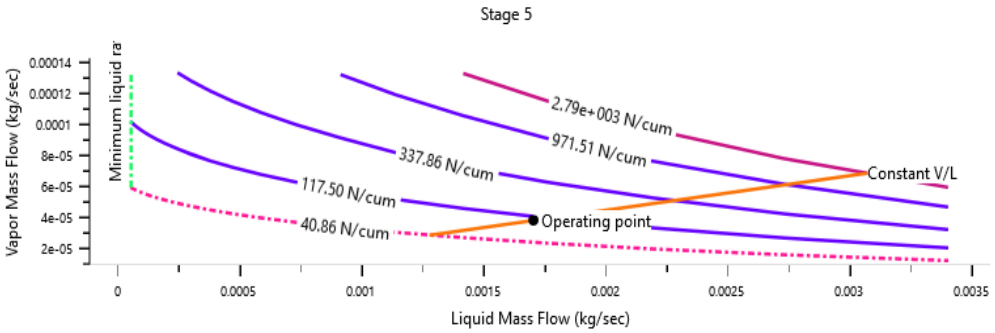

Figure 4.17 Vapor mass flow rate versus liquid mass flow rate inside absorber using MEA solution at 1.5 bar FLUEGAS pressure

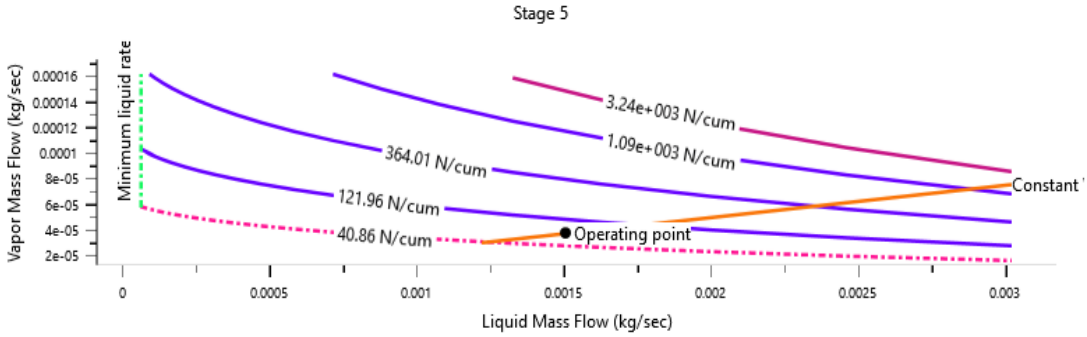

Figure 4.18 Vapor mass flow rate versus liquid mass flow rate inside absorber using PZ solution at 1.5 bar FLUEGAS pressure

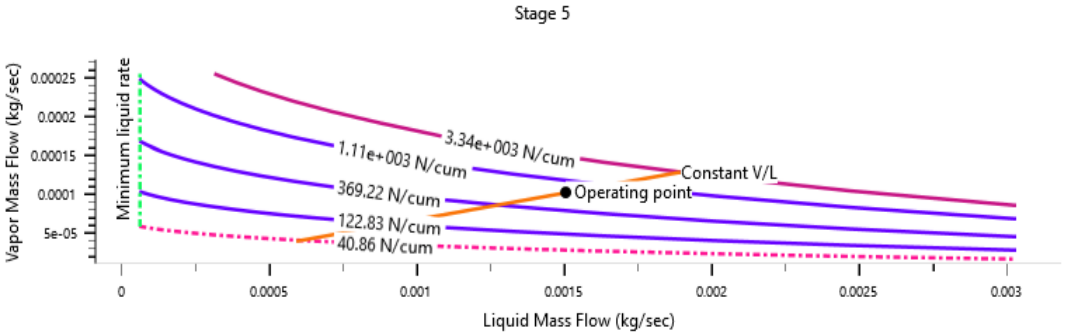

Figure 4.19 Vapor mass flow rate versus liquid mass flow rate inside absorber using MEA solution at 4 bar FLUEGAS pressure

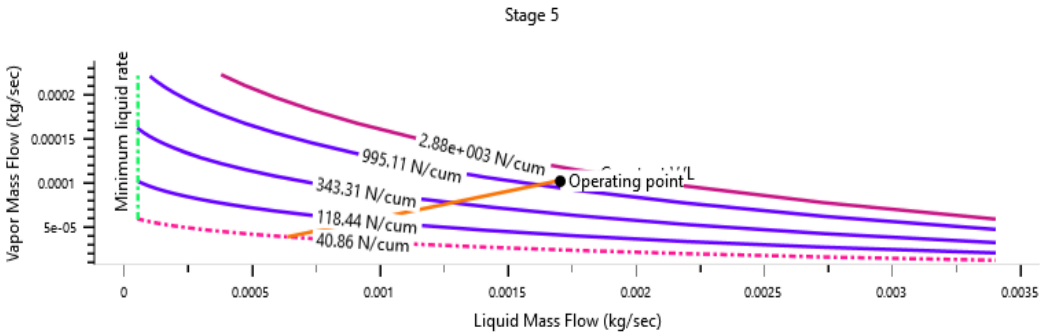

Figure 4.20 Vapor mass flow rate versus liquid mass flow rate inside absorber using PZ solution at 4 bar FLUEGAS pressure

4.4. Open Loop Studies

In the open loop studies, we mainly focused on the stripper operation. A column with a packed height of 2.1 m and a diameter of 0.1 m is selected for the stripper in the open loop studies by doing a similar analysis presented in section 4.3.3. As explained in section 3.4.2, first stage (top) of stripper has a partial-vapor condenser and the bottom stage of stripper has a kettle reboiler. Here, we do a similar type analysis to the stripper column as we did for the absorber column in section 4.3.5.

Figure 4.21 shows the column temperature and CO_2 reaction rate using MEA solution versus stage (1: top, 20: bottom) of STRIPPER column at 1.5 bar, 2 bar, 3 bar and 4 bar FLUEGAS pressures. As seen, the temperature stays almost constant throughout the column, except the top portion where the temperature drops and the bottom portion where the temperature increases. The decrease at the top portion is due to design specification for temperature provided at the top of the column, as explained in section 3.4.2. The increase at the bottom portion is due to the presence of the kettle reboiler at the bottom. FLUEGAS pressure is found to be ineffective in the column temperature.

Regarding the CO_2 reaction rate (which can be called as release rate in the stripper), we see that a higher release rate at the bottom of the stripper (note that the CO_2 reaction rate is positive if CO_2 is released and negative if CO_2 is absorbed). This is again due to presence of the kettle reboiler providing heat that drives the CO_2 release reaction. We also see that CO_2 reaction rate is almost constant throughout most of the stripper column, except a reversal in the CO_2 reaction rate at the top portion of the column

(reversal means the change in the sign of reaction rate). At the top portion of the section, we interestingly see a negative CO_2 reaction rate which indicates CO_2 absorption. That means that at the top of the column where the temperature drops, stripper column acts like an absorber by trying to absorb CO_2. The column tends to absorb as soon as the temperature drops. Little-to-no effect of FLUEGAS pressure is observed on the CO_2 reaction rate.

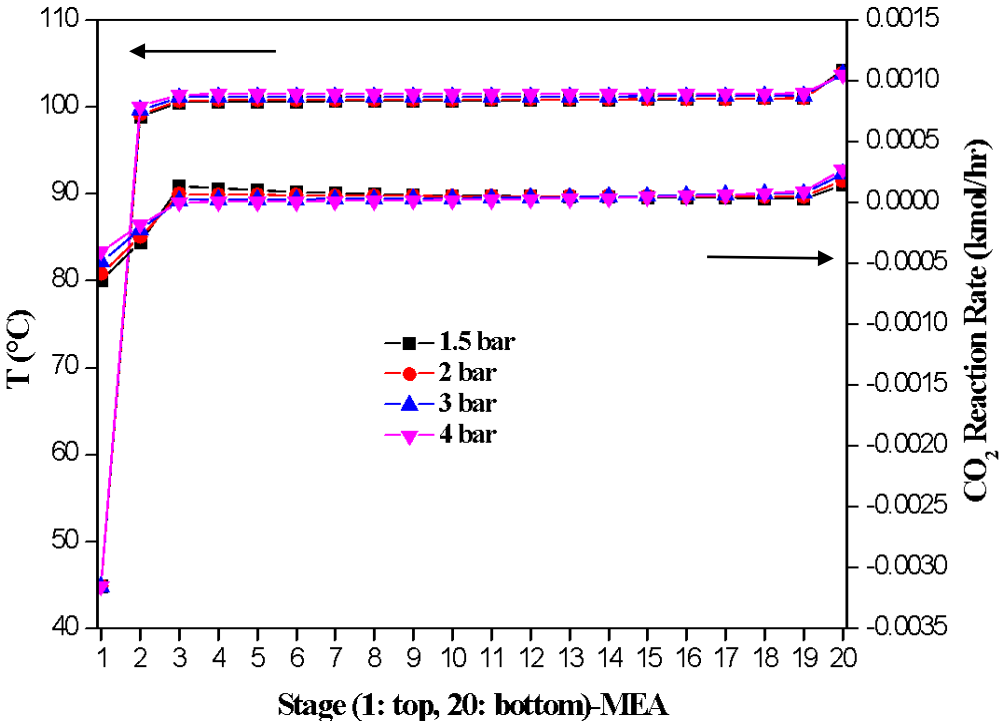

Figure 4.21 Column temperature and CO_2 reaction rate using MEA solution versus stage (1: top, 20: bottom) of stripper at 1.5 bar, 2 bar, 3 bar and 4 bar FLUEGAS pressures in open loop process

A similar trend is observed using PZ solution, as shown in Figure 4.22. The obvious difference is the much-pronounced CO_2 reaction rates at the bottom and at the top of bottom of the stripper column. This shows the faster kinetics of CO_2 reaction in the PZ solution compared to MEA solution.

The major results of stripper column obtained from open loop process are shown in Table 4.3 and Table 4.4, respectively, for MEA solution and PZ solution. These major results include distillate rate, distillate to feed ratio in mass terms, mass reflux rate, bottoms to feed ratio, boil-up ratio, and boil-up rate at different FLUEGAS pressures.

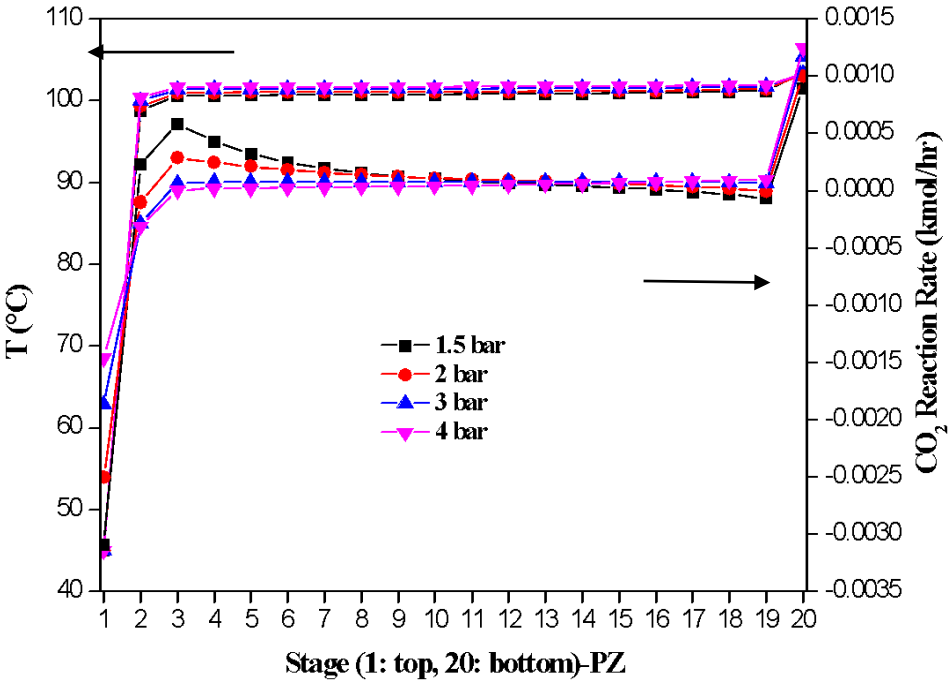

Figure 4.22 Column temperature and CO_2 reaction rate using PZ solution versus stage (1: top, 20: bottom) of stripper at 1.5 bar, 2 bar, 3 bar and 4 bar FLUEGAS pressures in open loop process

As seen in Table 4.3 and Table 4.4, all the metrics decrease with increasing pressure for both MEA and PZ solutions. A striking difference is observed especially in the distillate rate between the amine solutions. In the converged results, it is seen that the distillate rate in the stripper using PZ solution is about 40% higher than that of MEA solution. This is partly due to the fast kinetics of CO_2 release reaction using PZ solution. Another result is that the mass reflux rate, boilup ratio, boilup rate, and bottoms to feed ratio are smaller in PZ solution compared to MEA solution.

Table 4.3 Major results of stripper column in open loop design with MEA solution

MEA				
Inlet gas pressure	**1.5 bar**	**2 bar**	**3 bar**	**4 bar**
Distillate rate (kg/hr)	0.0114	0.0112	0.0109	0.0107
Mass distillate to feed ratio	0.00209	0.00205	0.00199	0.00195
Mass reflux rate	19.654	12.974	7.403	4.837
Mass boilup ratio	4.053	2.681	1.538	1.013
Boilup rate (kg/hr)	21.980	14.566	8.390	5.547
Bottoms to feed ratio	0.99791	0.99794	0.998	0.9981

Table 4.4 Major results of stripper column for open loop design with PZ solution

PZ				
Inlet gas pressure	**1.5 bar**	**2 bar**	**3 bar**	**4 bar**
Distillate rate (kg/hr)	0.0185	0.0172	0.0158	0.0148
Mass distillate to feed ratio	0.00301	0.00280	0.00255	0.00238
Mass reflux rate	14.06108	7.457221	3.989805	2.64267
Mass boilup ratio	2.716	1.441	0.776	0.520
Boilup rate (kg/hr)	16.663	8.856	4.786	3.218
Bottoms to feed ratio	0.99699	0.99719	0.99745	0.99761

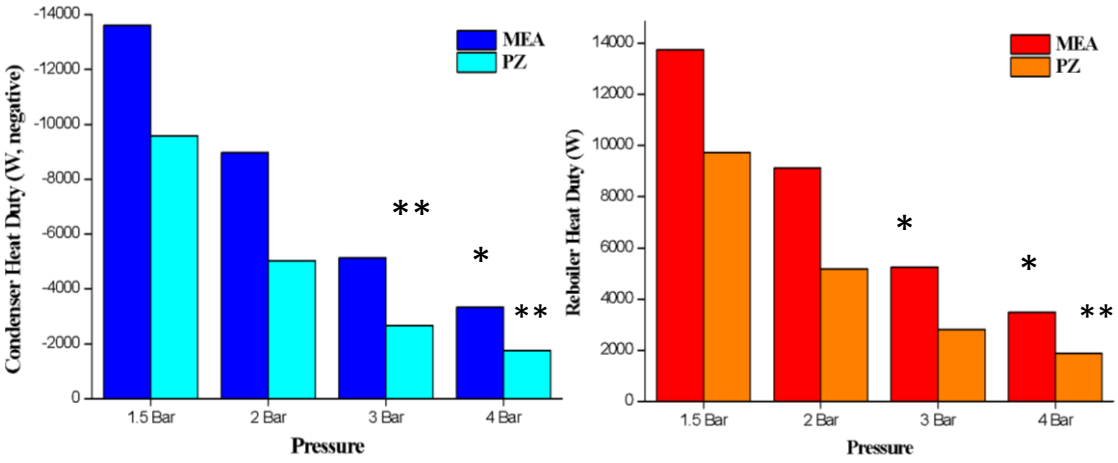

Figure 4.23 a) Condenser duty and b) reboiler duty of MEA and PZ solutions in the stripper in open loop process (*: MEA, **: PZ simulations converged but hydraulic plots are troubled. Flooding occurs inside the column.)

This condition is reflected in heat duty results. Figure 4.23 shows condenser and reboiler duties of MEA and PZ solutions at different FLUEGAS pressures. These are given together to create a clear comparison between bar graphs. As can be seen from graphs, condenser and reboiler duties decrease as the pressure increases. Strikingly, it is observed that use of PZ solution reduced both the condenser and reboiler heat duty at all FLUEGAS pressures. This result might be due to smaller reflux rate and boilup rate observed in the converged results with PZ solution, as mentioned above. Under the given conditions, we can say that PZ solution is more energy efficient than MEA solution in the open loop process.

4.4.1. Hydraulic Plots of Open Loop Studies

Hydraulic plots of open loop studies of MEA and PZ are shown in Figures 4.24-4.27. Stripper column using PZ solution at 3 bar and 4 bar FLUEGAS pressures and stripper column using MEA solution at 4 bar FLUEGAS pressure converge, however have problems regarding column hydraulics. Flooding occurs inside these columns. The reason is that vapor flow is lower than it should be. These problematic hydraulic plots are given in Appendix G. The hydraulics plots given at 1.5 bar and 2 bar FLUEGAS pressures show good column hydraulics.

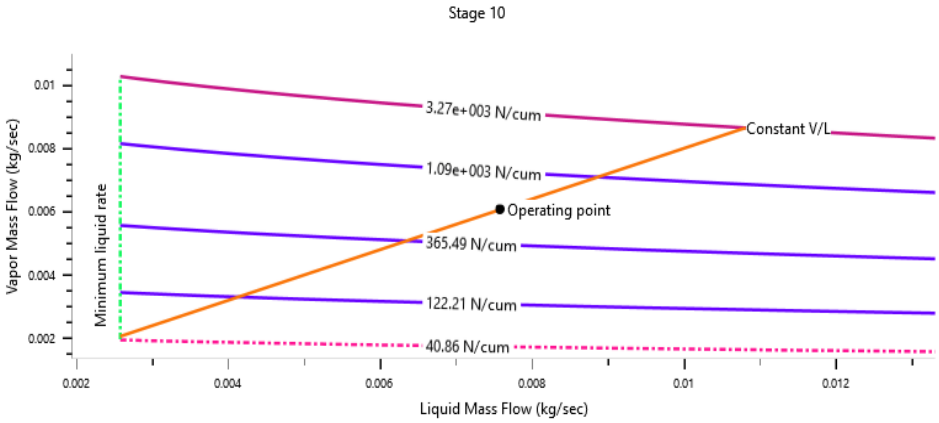

Figure 4.24 Vapor mass flow rate versus liquid mass flow rate inside stripper using MEA solution at 1.5 bar FLUEGAS pressure in open loop process

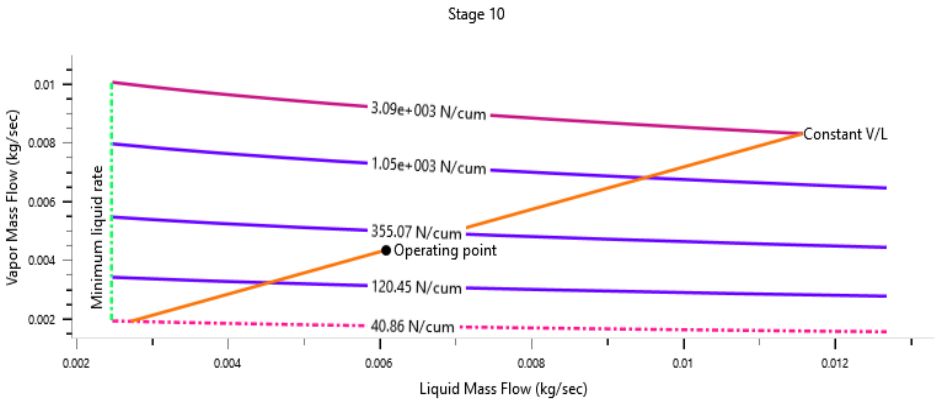

Figure 4.25 Vapor mass flow rate versus liquid mass flow rate inside stripper using PZ solution at 1.5 bar FLUEGAS pressure in open loop process

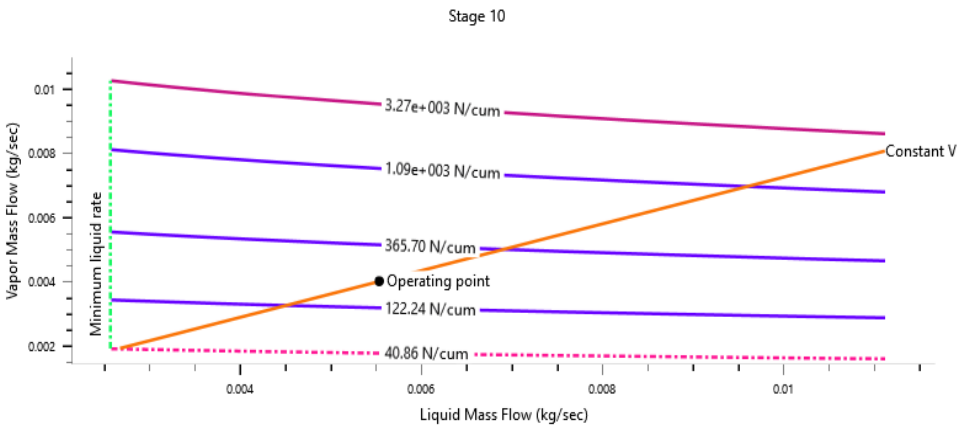

Figure 4.26 Vapor mass flow rate versus liquid mass flow rate inside stripper using MEA solution at 2 bar FLUEGAS pressure in open loop process

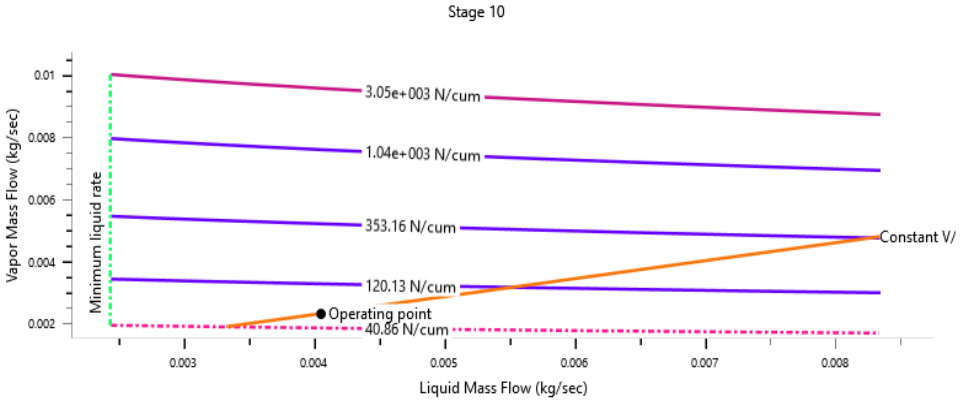

Figure 4.27 Vapor mass flow rate versus liquid mass flow rate inside stripper using PZ solution at 2 bar FLUEGAS pressure in open loop process

4.5. Closed Loop Studies (Recycle Studies)

In the closed loop studies, our focus is again on the stripper operation. The stripper column diameter calculated for closed loop simulations is 0.085 m, and the column height was calculated to be 2.1 m, as explained in section 4.3.3. Here, we have the same configuration of the top and bottom stages of the stripper as in open loop process, i.e. top stage has partial condenser and bottom stage has kettle reboiler. We follow the same line of analyses as the open loop stripper column. It must be pointed out that achieving convergence in closed loop simulations are far more challenging than those in open loop simulations. Figure 4.28 shows the column temperature and CO_2 reaction rate using MEA solution versus stage (1: top, 20: bottom) of STRIPPER column at 1.5 bar, 2 bar, 3 bar and 4 bar FLUEGAS pressures. The temperature and CO_2 reaction rate inside the stripper

in closed loop process resembles closely to that in open loop process, as expected (see Figure 4.23).

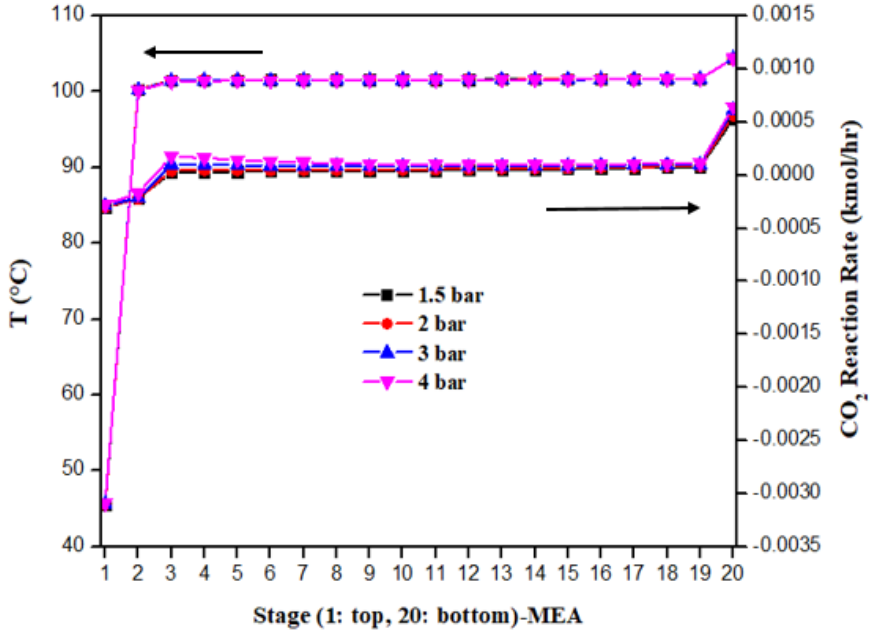

Figure 4.28 Column temperature and CO_2 reaction rate using MEA solution versus stage (1: top, 20: bottom) of stripper at 1.5 bar, 2 bar, 3 bar and 4 bar FLUEGAS pressures in closed loop process

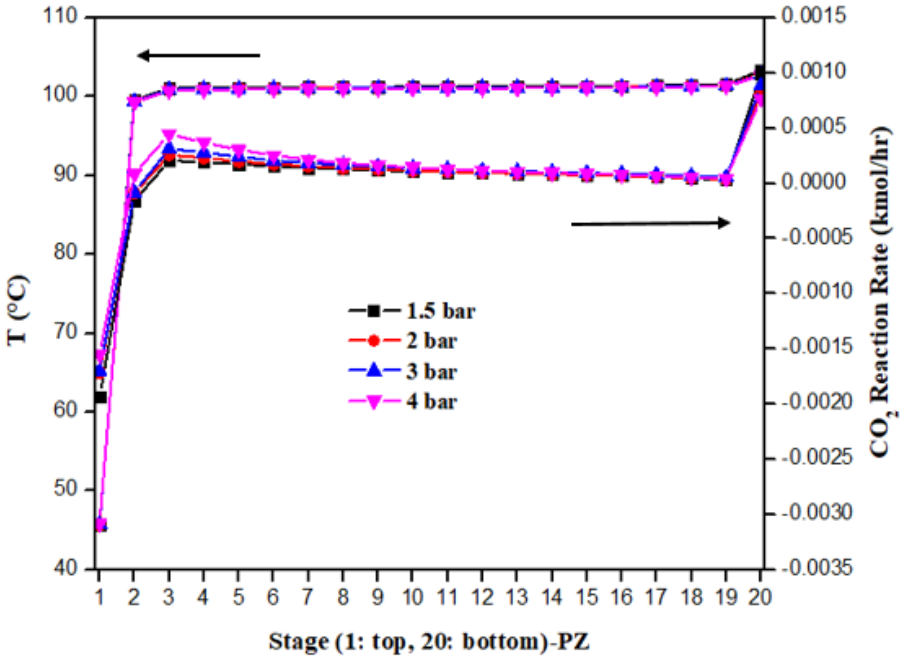

Figure 4.29 Column temperature and CO_2 reaction rate using PZ solution versus stage (1: top, 20: bottom) of stripper at 1.5 bar, 2 bar, 3 bar and 4 bar FLUEGAS pressures in closed loop process

Also, similar trends are observed for PZ solution shown in Figure 4.29 as in open loop process, as expected (see Figure 4.24), although the effect of FLUEGAS pressure on the CO_2 reaction rate is less pronounced in closed loop process compared to open loop process. In both open loop and closed loop processes, the PZ solution is found to provide a higher CO_2 reaction rate at the top and the bottom of the stripper column. This is in part due to faster kinetics with PZ solution.

The major results of stripper column obtained from closed loop process are given in Table 4.5 and Table 4.6, respectively, for MEA solution and PZ solution at different FLUEGAS pressures. As opposed to open loop process, all metrics except the bottoms to feed ratio are found to increase with FLUEGAS pressure. This might be due to the fact that the effect of the FLUEGAS pressure is now continuously present on the process due to recycle streams. Another interesting result is that PZ solution distillate to feed ratio is almost the same as MEA solution (marginally higher, in fact), as opposed to open loop process. One reason might be the fact that the closed loop process required relaxation of design specifications where the variables such as reflux rate can be searched algorithmically by Aspen Plus to achieve convergence. Remember that only one design specification of CO_2 mole purity of 0.9 is used with the corresponding variable of distillate to feed ratio in closed loop process where the reflux ratio is held constant (On the other hand, two design specifications are used in the open loop process, see sections 3.4.2 and 3.4.3). The constant reflux ratio can be seen in Table 4.5 and Table 4.6. Although the PZ solution has a faster CO_2 reaction kinetics as we showed above, it does not manifest itself in closed loop process due to different design specifications in the closed loop process.

Table 4.5 Major results of stripper column in closed loop design with MEA solution

MEA				
Inlet gas pressure	**1.5 bar**	**2 bar**	**3 bar**	**4 bar**
Distillate rate (kg/hr)	0.0378	0.0500	0.0752	0.1002
Mass distillate to feed ratio	0.00683	0.00902	0.013510	0.01793
Mass reflux rate	5	5	5	5
Mass boilup ratio	1.044	1.047	1.053	1.059
Boilup rate (kg/hr)	5.746	5.757	5.782	5.807
Bottoms to feed ratio	0.99317	0.99098	0.98650	0.98201

Table 4.6 Major results of stripper column in closed loop design with PZ solution

PZ				
Inlet gas pressure	**1.5 bar**	**2 bar**	**3 bar**	**4 bar**
Distillate rate (kg/hr)	0.0376	0.0502	0.0754	0.1004
Mass distillate to feed ratio	0.00677	0.00903	0.01235	0.01790
Mass reflux rate	5	5	5	5
Mass boilup ratio	1.083	1.078	0.992	1.087
Boilup rate (kg/hr)	5.977	5.952	5.978	5.989
Bottoms to feed ratio	0.99323	0.99097	0.98764	0.98210

The heat duties of condenser and reboiler in the stripper column using MEA and PZ solutions in closed loop process are compared in Figure 4.30 at different FLUEGAS pressures. The effect of pressure is found to be negligible as opposed to open loop process for both amine solutions. This might be related to the constant mass reflux rate used in the simulations. Even though same reflux rates are used, the PZ solution is still found to have lower heat duties (although marginally) in both condenser and reboiler in closed loop compared to that in MEA solution. This indicates that PZ is found to be more energy efficient in both open loop and closed loop studies.

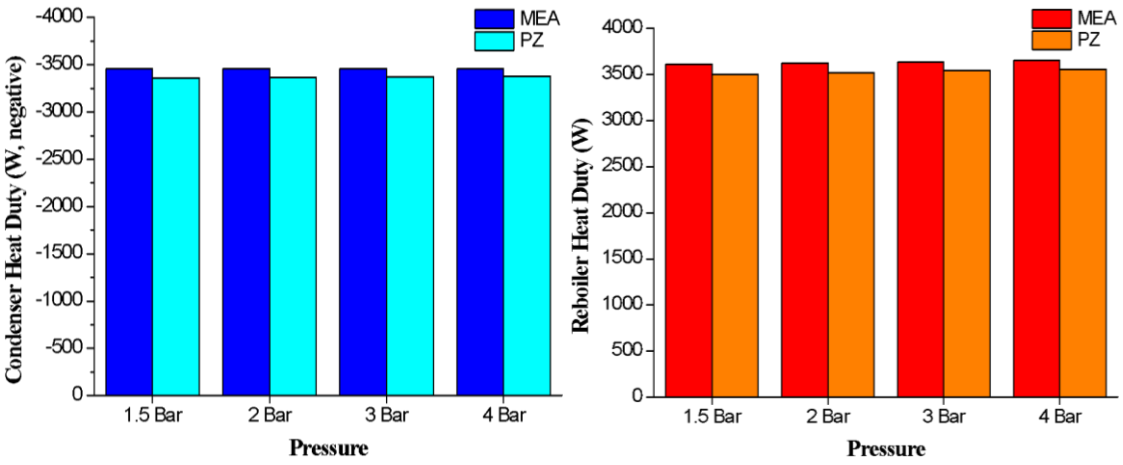

Figure 4.30 a) Condenser duty and b) reboiler duty of MEA and PZ solutions in the stripper in closed loop process

4.5.1. Hydraulic Plots of Closed Loop Studies

Representative hydraulic plots of stripper columns in closed loop studies are shown in Figure 4.31-4.34. In general, the hydraulics of stripper columns are fine. A slight

flooding occurs at 4 bar FLUEGAS pressure columns even though hydraulics seems to work properly. Also, 2 bar and 3 bar studies are given in Appendix H.

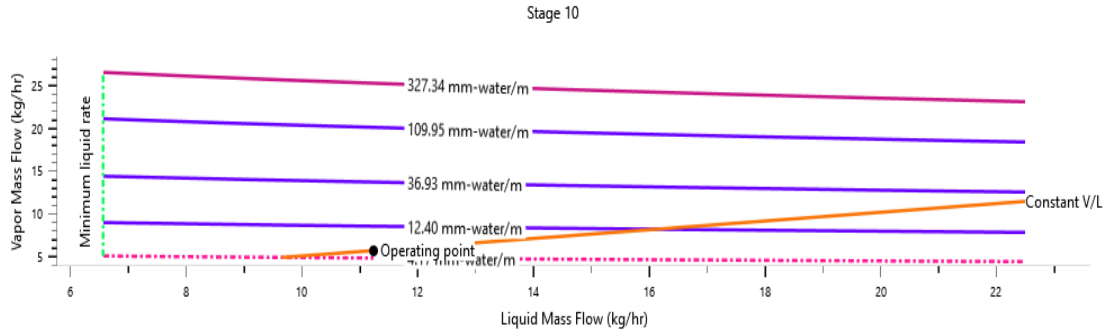

Figure 4.31 Vapor mass flow rate versus liquid mass flow rate inside stripper using MEA solution at 1.5 bar FLUEGAS pressure in closed loop process

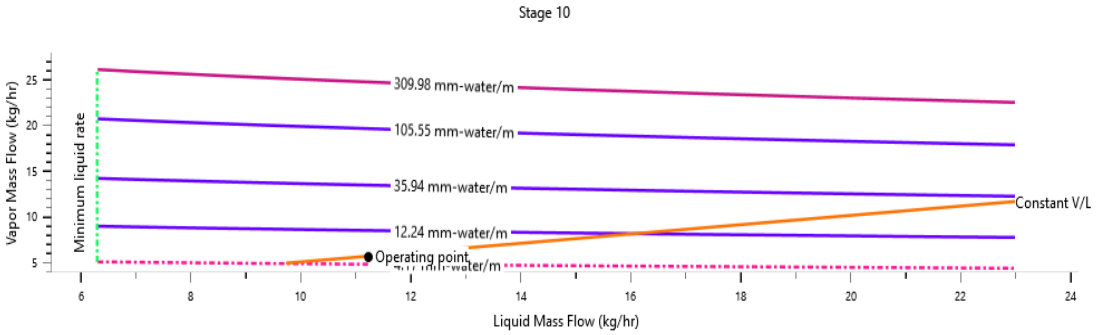

Figure 4.32 Vapor mass flow rate versus liquid mass flow rate inside stripper using PZ solution at 1.5 bar FLUEGAS pressure in closed loop process

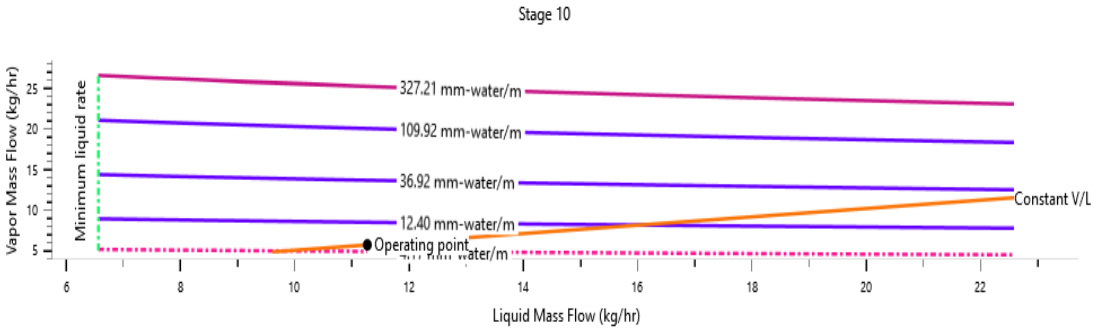

Figure 4.33 Vapor mass flow rate versus liquid mass flow rate inside stripper using MEA solution at 4 bar FLUEGAS pressure in closed loop process

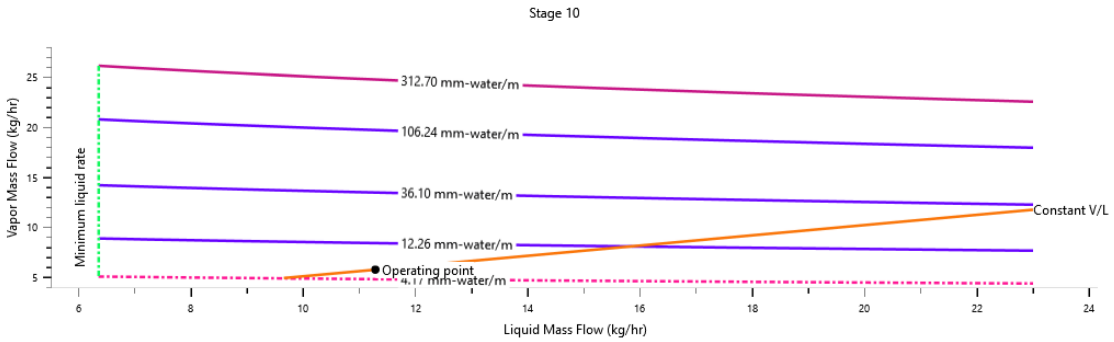

Figure 4.34 Vapor mass flow rate versus liquid mass flow rate inside stripper using PZ solution at 4 bar FLUEGAS pressure in closed loop process

CHAPTER 5

CONCLUSION AND RECOMMENDATIONS

This thesis study investigated the design and simulation of laboratory scale, post-combustion CO_2 capture process using Aspen Plus software. The following conclusions were reached based on results obtained.

- Speciation in MEA-CO_2-H_2O and PZ-CO_2-H_2O systems obtained by simulations can be validated by comparison with literature data.
- PZ absorbs higher amount of CO_2 than MEA.
- PZ solution has faster CO_2 reaction kinetics than MEA solution.
- PZ solution is more energy efficient than MEA solution under the given conditions in both open loop and closed loop processes.
- Achieving convergence of closed loop process is much more difficult than that in open loop design.
- The choice of design specifications in Aspen Plus determine how the results should be interpreted.
- Hydraulic design is important for absorber and stripper column design and simulation.

The recommendations for further studies can be listed as follows.

- The simulation results obtained in this study can be used to construct a working laboratory-scale CO_2 capture system.
- Not only MEA and PZ but also other novel solvents and their possible blends could be simulated on Aspen.
- Instead of using default examples on Aspen Plus graphical user interface, both MEA-CO_2-H_2O and PZ-CO_2-H_2O equilibrium systems and their thermodynamic and kinetic parameters could be taken from literature, inserted into Aspen Plus and more realistic simulations can be performed.

REFERENCES

(1) Dugas, R. E. Carbon Dioxide Absorption, Desorption and Diffusion in Aqueous Piperazine and Monoethanolamine. Ph.D. Dissertation, The University of Texas: Austin, **2009**.

(2) Arachchige, U. S. P. R. Carbon Dioxide Capture by Chemical Absorption: Energy Optimization and Analysis of Dynamic Viscosity of Solvents. Ph.D. Dissertation, University of South-Eastern Norway, **2019**.

(3) Kothandaraman, A. Carbon Dioxide Capture by Chemical Absorption: A Solvent Comparison Study. Ph.D. Dissertation, Massachusetts Institute of Technology, **2010**.

(4) Global Temperature https://climate.nasa.gov/vital-signs/global-temperature/ (accessed May 31, **2020**).

(5) Pachauri, R.K and Reisinger, A. *Climate Change 2007: Synthesis Report*; Geneva, Switzerland, **2007**.

(6) Trends in Atmospheric Carbon Dioxide: Global Monthly Mean CO2 https://www.esrl.noaa.gov/gmd/ccgg/trends/global.html#global (accessed May 31, **2020**).

(7) Gonçalves-Araujo, R. Tracing Environmental Variability in the Changing Arctic Ocean with Optical Measurements of Dissolved Organic Matter. Ph.D. Dissertation, Technical University of Denmark, **2016**. https://doi.org/10.13140/RG.2.2.16968.32001.

(8) International Energy Agency. *World Energy Outlook 2001: Assessing Today's Supplies to Fuel Tomorrow's Growth, OECD Publishing*; Paris, **2001**. https://doi.org/10.1787/weo-2001-en.

(9) Birkelund, E. S. CO2 Absorption and Desorption Simulation with Aspen HYSYS. MSc. Dissertation, University of Tromsø, **2013**.

(10) Gupta, V. Modelling of CO2 Capture Using Aspen Plus for EDF Power Plant, Krakow, Poland. MSc. Dissertation, Técnico Lisboa, **2016**.

(11) Shaddix, C.; Molina, A. Ignition, Flame Stability, and Char Combustion in Oxy-Fuel Combustion. In *Oxy-Fuel Combustion for Power Generation and Carbon Dioxide (CO2) Capture*; Elsevier, **2011**; pp 101–124. https://doi.org/10.1533/9780857090980.2.101.

(12) Carpenter, S. M.; Long III, H. A. Integration of Carbon Capture in IGCC Systems. In *Integrated Gasification Combined Cycle (IGCC) Technologies*; Elsevier, **2017**; pp 445–463.

(13) Merkel, T. C.; Lin, H.; Wei, X.; Baker, R. Power Plant Post-Combustion Carbon Dioxide Capture: An Opportunity for Membranes. *J. Memb. Sci.* **2010**, *359* (1–2), 126–139. https://doi.org/10.1016/j.memsci.2009.10.041.

(14) Thomaser, T. Analysis and Optimization of an Industrial-Scale Pre-Combustion CO2 Capture Unit of an IGCC Power Plant. MSc. Dissertation, Politecnico Di Milano, **2013**.

(15) Allahyari, N. Economic Evaluation Of Capturing Co2 From Natural Gas Power Plant And Injecting CO2 For Enhanced Oil Recovery As An Integrated System. MSc. Dissertation, University of Regina, **2013**.

(16) Leung, D. Y. C.; Caramanna, G.; Maroto-Valer, M. M. An Overview of Current Status of Carbon Dioxide Capture and Storage Technologies. *Renew. Sustain. Energy Rev.* **2014**, *39*, 426–443. https://doi.org/10.1016/j.rser.2014.07.093.

(17) Mustafa, J.; Farhan, M.; Hussain, M. CO2 Separation from Flue Gases Using Different Types of Membranes. *J Membr Sci Technol* **2016**, *6*, 153–159. https://doi.org/10.4172/2155-9589.1000153.

(18) Sayre, R. Microalgae: The Potential for Carbon Capture. *Bioscience* **2010**, *60* (9), 722–727. https://doi.org/10.1525/bio.2010.60.9.9.

(19) Ban, Z. H.; Keong, L. K.; Mohd Shariff, A. Physical Absorption of CO2 Capture: A Review. In *Advanced Materials Research*; Trans Tech Publ, **2014**; Vol. 917, pp 134–143. https://doi.org/10.4028/www.scientific.net/AMR.917.134.

(20) Plaza, J. M.; Chen, E.; Rochelle, G. T. Absorber Intercooling in CO2 Absorption by Piperazine-Promoted Potassium Carbonate. *AIChE J.* **2010**, *56* (4), 905–914. https://doi.org/10.1002/aic.12041.

(21) Calle, R. G. Modelling of an Amine-Organic Solvent Based Carbon-Capture Process for Efficient Excess Heat Utilization. MSc. Dissertation, Chalmers University of Technology, Sweden, **2018**.

(22) Boot-Handford, M. E.; Abanades, J. C.; Anthony, E. J.; Blunt, M. J.; Brandani, S.; Mac Dowell, N.; Fernández, J. R.; Ferrari, M. C.; Gross, R.; Hallett, J. P.; Haszeldine, R. S.; Heptonstall, P.; Lyngfelt, A.; Makuch, Z.; Mangano, E.; Porter, R. T. J.; Pourkashanian, M.; Rochelle, G. T.; Shah, N.; Yao, J. G.; Fennell, P. S. Carbon Capture and Storage Update. *Energy Environ. Sci.* **2014**, *7* (1), 130–189.

https://doi.org/10.1039/c3ee42350f.

(23) Dugas, R.; Rochelle, G. Absorption and Desorption Rates of Carbon Dioxide with Monoethanolamine and Piperazine. *Energy Procedia* **2009**, *1* (1), 1163–1169. https://doi.org/10.1016/j.egypro.2009.01.153.

(24) Rochelle, G.; Chen, E.; Freeman, S.; Van Wagener, D.; Xu, Q.; Voice, A. Aqueous Piperazine as the New Standard for CO2 Capture Technology. *Chem. Eng. J.* **2011**, *171* (3), 725–733. https://doi.org/10.1016/j.cej.2011.02.011.

(25) Chen, X.; Rochelle, G. T. Aqueous Piperazine Derivatives for CO2 Capture: Accurate Screening by a Wetted Wall Column. *Chem. Eng. Res. Des.* **2011**, *89* (9), 1693–1710. https://doi.org/10.1016/j.cherd.2011.04.002.

(26) Van Wagener, D. H.; Rochelle, G. T. Stripper Configurations for CO2 Capture by Aqueous Monoethanolamine and Piperazine. *Energy Procedia* **2011**, *4*, 1323–1330. https://doi.org/10.1016/j.egypro.2011.01.190.

(27) Freguia, S. Modeling of CO2 Removal from Flue Gases with Monoethanolamine. MSc. Dissertation, The University of Texas at Austin, **2002**.

(28) Lewis, W. K.; Whitman, W. G. Principles of Gas Absorption. *Ind. Eng. Chem.* **1924**, *16* (12), 1215–1220. https://doi.org/10.1021/ie50180a002.

(29) Rousseau, R. W. *Handbook of Separation Process Technology*; John Wiley & Sons, **1987**.

(30) Billet, R. *Packed Towers: In Processing and Environmental Technology*; VCH New York, **1995**.

(31) Pérez, A. P.; Segura, R. S. Design of a Packed-Bed Absorption Column Considering Four Packing Types and Applying Matlab. **2016**, *29* (02), 83–104. https://doi.org/10.5377/nexo.v29i2.4577.

(32) Benitez, J. *Principles and Modern Applications of Mass Transfer Operations*; Wiley, **2009**.

(33) Absorbers http://encyclopedia.che.engin.umich.edu/Pages/SeparationsChemical/Absorbers/Absorbers.html (accessed May 31, **2020**).

(34) Peters, M. S.; Timmerhaus, K. D. *Plant Design and Economics for Chemical Engineers, McGraw-Hili International Editions*; McGraw-Hill, **1991**.

(35) Towler, G.; Sinnott, R. *Chemical Engineering Design Principles, Practice and Economics of Plant and Process Design*; Elsevier Ltd., **2013**. https://doi.org/10.1016/B978-0-08-096659-5.00022-5.

(36) Kolev, N. *Packed Bed Columns: For Absorption, Desorption, Rectification and Direct Heat Transfer*; Elsevier, **2006**.

(37) Hanley, B.; Lew, M.; Dyment, J. *Column Analysis in Aspen Plus ® and Aspen HYSYS ® : Validation with Experimental and Plant Data*; **2016**.

(38) *Column Analysis in Aspen HYSYS ® and Aspen Plus ® V9*. https://doi.org/10.1016/S1350-4533(00)00034-5.

(39) Sinnot, R. K. *Coulson & Richardson's Chemical Engineering*; Elsevier Ltd, **1993**; Vol. 2.

(40) Kister, H. Z.; Haas, J. R.; Hart, D. R.; Gill, D. R. *Distillation Design*; McGraw-Hill New York, **1992**; Vol. 1.

(41) Kohl, A. L.; Nielsen, R. *Gas Purification*; Elsevier: Houston, Texas, **1997**.

(42) Harun, N. Dynamic Simulation of MEA Absorption Process for CO2 Capture from Power Plants. Ph.D. Dissertation, University of Waterloo, **2012**.

(43) Sartori, G.; Savage, D. W. Sterically Hindered Amines for Carbon Dioxide Removal from Gases. *Ind. Eng. Chem. Fundam.* **1983**, *22* (2), 239–249. https://doi.org/10.1021/i100010a016.

(44) Zhang, Y.; Sachde, D.; Chen, E.; Rochelle, G. Modeling of Absorber Pilot Plant Performance for CO2 Capture with Aqueous Piperazine. *Int. J. Greenh. Gas Control* **2017**, *64* (July), 300–313. https://doi.org/10.1016/j.ijggc.2017.08.004.

(45) Edwards, T. J.; Maurer, G.; Newman, J.; Prausnitz, J. M. Vapor-Liquid Equilibria in Multicomponent Aqueous Solutions of Volatile Weak Electrolytes. *AIChE J.* **1978**, *24* (6), 966–976. https://doi.org/10.1002/aic.690240605.

(46) Orestes, E.; Machado Ronconi, C.; Carneiro, J. W. de M. Insights into the Interactions of CO2 with Amines: A DFT Benchmark Study. *Phys. Chem. Chem. Phys.* **2014**, *16* (32), 17213–17219. https://doi.org/10.1039/c4cp02254h.

(47) Hwang, G. S.; Stowe, H. M.; Paek, E.; Manogaran, D. Reaction Mechanisms of Aqueous Monoethanolamine with Carbon Dioxide: A Combined Quantum Chemical and Molecular Dynamics Study. *Phys. Chem. Chem. Phys.* **2015**, *17* (2), 831–839. https://doi.org/10.1039/c4cp04518a.

(48) Wong, M. K.; Bustam, M. A.; Shariff, A. M. Chemical Speciation of CO2 Absorption in Aqueous Monoethanolamine Investigated by in Situ Raman Spectroscopy. *Int. J. Greenh. Gas Control* **2015**, *39*, 139–147. https://doi.org/10.1016/j.ijggc.2015.05.016.

(49) Dang, H.; Rochelle, G. T. CO2 Absorption Rate and Solubility in

Monoethanolamine/Piperazine/Water. *Sep. Sci. Technol.* **2003**, *38* (2), 337–357. https://doi.org/10.1081/SS-120016678.

(50) Arachchige, U. S. P. R.; Melaaen, M. C. Aspen plus Simulation of CO2 Removal from Coal and Gas Fired Power Plants. *Energy Procedia* **2012**, *23* (1876), 391–399. https://doi.org/10.1016/j.egypro.2012.06.060.

(51) Ferrara, F.; Calì, G.; Frau, C.; Pettinau, A.; Sotacarbo, S. a; Miniera, G. Experimental and Numerical Assessment of the CO2 Absorption Process in the Sotacarbo Pilot Platform. In *1st International Conference on Sustainable Fossil Fuels for Future Energy*; **2009**; pp 1–12.

(52) Zhang, Y.; Que, H.; Chen, C. C. Thermodynamic Modeling for CO2 Absorption in Aqueous MEA Solution with Electrolyte NRTL Model. *Fluid Phase Equilib.* **2011**, *311* (1), 67–75. https://doi.org/10.1016/j.fluid.2011.08.025.

(53) Jin, H.; Liu, P.; Li, Z. Energy-Efficient Process Intensification for Post-Combustion CO2 Capture: A Modeling Approach. *Energy* **2018**, *158*, 471–483. https://doi.org/10.1016/j.energy.2018.06.045.

(54) Dubois, L.; Thomas, D. Comparison of Various Configurations of the Absorption-Regeneration Process Using Different Solvents for the Post-Combustion CO2 Capture Applied to Cement Plant Flue Gases. *Int. J. Greenh. Gas Control* **2018**, *69* (March 2017), 20–35. https://doi.org/10.1016/j.ijggc.2017.12.004.

(55) Soltani, S. M.; Fennell, P. S.; Mac Dowell, N. A Parametric Study of CO2 Capture from Gas-Fired Power Plants Using Monoethanolamine (MEA). *Int. J. Greenh. Gas Control* **2017**, *63* (May), 321–328. https://doi.org/10.1016/j.ijggc.2017.06.001.

(56) Kalatjari, H. R.; Haghtalab, A.; Nasr, M. R. J.; Heydarinasab, A. Experimental, Simulation and Thermodynamic Modeling of an Acid Gas Removal Pilot Plant for CO2 Capturing by Mono-Ethanol Amine Solution. *J. Nat. Gas Sci. Eng.* **2019**, *72* (September), 103001. https://doi.org/10.1016/j.jngse.2019.103001.

(57) Øi, L. E. Aspen HYSYS Simulation of CO 2 Removal by Amine Absorption from a Gas Based Power Plant. In *SIMS2007 Conference*; **2007**; pp 73–81.

(58) Liu, Y.; Zhang, L.; Watanasiri, S. Representing Vapor-Liquid Equilibrium for an Aqueous MEA-CO2 System Using the Electrolyte Nonrandom-Two-Liquid Model. *Ind. Eng. Chem. Res.* **1999**, *38* (5), 2080–2090. https://doi.org/10.1021/ie980600v.

(59) Stowe, H. M.; Paek, E.; Hwang, G. S. First-Principles Assessment of CO2 Capture

Mechanisms in Aqueous Piperazine Solution. *Phys. Chem. Chem. Phys.* **2016**, *18* (36), 25296–25307. https://doi.org/10.1039/c6cp03584a.

(60) Oexmann, J.; Hensel, C.; Kather, A. Post-Combustion CO2-Capture from Coal-Fired Power Plants: Preliminary Evaluation of an Integrated Chemical Absorption Process with Piperazine-Promoted Potassium Carbonate. *Int. J. Greenh. Gas Control* **2008**, *2* (4), 539–552. https://doi.org/10.1016/j.ijggc.2008.04.002.

(61) Stefania Moioli, L. A. P. Improved Rate-Based Modeling of the Process of C02 Capture with PZ Solution. *Chem. Eng. Res. Des.* **2015**, *93* (January), 611–620. https://doi.org/10.1016/j.cherd.2014.03.022.

(62) Mudhasakul, S.; Ku, H. ming; Douglas, P. L. A Simulation Model of a CO2 Absorption Process with Methyldiethanolamine Solvent and Piperazine as an Activator. *Int. J. Greenh. Gas Control* **2013**, *15*, 134–141. https://doi.org/10.1016/j.ijggc.2013.01.023.

(63) Cullinane, J. T.; Rochelle, G. T. Kinetics of Carbon Dioxide Absorption into Aqueous Potassium Carbonate and Piperazine. *Ind. Eng. Chem. Res.* **2006**, *45* (8), 2531–2545. https://doi.org/10.1021/ie050230s.

(64) Dash, S. K.; Samanta, A.; Samanta, A. N.; Bandyopadhyay, S. S. Vapour Liquid Equilibria of Carbon Dioxide in Dilute and Concentrated Aqueous Solutions of Piperazine at Low to High Pressure. *Fluid Phase Equilib.* **2011**, *300* (1–2), 145–154. https://doi.org/10.1016/j.fluid.2010.11.004.

(65) Zhang, W.; Chen, J.; Luo, X.; Wang, M. Modelling and Process Analysis of Post-Combustion Carbon Capture with the Blend of 2-Amino-2-Methyl-1-Propanol and Piperazine. *Int. J. Greenh. Gas Control* **2017**, *63* (March), 37–46. https://doi.org/10.1016/j.ijggc.2017.04.018.

(66) Lu, R.; Li, K.; Chen, J.; Yu, H.; Tade, M. CO2 Capture Using Piperazine-Promoted, Aqueous Ammonia Solution: Rate-Based Modelling and Process Simulation. *Int. J. Greenh. Gas Control* **2017**, *65* (March), 65–75. https://doi.org/10.1016/j.ijggc.2017.08.018.

(67) Dash, S. K.; Samanta, A. N.; Bandyopadhyay, S. S. Simulation and Parametric Study of Post Combustion CO2 Capture Process Using (AMP+PZ) Blended Solvent. *Int. J. Greenh. Gas Control* **2014**, *21*, 130–139. https://doi.org/10.1016/j.ijggc.2013.12.003.

(68) Samanta, A.; Bandyopadhyay, S. S. Kinetics and Modeling of Carbon Dioxide Absorption into Aqueous Solutions of Piperazine. *Chem. Eng. Sci.* **2007**, *62* (24),

7312–7319. https://doi.org/10.1016/j.ces.2007.08.022.

(69) Derks, P. W. J.; Kleingeld, T.; van Aken, C.; Hogendoorn, J. A.; Versteeg, G. F. Kinetics of Absorption of Carbon Dioxide in Aqueous Piperazine Solutions. *Chem. Eng. Sci.* **2006**, *61* (20), 6837–6854. https://doi.org/10.1016/j.ces.2006.07.009.

(70) Hilliard, M. D. A Predictive Thermodynamic Model for an Aqueous Blend of Potassium Carbonate, Piperazine, and Monoethanolamine for Carbon Dioxide Capture from Flue Gas. Ph.D. Dissertation, University of Texas at Austin, **2008**.

(71) Derks, P. W. J.; Dijkstra, H. B. S.; Hogendoorn, J. A.; Versteeg, G. F. Solubility of Carbon Dioxide in Aqueous Piperazine Solutions. *AIChE J.* **2005**, *51* (8), 2311–2327. https://doi.org/10.1002/aic.10442.

(72) Madeddu, C.; Errico, M.; Baratti, R. *CO2 Capture by Reactive Absorption-Stripping Modeling, Analysis and Design*; Springer, **2019**. https://doi.org/10.1007/978-3-030-04579-1.

(73) Plaza, J. M.; Wagener, D. Van; Rochelle, G. T. Modeling CO2 Capture with Aqueous Monoethanolamine. *Energy Procedia* **2009**, *1* (1), 1171–1178. https://doi.org/10.1016/j.egypro.2009.01.154.

(74) Nakagaki, T.; Yamabe, R.; Furukawa, Y.; Sato, H.; Yamanaka, Y. Experimental Evaluation of Temperature and Concentration Effects on Heat of Dissociation of CO2-Loaded MEA Solution in Strippers. In *13th International Conference on Greenhouse Gas Control Technologies, GHGT-13*; The Author(s), **2017**; Vol. 114, pp 1910–1918. https://doi.org/10.1016/j.egypro.2017.03.1322.

(75) Niu, Z.; Guo, Y.; Zeng, Q.; Lin, W. Experimental Studies and Rate-Based Process Simulations of CO2 Absorption with Aqueous Ammonia Solutions. *Ind. Eng. Chem. Res.* **2012**, *51* (14), 5309–5319. https://doi.org/10.1021/ie2030536.

(76) Liu, J.; Gao, H. C.; Peng, C. C.; Wong, D. S. H.; Jang, S. S.; Shen, J. F. Aspen Plus Rate-Based Modeling for Reconciling Laboratory Scale and Pilot Scale CO2 Absorption Using Aqueous Ammonia. *Int. J. Greenh. Gas Control* **2015**, *34*, 117–128. https://doi.org/10.1016/j.ijggc.2015.01.009.

(77) Qi, G.; Wang, S. Experimental Study and Rate-Based Modeling on Combined CO2 and SO2 Absorption Using Aqueous NH3 in Packed Column. *Appl. Energy* **2017**, *206* (October), 1532–1543. https://doi.org/10.1016/j.apenergy.2017.09.110.

(78) Thiels, M.; Wong, D. S. H.; Yu, C. H.; Kang, J. L.; Jang, S. S.; Tan, C. S. Modelling and Design of Carbon Dioxide Absorption in Rotating Packed Bed and Packed Column. In *IFAC-PapersOnLine*; Elsevier B.V., **2016**; Vol. 49, pp 895–

900. https://doi.org/10.1016/j.ifacol.2016.07.303.

(79) Errico, M.; Madeddu, C.; Pinna, D.; Baratti, R. Model Calibration for the Carbon Dioxide-Amine Absorption System. *Appl. Energy* **2016**, *183*, 958–968. https://doi.org/10.1016/j.apenergy.2016.09.036.

(80) Pinsent, B. R. W.; Pearson, L.; Roughton, F. J. W. The Kinetics of Combination of Carbon Dioxide with Hydroxide Ions. *Trans. Faraday Soc.* **1956**, *52*, 1512–1520.

(81) Sanjay Bishnoi, G. T. R. Absorption of Carbon Dioxide in Aqueous Piperazine/Methyldiethanolamine. *AIChE J.* **2002**, *48* (12), 2788–2799. https://doi.org/10.1002/aic.690481208.

(82) Haydary, J. *Chemical Process Design and Simulation: Aspen Plus and Aspen Hysys Applications*; John Wiley & Sons, **2019**.

(83) Lawal, A.; Wang, M.; Stephenson, P.; Yeung, H. Dynamic Modelling of CO2 Absorption for Post Combustion Capture in Coal-Fired Power Plants. *Fuel* **2009**, *88* (12), 2455–2462. https://doi.org/10.1016/j.fuel.2008.11.009.

(84) Fogler, H. S. *Elements of Chemical Reaction Engineering*; Prentice Hall: Westford, Massachusetts, **2006**.

(85) Taylor, R.; Krishna, R. *Multicomponent Mass Transfer*; John Wiley & Sons: New York, **1993**.

(86) Kvamsdal, H. M.; Rochelle, G. T. Effects of the Temperature Bulge in CO2 Absorption from Flue Gas by Aqueous Monoethanolamine. *Ind. Eng. Chem. Res.* **2008**, *47* (3), 867–875. https://doi.org/10.1021/ie061651s.

(87) Kvamsdal, H. M.; Jakobsen, J. P.; Hoff, K. A. Dynamic Modeling and Simulation of a CO2 Absorber Column for Post-Combustion CO2 Capture. *Chem. Eng. Process. Process Intensif.* **2009**, *48* (1), 135–144. https://doi.org/10.1016/j.cep.2008.03.002.

(88) Kvamsdal, H. M.; Hillestad, M. Selection of Model Parameter Correlations in a Rate-Based CO2 Absorber Model Aimed for Process Simulation. *Int. J. Greenh. Gas Control* **2012**, *11*, 11–20. https://doi.org/10.1016/j.ijggc.2012.07.013.

(89) Finn Andrew Tobiesen, H. F. S. Experimental Validation of a Rigorous Absorber Model for CO2 Postcombustion Capture. *AIChE J.* **2007**, *53* (4), 846–865. https://doi.org/10.1002/aic.

(90) Kucka, L.; Müller, I.; Kenig, E. Y.; Górak, A. On the Modelling and Simulation of Sour Gas Absorption by Aqueous Amine Solutions. *Chem. Eng. Sci.* **2003**, *58* (16),

3571–3578. https://doi.org/10.1016/S0009-2509(03)00255-0.

(91) Yang, H.; Xu, Z.; Fan, M.; Gupta, R.; Slimane, R. B.; Bland, A. E.; Wright, I. Progress in Carbon Dioxide Separation and Capture: A Review. *J. Environ. Sci.* **2008**, *20* (1), 14–27. https://doi.org/10.1016/S1001-0742(08)60002-9.

(92) Mikkelsen, M.; Jørgensen, M.; Krebs, F. C. The Teraton Challenge. A Review of Fixation and Transformation of Carbon Dioxide. *Energy Environ. Sci.* **2010**, *3* (1), 43–81. https://doi.org/10.1039/b912904a.

(93) MacDowell, N.; Florin, N.; Buchard, A.; Hallett, J.; Galindo, A.; Jackson, G.; Adjiman, C. S.; Williams, C. K.; Shah, N.; Fennell, P. An Overview of CO2 Capture Technologies. *Energy Environ. Sci.* **2010**, *3* (11), 1645–1669. https://doi.org/10.1039/c004106h.

(94) Chen, E. Carbon Dioxide Absorption into Piperazine Promoted Potassium Carbonate Using Structured Packing. Ph.D. Dissertation, The University of Texas at Austin, **2007**.

(95) Aboudheir, A. Kinetics, Modeling, and Simulation Ofcarbon Dioxide Absorption into Highly Concentrated and Loaded Monoethanolamine Solutions. Ph.D. Dissertation, University ofRegina, Canada, 2002.

(96) Rochelle, G. T. *Research Needs for CO2 Capture from Flue Gas by Aqueous Absorption/Stripping*; **2001**.

(97) Austgen, D. M.; Rochelle, G. T.; Peng, X.; Chen, C. C. Model of Vapor-Liquid Equilibria for Aqueous Acid Gas-Alkanolamine Systems Using the Electrolyte-NRTL Equation. *Ind. Eng. Chem. Res.* **1989**, *28* (7), 1060–1073.

(98) Aboudheir, A.; Tontiwachwuthikul, P.; Chakma, A.; Idem, R. Kinetics of the Reactive Absorption of Carbon Dioxide in High CO2-Loaded, Concentrated Aqueous Monoethanolamine Solutions. *Chem. Eng. Sci.* **2003**, *58* (23–24), 5195–5210. https://doi.org/10.1016/j.ces.2003.08.014.

(99) Hikita, H.; Asai, S.; Ishikawa, H.; Honda, M. The Kinetics of Reactions of Carbon Dioxide with Monoethanolamine, Diethanolamine and Triethanolamine by a Rapid Mixing Method. *Chem. Eng. J.* **1977**, *13* (1), 7–12. https://doi.org/10.1016/0300-9467(77)80002-6.

(100) Plaza, J. M.; Rochelle, G. T. Modeling Pilot Plant Results for CO2 Capture by Aqueous Piperazine. *Energy Procedia* **2011**, *4*, 1593–1600. https://doi.org/10.1016/j.egypro.2011.02.029.

(101) Frailie, P.; Plaza, J.; Van Wagener, D.; Rochelle, G. T. Modeling Piperazine

Thermodynamics. *Energy Procedia* **2011**, *4*, 35–42. https://doi.org/10.1016/j.egypro.2011.01.020.

(102) Gao, T.; Selinger, J. L.; Rochelle, G. T. Demonstration of 99% CO2 Removal from Coal Flue Gas by Amine Scrubbing. *Int. J. Greenh. Gas Control* **2019**, *83* (February), 236–244. https://doi.org/10.1016/j.ijggc.2019.02.013.

(103) Yu, J.; Wang, S.; Yu, H. Experimental Studies and Rate-Based Simulations of CO2 Absorption with Aqueous Ammonia and Piperazine Blended Solutions. *Int. J. Greenh. Gas Control* **2016**, *50*, 135–146. https://doi.org/10.1016/j.ijggc.2016.04.019.

(104) Chen, C.; Britt, H. I.; Boston, J. F.; Evans, L. B. Local Composition Model for Excess Gibbs Energy of Electrolyte Systems. Part I: Single Solvent, Single Completely Dissociated Electrolyte Systems. *AIChE J.* **1982**, *28* (4), 588–596.

(105) Chen, C.; Evans, L. B. A Local Composition Model for the Excess Gibbs Energy of Aqueous Electrolyte Systems. *AIChE J.* **1986**, *32* (3), 444–454.

(106) Yildirim, O.; Flechsig, S.; Brinkmann, U.; Kenig, E. Y. Application of the Wallis Plot for the Determination of the Loading Limits of Structured Packings and Sandwich Packings. *Chem. Eng. Trans.* **2015**, *45*, 1165–1170. https://doi.org/10.1002/cite.201500043.

(107) Du Preez, L. J.; Motang, N.; Callanan, L. H.; Burger, A. J. Determining the Liquid Phase Equilibrium Speciation of the CO2-MEA-H2O System Using a Simplified in Situ Fourier Transform Infrared Method. *Ind. Eng. Chem. Res.* **2019**, *58* (1), 469–478. https://doi.org/10.1021/acs.iecr.8b04437.

(108) Huertas, J. I.; Gomez, M. D.; Giraldo, N.; Garzón, J. CO2 Absorbing Capacity of MEA. *J. Chem.* **2015**, *2015* (2). https://doi.org/10.1155/2015/965015.

(109) Pacheco, M. A. Mass Transfer, Kinetics and Rate-Based Modeling of Reactive Absorption. Ph.D. Dissertation, The University of Texas at Austin, **1999**.

APPENDICES

APPENDIX A. Fundamentals of Gas Absorption

Absorption columns are traditionally modeled using models based on equilibrium. A series of stages are assumed to be present in the column. The liquid phase and vapor phase exiting each stage are assumed to be at equilibrium. However, that condition is not valid in real cases. Because of that, height of packing equivalent to a theoretical plate (HETP), stage and Murphree efficiencies are utilized to correct for this.

In each stage, a suitable mass transfer between gas and liquid phases is generally expressed using a term called the height of packing equivalent to one transfer unit (HTU) or HETP. HTU can be calculated based on the number of transfer units which can be expressed using the driving force for mass transfer in the gas phase (NTU_G) or the driving force in the liquid phase (NTU_L), as displayed in the following equations:

$$NTU_G = \int_{y_1}^{y_2} \frac{dy}{y - {y_G}^*} \qquad Eqn.1$$

$$NTU_L = \int_{x_1}^{x_2} \frac{dx}{{x_L}^* - x} \qquad Eqn.2$$

$$HTU_G = \frac{Z}{NTU_G} \qquad Eqn.3$$

$$HTU_L = \frac{Z}{NTU_L} \qquad Eqn.4$$

where y and x are gas phase and liquid phase concentrations, respectively, and ${y_G}^*$ and ${x_L}^*$ are gas phase and liquid phase concentrations corresponding to values in equilibrium with the liquid phase and gas phase concentrations, respectively, and Z is height of packing which corresponds to distance from the lower to upper limits showed by the subscripts on x and y.

APPENDIX B. Packed Column Model

RateSep^{TM} model on Aspen Plus allows the researcher to divide the column into segments, carry out the material and energy balances, heat transfer, mass transfer, and phase equilibrium calculations at each stage and integrate across the column. So, mass and energy balances are modeled using rate-based equations.

Chemical reaction is assumed to be at equilibrium in rate-based model. Chemical kinetics is considered to be in the liquid bulk phase. Rate-based model complexity increases substantially if kinetically controlled chemical reactions occurs in the liquid film and liquid bulk phase. Modeling a rigorous reactive absorption causes to a large set of equations.

In this study, a steady state rate-based model was selected by using film theory with chemical equilibrium assumption. Mathematically, packed column model (absorber and stripper columns) requires these equations:

1. Material Balance Equations
2. Energy Balance Equations
3. Rate Equations
4. Equilibrium Relations
5. Chemical Kinetics

The partial differential equations for mass and energy balances integrate the model for the column. The equations are derived over a volume element representing a small part of the column. Temperature and concentration profiles inside the columns are found by the integration of these equations with appropriate boundary conditions. Along with these equations, solubility, diffusivity, viscosity, and density must be included to provide a good description of the process. For the packed column model, following assumptions are made:

1. Linear pressure drop
2. The fluid is in turbulent flow
3. Due to low pressure, there is ideal gas phase
4. No accumulation in gas films and liquid films
5. Mass fluxes of H_2O, MEA/PZ and CO_2 are allowed in both directions between the two phases

APPENDIX C. Material and Energy Balance for the Gas and Liquid Phases

Material balances are expressed in a derivative form to consider the spatial and temporal behavior of the column. The packed column is divided into height elements, Δz. The axial position of z is selected to be positive in the direction of gas flow, that is, positive starting at the bottom going to the top. This model was obtained by implementation of an approach based on differential volume element with a height of Δz in the packed column. Thus, the differential material balances of component i in liquid and gas phases over a volume element as displayed in both Equations and Figure C.1 are as follows:

$$0 = -u_g \frac{\partial C_{g,i}}{\partial z} - C_{g,i} \frac{\partial u_g}{\partial z} - a_{gl} N_i \qquad Eqn.5$$

$$0 = u_l \frac{\partial C_{l,i}}{\partial z} + a_{gl} N_i \qquad Eqn.6$$

where $C_{g,i}$ (mol/m^3) and $C_{l,i}$ (mol/m^3) are the molar concentrations of component i in the gas and liquid phase, u_g (m/s) and u_l (m/s) are the gas and liquid velocities, a_{gl} (m^2/m^3) is for the specific gas-liquid interfacial area and N_i (mol/m^2/s) is the molar flux of component i. As seen in Eqn 5. and 6., the concentration of i in the liquid and gas phase changes with distance (z) along the height of the column.

For the absorber, the molar flux of N_i in Equations 5 and 6 are defined as the net loss of component i in the gas phase and the net gain of the same component in the liquid phase. At the same time, in the stripper, the interfacial mass transfer will happen in the opposite direction such as the net loss and gain of component i take place in the liquid and gas phase, respectively. The component i in the column might be MEA, CO_2, N_2 or H_2O. However, N_2 is not involved in the reaction and is not considered to be transferred between the phases.

The energy balance for the gas and liquid phase might be acquired from the application of the differential volume element approach for a section inside the packed column. The equations are:

$$0 = -u_g \frac{\partial T_g}{\partial z} - T_g \frac{\partial u_g}{\partial z} - \frac{q_g a_{gl}}{\sum C_{g,i} C_{p,i}} \qquad Eqn.7$$

$$0 = -u_l \frac{\partial T_l}{\partial z} - \frac{q_l a_{gl}}{\sum C_{l,i} C_{p,i}} \qquad Eqn.8$$

where, T_l (K) and T_g (K) are the liquid (solvent) and gas temperature, q_g (J/m^3/s) and q_l (J/m^3/s) show interfacial heat transfer in the gas and liquid phase, a_{gl} (m^2/m^3) is for the specific gas-liquid interfacial area and C_p (J/mol/K) is the specific heat capacity.

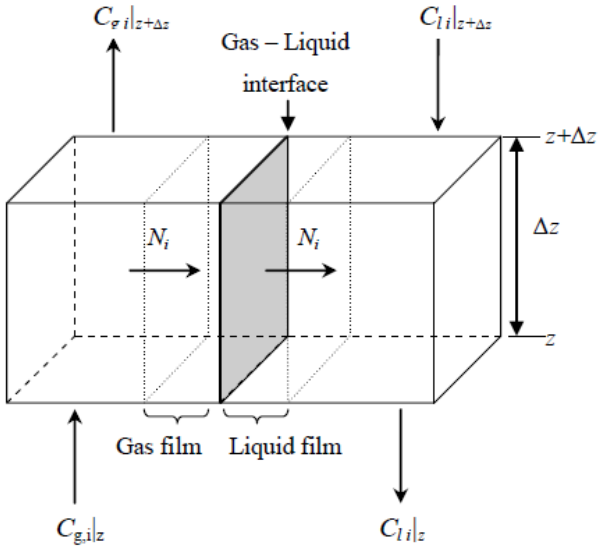

Figure C.1 Mass Balance over a volume element (from N. Harun Ph.D. Dissertation)

The interfacial heat transfer consists of a conductive heat flux due to temperature gradients in the fluid and a convective heat flux by interface transport due to transport enthalpy. Conductive heat flux is considered as

$$q_g = h_{gl}(T_l - T_g) \qquad Eqn.9$$

where h_{gl} (W/m^2/K) is the interfacial heat transfer coefficient. The liquid heat transfer thanks to the temperature difference between the two phases, heat of vaporization of H_2O, heat of reaction (exothermic reaction between CO_2 and MEA or PZ) and heat loss to the surroundings are calculated in the model:

$$q_l = h_{gl}(T_l - T_g) + \Delta H_{rxn} N_{CO_2} + \Delta H_{vap} N_{H_2O} + h_{out}(T_l - T_{amb}) \qquad Eqn.10$$

where ΔH_{rxn} (J/mol) is the heat of reaction per mol CO_2, h_{out} (W/m^2/K) is the wall heat transfer coefficient and T_{amb} (K) is the ambient temperature. The present model assumes that chemical reaction of CO_2 occurs in the liquid phase. For example, the heat of reaction is only taken into account in the energy balance for the liquid bulk like in Equation 10. The heat losses to the surroundings are deeply taken into consideration in the liquid phase.

APPENDIX D. Solution Chemistry

Reversible reactions of MEA-CO_2-H_2O and PZ-CO_2-H_2O systems in liquid phases are given in the introduction chapter. Every reaction shows an equilibrium constraint. Solving the thermodynamic problem for the MEA and PZ solution systems at a specific pressure and temperature means finding the mole fractions of each of the components in both vapor and liquid phases. Since the ions are non-volatile, only CO_2, MEA, PZ and H_2O are present in the vapor phase. For the MEA and PZ systems, there are 5 and 7 equilibrium constraints, respectively.

$$K_j = \frac{\prod_1^{prod}(a_i)^{vi}}{\prod_1^{reactant}(a_i)^{vi}} \qquad Eqn.11$$

In Equation 11, a_i is the activity of component i in the solution and v_i is the stoichiometric coefficient of component i in reaction j. Activity of component i is also expressed by mole fraction times activity coefficient which is shown in Equation 12. Aspen Plus also uses these activity coefficient models in the simulations. Activity coefficients are represented with ELEC-NRTL thermodynamic model including for both ionic and molecular species in mixed solvent systems.

$$a_i = x_i \gamma_i \qquad Eqn.12$$

APPENDIX E. CO_2 Capture Rate

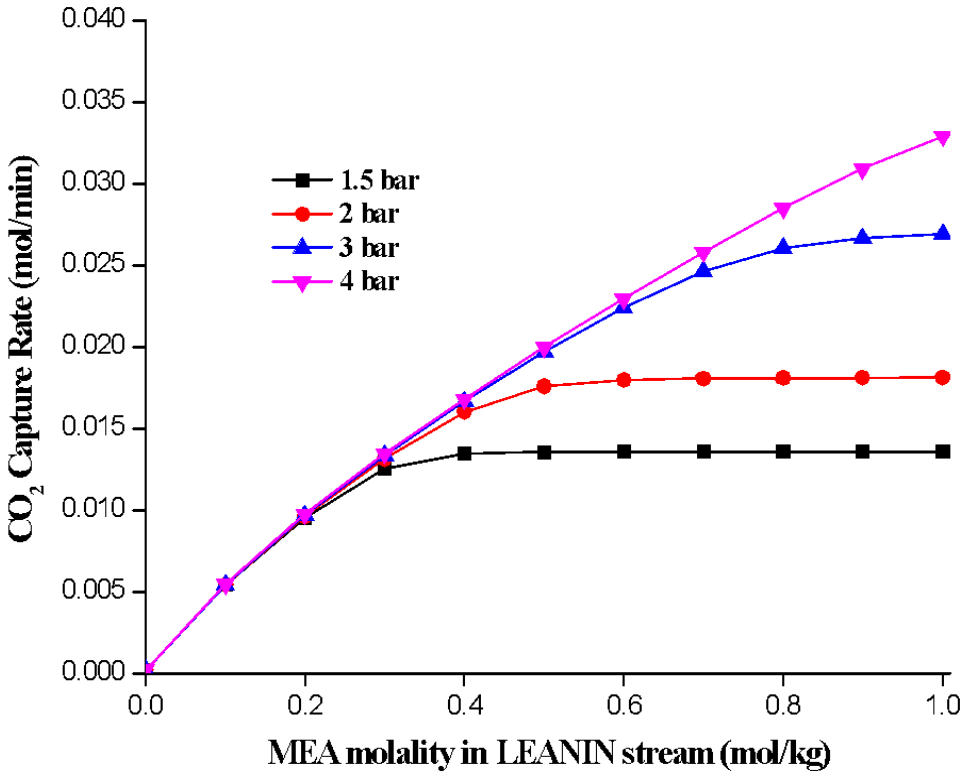

Figure E.1 CO_2 capture rate versus molality of MEA in LEANIN stream at 1.5 bar, 2 bar, 3 bar and 4 bar FLUEGAS inlet pressures

In Figure E.1, CO_2 capture rate (mol/min) versus molality of MEA (mol/kg) in LEANIN stream is shown. Equilibrium calculations are done under non-ideal conditions to find molality. CO_2 capture rate (mol/min) is calculated as a function of apparent molar concentrations of CO_2 and volumetric flow rates at inlet and outlet gas streams in Equation 1.

$$CO_2\ capture\ rate\ \left(\frac{mol}{min}\right) = C_{inlet} * G_{inlet} - C_{outlet} * G_{outlet} \qquad Eqn\ 1.$$

Here, "C" stands for molar concentration of CO_2 (mol/L) and "G" stands for volumetric flow rate of that stream (L/min). Between 0 m and 1 m (m: molality), simulations are converged to see the effect of increasing molality of MEA on CO_2 capture rate. For MEA, for three of pressure values (1.5 bar, 2 bar, 3 bar), CO_2 capture rate increases to a certain level and then levels off. At 4 bar inlet gas pressure, capture rate continues to increase over 1 m MEA in LEANIN stream.

In Figure E.2, CO_2 capture rate (mol/min) versus molality of PZ (mol/kg) in LEANIN stream is displayed.

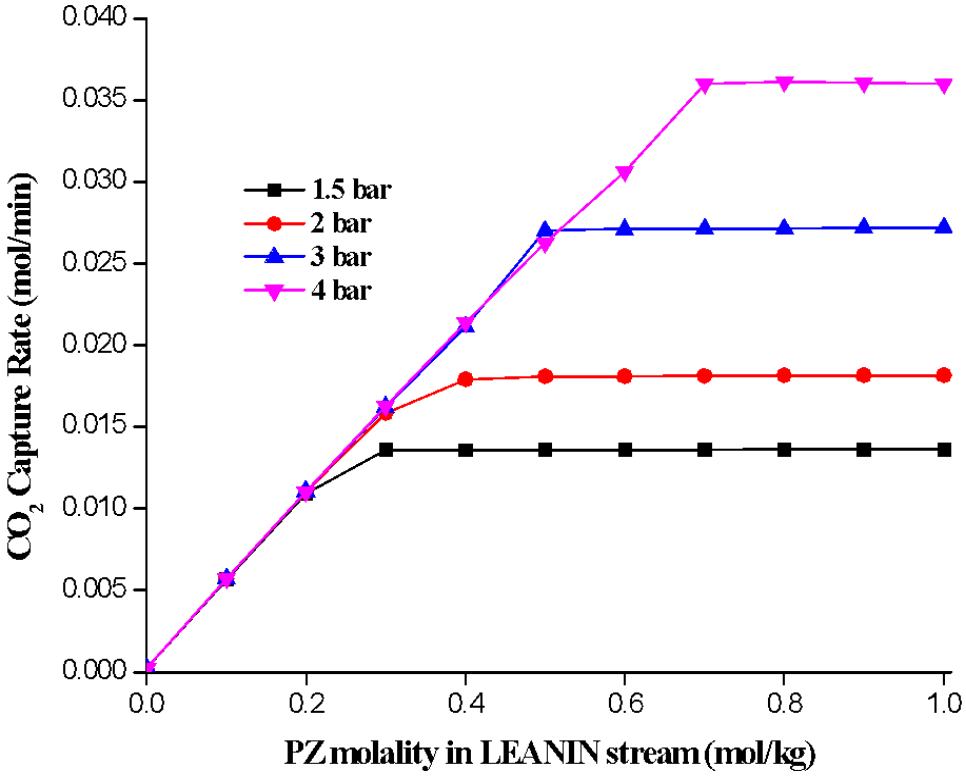

Figure E.2 CO_2 capture rate versus molality of PZ in LEANIN stream at 1.5 bar, 2 bar, 3 bar and 4 bar FLUEGAS inlet pressures

As seen, most of the trend is similar to that of MEA. The CO_2 capture rate is a bit higher in PZ solution compared to MEA solution. Only difference is that the CO_2 capture rate at 4 bar levels off after a certain molality of PZ unlike that in MEA. Considering both solvents, PZ shows a little higher CO_2 capture rate than MEA.

APPENDIX F. Hydraulic Plots of Absorber Studies

Hydraulic plots of absorber studies are shown in Figure F.1-F.4.

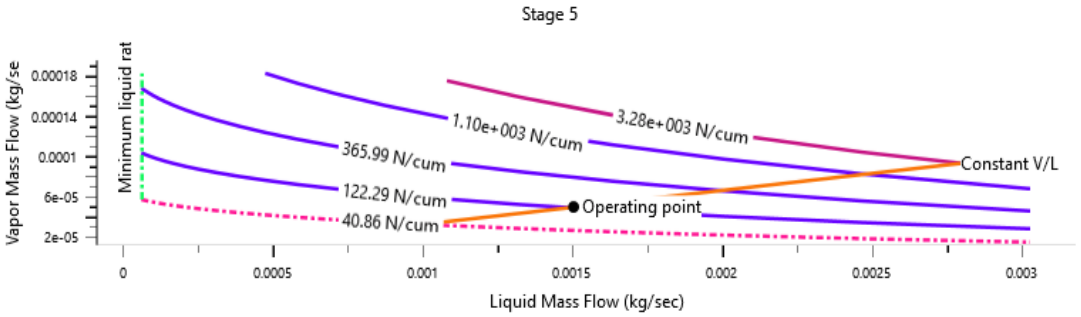

Figure F.1 Vapor mass flow versus liquid mass flow of MEA solution at 2 bar inlet gas pressure in the absorber

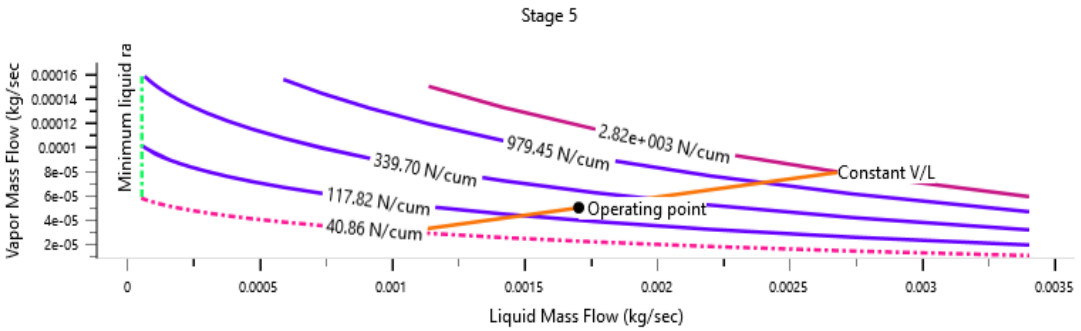

Figure F.2 Vapor mass flow versus liquid mass flow of PZ solution at 2 bar inlet gas pressure in the absorber

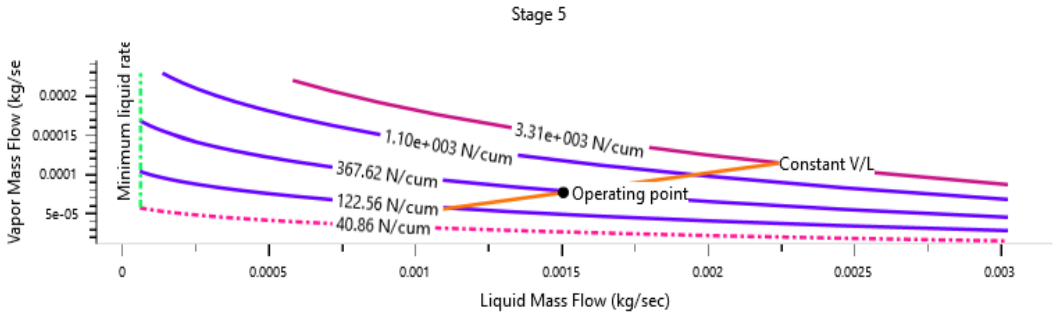

Figure F.3 Vapor mass flow versus liquid mass flow of MEA solution at 3 bar inlet gas pressure in the absorber

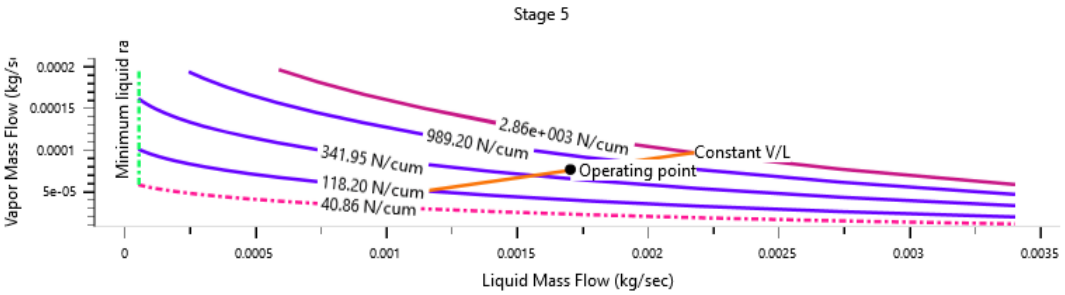

Figure F.4 Vapor mass flow versus liquid mass flow of PZ solution at 3 bar inlet gas pressure in the absorber

APPENDIX G. Hydraulic Plots of Open Loop Studies

Hydraulic plots of stripper in open loop studies are shown in Figure G.1-G.4.

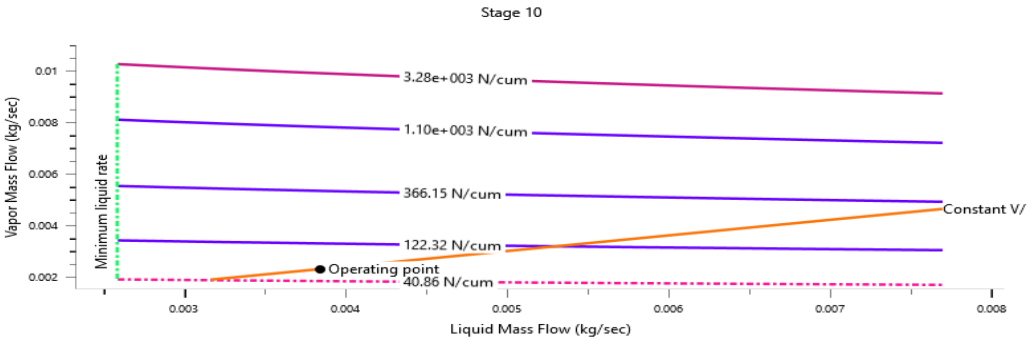

Figure G.1 Vapor mass flow versus liquid mass flow of MEA solution at 3 bar inlet gas pressure in the stripper in the open loop study

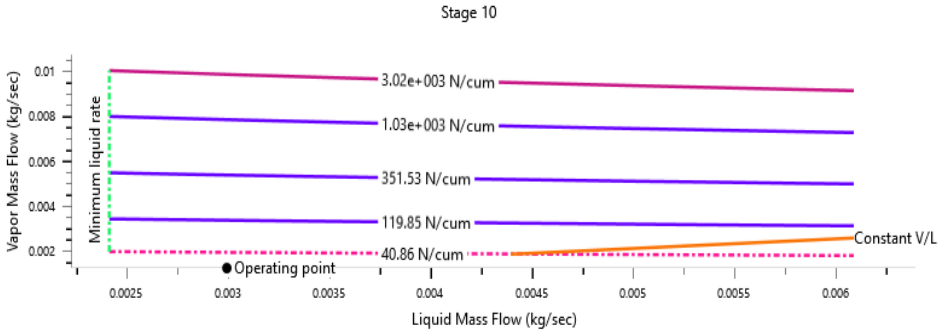

Figure G.2 Vapor mass flow versus liquid mass flow of PZ solution at 3 bar inlet gas pressure in the stripper in the open loop study

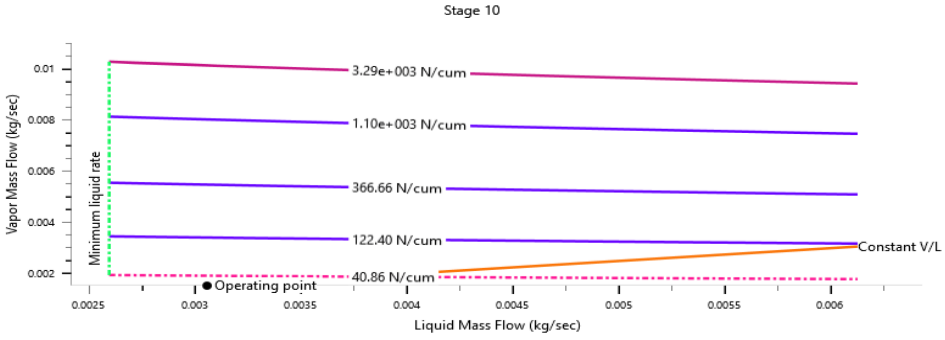

Figure G.3 Vapor mass flow versus liquid mass flow of MEA solution at 4 bar inlet gas pressure in the stripper in the open loop study

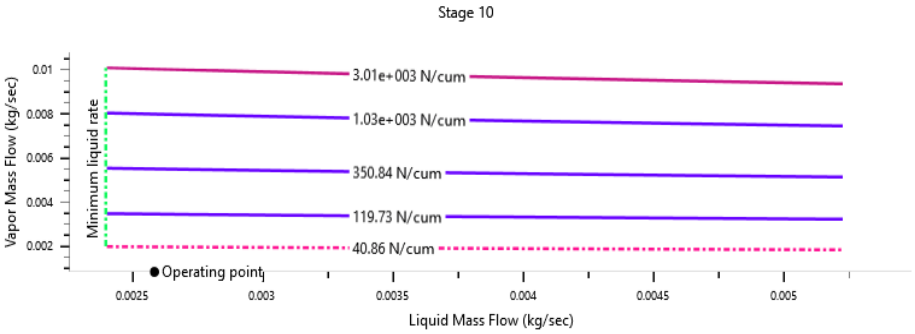

Figure G.4 Vapor mass flow versus liquid mass flow of PZ solution at 4 bar inlet gas pressure in the stripper in the open loop study

APPENDIX H. Hydraulic Plots of Closed Loop Studies

Hydraulic plots of closed loop studies are shown in Figure H.1-H.4.

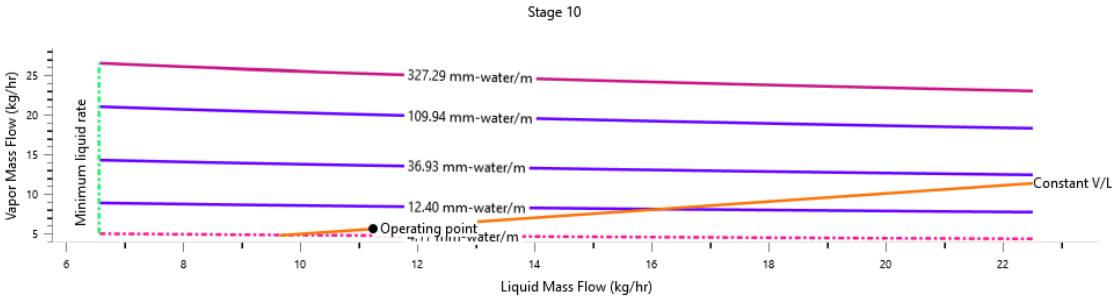

Figure H.1 Vapor mass flow versus liquid mass flow of MEA solution at 2 bar inlet gas pressure in the stripper in closed loop studies

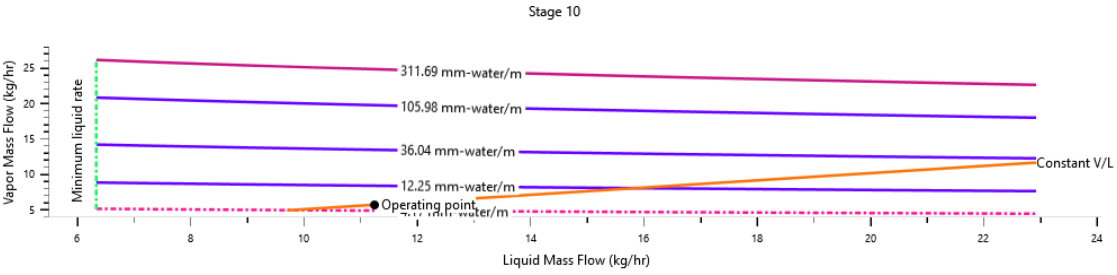

Figure H.2 Vapor mass flow versus liquid mass flow of PZ solution at 2 bar inlet gas pressure in the stripper in closed loop studies

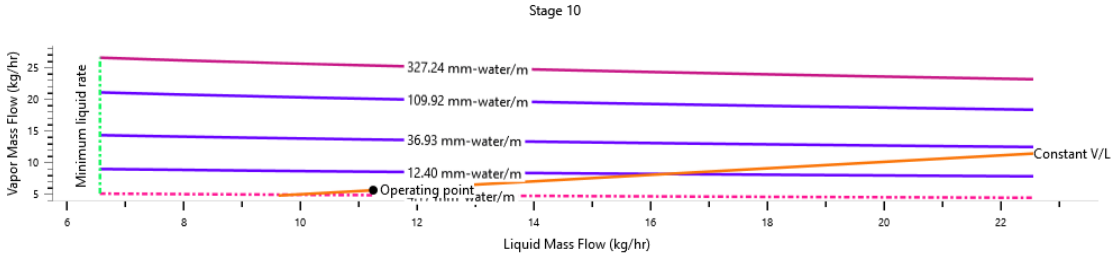

Figure H.3 Vapor mass flow versus liquid mass flow of MEA solution at 3 bar inlet gas pressure in the stripper in closed loop studies

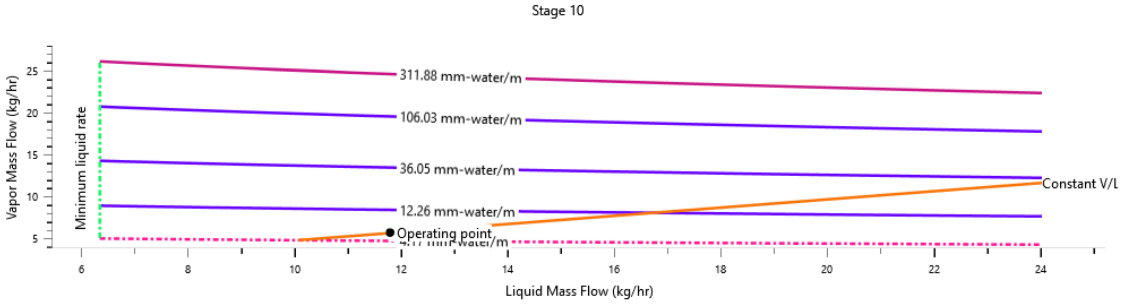

Figure H.4 Vapor mass flow versus liquid mass flow of PZ solution at 3 bar inlet gas pressure in the stripper in closed loop studies